CERN
INFN

EUROPEAN ORGANIZATION FOR NUCLEAR RESEARCH
ISTITUTO NAZIONALE DI FISICA NUCLEARE

CERN 98-02
INFN/AE-98/05
19 May 1998

THE CERN NEUTRINO BEAM TO GRAN SASSO

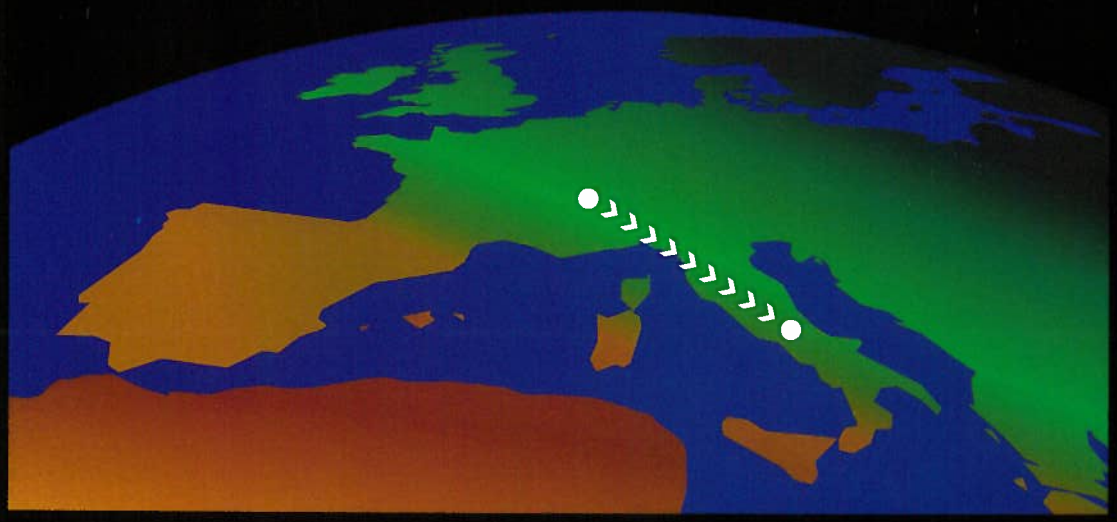

EDITOR:
K. ELSENER

CONCEPTUAL TECHNICAL DESIGN

ISSN 0007-8328
ISBN 92-9083-129-4

CERN – EUROPEAN LABORATORY FOR PARTICLE PHYSICS
INFN – ISTITUTO NAZIONALE DI FISICA NUCLEARE

CERN 98–02
INFN/AE–98/05
19 May 1998

THE CERN NEUTRINO BEAM TO GRAN SASSO (NGS)
Conceptual Technical Design

G. Acquistapace, J. L. Baldy, A. E. Ball, P. Bonnal, M. Buhler-Broglin, F. Carminati, E. Cennini, K. Elsener (Ed.), A. Ereditato, V. Falaleev, P. Faugeras, A. Ferrari, L. Foà, G. Fortuna, R. Genand, A. L. Grant, L. Henny, A. Hilaire, K. Hübner, J. Inigo-Golfin, K. H. Kissler, L. A. Lopez-Hernandez, J. M. Maugain, M. Mayoud, P. Migliozzi, D. Missiaen V. Palladino, I. M. Papadopoulos, S. Péraire, F. Pietropaolo, S. Rangod, J.-P. Revol, J. Roche, P. Sala, C. Sanelli, G. R. Stevenson, B. Tomat, E. Tsesmelis, R. Valbuena, H. Vincke, E. Weisse and M. Wilhelmsson

GENEVA
1998

CERN–Service d'information scientifique–RD/984–2000–mai 1998

ABSTRACT

The conceptual design of a new neutrino facility at CERN is presented. Starting with 400 GeV/c protons from the Super Proton Synchrotron (SPS), a neutrino beam is produced which is directed towards the underground Gran Sasso Laboratory in Italy, 732 km away from CERN, where large, complex detectors will allow long-baseline experiments searching for neutrino oscillation phenomena to be performed.

PREFACE

This report outlines the conceptual design of a new CERN Neutrino beam to Gran Sasso (NGS). The proposed facility consists of a neutrino beam directed towards the INFN Gran Sasso Laboratory (an underground laboratory in central Italy, 732 km from CERN) and an underground experimental area for neutrino physics approximately 2 km from the source at the boundary of Geneva airport. Such a new CERN neutrino beam, together with massive detectors at Gran Sasso will constitute a powerful tool for long-baseline (LBL) neutrino oscillation searches, sensitive to low mass differences squared Δm^2 between different neutrino flavours. The experimental area near CERN with a short-baseline (SBL) experiment, sensitive to low mixing parameters $\sin^2 2\theta$, will ideally complement this exciting physics programme.

Following CERN tradition, the new facility takes maximum advantage of existing installations such as the proton injectors (Linac, Booster, PS) and the SPS accelerator. Moreover, the extraction from the SPS, planned for the LHC, can be used with some modifications. The report also defines the restrictions for the new project, including those made by the approved CERN physics programme (SPS, LEP, LHC).

The result of studies made by a Technical Committee, mandated by INFN and CERN, in conjunction with extensive studies by a CERN internal working group are summarized in the report. These studies began in April 1997 and benefited from preliminary work on possible long-baseline neutrino experiments with a beam from CERN. The invaluable experience of running neutrino beam facilities at CERN for several decades is naturally reflected in this work.

In this first report, the physics motivation and the general layout of the facility are presented, together with a description of the technical aspects of the neutrino beam towards Gran Sasso. In a forthcoming report, an experimental area for a possible short-baseline neutrino oscillation experiment, located at 1850 m from the target, will be described.

Note: The NGS draft schedule presented in this report assumes that funding would be available to start the civil engineering construction in October 1998. This is now known not to be the case. A new draft schedule, with the NGS neutrino beam starting early in 2003, is being prepared.

CONTENTS

List of Figures

List of Tables

1 OUTLINE

This section gives an introduction to neutrino oscillation and recent developments in the field, followed by a description of the proposed CERN Neutrino Beam to Gran Sasso (NGS) facility. The main characteristics of the various parts in the system are given together with the expected neutrino beam performance. Therefore, this section also provides a summary of the NGS report.

1.1 Neutrino oscillation

One of the most intriguing questions in the present scenario of particle physics is whether neutrinos have non-vanishing mass. A massive neutrino would be a direct indication of physics beyond the Standard Model, representing a fundamental milestone in particle physics. Moreover, it would have profound implications for cosmology and astrophysics, giving a clue to the explanation of the dark matter puzzle [1]. Most likely, the neutrino mass is out of reach of direct measurements. The only way to assess this issue is to search for neutrino oscillation [2], which may occur only for massive neutrinos.

In the first approximation, oscillation phenomena occur between two neutrino flavours and are described by two parameters: the mixing parameter $\sin^2 2\theta$ and the mass-squared difference Δm^2. The sensitivity of the experimental searches to these parameters depends on the neutrino energy E and on the distance L of the detector from the neutrino source. For experiments at high-energy accelerators, one usually refers to short- ($L \sim 1\,\mathrm{km}$) or long- ($L \sim 1000\,\mathrm{km}$) baseline experiments.

At the moment, there are three experimental indications for neutrino oscillation:

- The solar neutrino deficit with parameters $\Delta m^2 = (0.5\text{–}1.6) \times 10^{-5}\,\mathrm{eV}^2$ and $\sin^2 2\theta = (0.4\text{–}1.2) \times 10^{-2}$ [3] as explained by matter-enhanced oscillations (MSW model) [4].
- The apparent deficit of atmospheric muon neutrinos, as measured in the Kamiokande [5] and Superkamiokande [6] experiments, with a small Δm^2 ($\sim 10^{-2} - 10^{-3}\,\mathrm{eV}^2$) and a large mixing angle ($\sin^2 2\theta > 0.5$). The recent result of the reactor experiment CHOOZ [7], which explores the same parameter region, excludes $\nu_\mu - \nu_e$ oscillation down to the level of $10^{-3}\,\mathrm{eV}^2$, thus favouring the explanation of the Kamiokande and Superkamiokande results in terms of $\nu_\mu - \nu_\tau$ oscillation.
- The LSND experiment [8] suggests the existence of $\overline{\nu}_\mu - \overline{\nu}_\mathrm{e}$ oscillation with $\Delta m^2 \sim 1\,\mathrm{eV}^2$.

In Fig. 1, the results from the Kamiokande, Superkamiokande and CHOOZ experiments are summarized. The data in the Kamiokande experiment is divided into sub- and multi-GeV regions. Figure 1 shows the combined region of oscillation parameters favoured by the experiments (shaded areas) for the $\nu_\mu - \nu_\mathrm{e}$ and the $\nu_\mu - \nu_\tau$ channels.

Within the conventional two-flavour oscillation scheme, two independent Δm^2 are available as oscillation parameters. The three Δm^2 values indicated by the experiments would thus require a fourth (sterile) neutrino [9]. Several phenomenological analyses of the present data have been published [10]–[15] where the full mixing matrix of a general three-flavour approach is exploited. Such three-flavour analyses can, without a 'sterile' neutrino, accommodate the experimental observations to a larger extent by attributing at least two of the observed phenomena to the same mass difference.

The next generation of solar and atmospheric neutrino experiments is expected to contribute substantially to the experimental scenario on neutrino mixing. The SNO [16] and ICARUS [17] experiments will measure the ratio of charged to neutral current events, studying oscillations independent of the Solar Model. Superkamiokande will be able to observe effects that can discriminate between different neutrino oscillation schemes, such as time variation of the solar signal. The BOREXINO experiment [18] can address the energy dependence of the solar neutrino deficit.

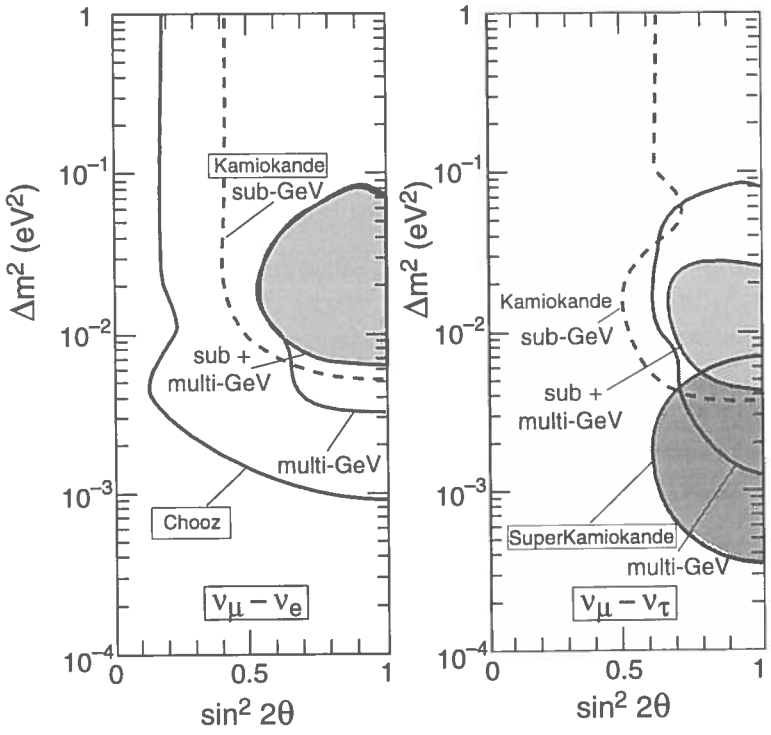

Fig. 1: Results from the Kamiokande, Superkamiokande and CHOOZ experiments

Specific appearance searches are being pursued by accelerator experiments. The evidence for $\overline{\nu}_\mu - \overline{\nu}_e$ oscillation reported by LSND may soon be verified by the upgraded KARMEN experiment [19]. A proposed project at CERN [20] aims at a $\nu_\mu - \nu_e$ appearance search with a low-energy neutrino beam from the PS, to study the LSND signal.

In the $\nu_\mu - \nu_\tau$ channel, the two experiments running at CERN, CHORUS [21] and NOMAD [22] have recently reported [23, 24] no evidence for oscillations at the level of the previous best limit [25]. These are short-baseline (SBL) experiments, sensitive to small mixing angles ($\sin^2 2\theta_{\mu\tau} \sim 2 \times 10^{-4}$) and relatively large Δm^2. A positive signal would call for a new dedicated experiment with higher sensitivity, to confirm the discovery and to learn more. In case no oscillation is found, theoretical speculations [26]–[28] suggest a further extension of the investigation to smaller mixing angles. Interest in a new experiment has recently been expressed at CERN by a Letter of Intent (I213/TOSCA [29]). It is able to increase the sensitivity by more than one order of magnitude with respect to the searches presently under way. Within the three-flavour analysis, a new SBL experiment can have sufficient sensitivity to mixing in order to probe a proposed solution for all oscillation evidence and in this framework, the LSND signal [30]. The limits expected from the sensitivity of CHORUS and NOMAD are shown in Fig. 2, together with the expected extent of a future SBL experiment.

The present experimental evidence from Kamiokande, Superkamiokande and CHOOZ points strongly towards $\nu_\mu - \nu_\tau$ oscillation in the small Δm^2 ($\sim 10^{-2} - 10^{-3}\,\mathrm{eV}^2$) region (see Fig. 1). To explore this region by an independent method, long-baseline (LBL) neutrino-beam experiments are needed. The sensitivity to small Δm^2 improves with increasing L/E; the physics requirements for such LBL experiments are described in detail in Section 2.1.

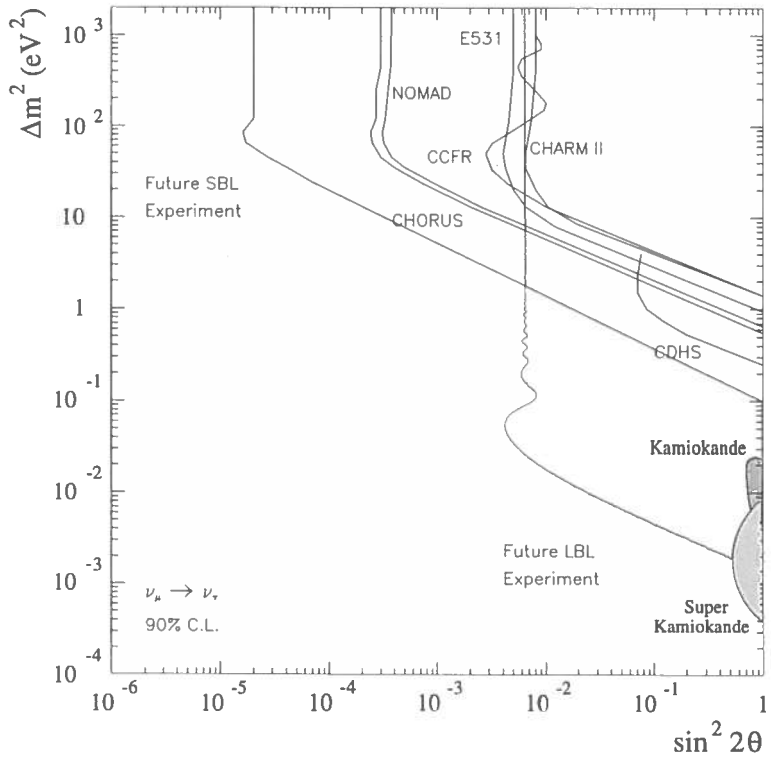

Fig. 2: Oscillation parameter range to be covered by future SBL and LBL $\nu_\mu - \nu_\tau$ experiments

Currently, a new neutrino facility (K2K) is under construction at KEK (see Section 3.10.2), providing a $\sim$1 GeV ν_μ beam with the Superkamiokande detector (250 km away). This low-energy beam, operational in 1999, will not allow ν_τ appearance measurements.

Another project (NuMI, see Section 3.10.1) is proposed at Fermilab. It exploits the future Main Injector to produce a neutrino beam of about 10 GeV pointing towards the SOUDAN mine (730 km away) where a new detector (MINOS [31]) will be installed.

In Europe, CERN has a long experience of neutrino beam physics. In the last twenty years the SPS accelerator was successfully used to produce high-energy neutrino beams (see Section 1.2). The SPS is expected to be operational well into the next century. It is, therefore, a natural candidate to provide protons for a new neutrino beam to the INFN Gran Sasso Laboratory in Italy (732 km away from CERN), the NGS, which is the subject of this report. A 'near' location for an SBL experiment is also foreseen in the beam design.

A high-energy [$\mathcal{O}$(20 GeV)] neutrino beam from the SPS to Gran Sasso was originally proposed for neutrino oscillation studies with the ICARUS detector [17]. Several other projects for LBL experiments at Gran Sasso have since been proposed (NOE [32], AQUARICH [33], OPERA [34] and NICE [35]) covering a broad range of detector techniques. The above experiments aim at a sensitivity which covers the oscillation parameter region indicated by the atmospheric neutrino anomaly (Fig. 2). Both $\nu_\mu - \nu_\tau$ appearance and ν_μ disappearance searches are possible with the NGS.

1.2 The present CERN-SPS neutrino programme (WANF)

The West Area Neutrino Facility (WANF) on the CERN 450 GeV Super Proton Synchrotron (SPS) has been operating continuously, with only minor interruptions for changes in the beam

configuration, since 1976. For many years now, it has provided a very intense beam of high-energy muon neutrinos to the particle physics community and has a proven track record for high operational reliability.

A schematic layout of the present WANF is shown in Fig. 3. Protons extracted from the straight section 6 of the SPS at 450 GeV are directed towards the West Experimental Area and focused onto a beryllium target (T9). A fast resonant (FS) extraction is used which produces two beam spills of ≈ 6 ms duration, separated by 2.7 s, for each 14.4 s cycle of the accelerator.

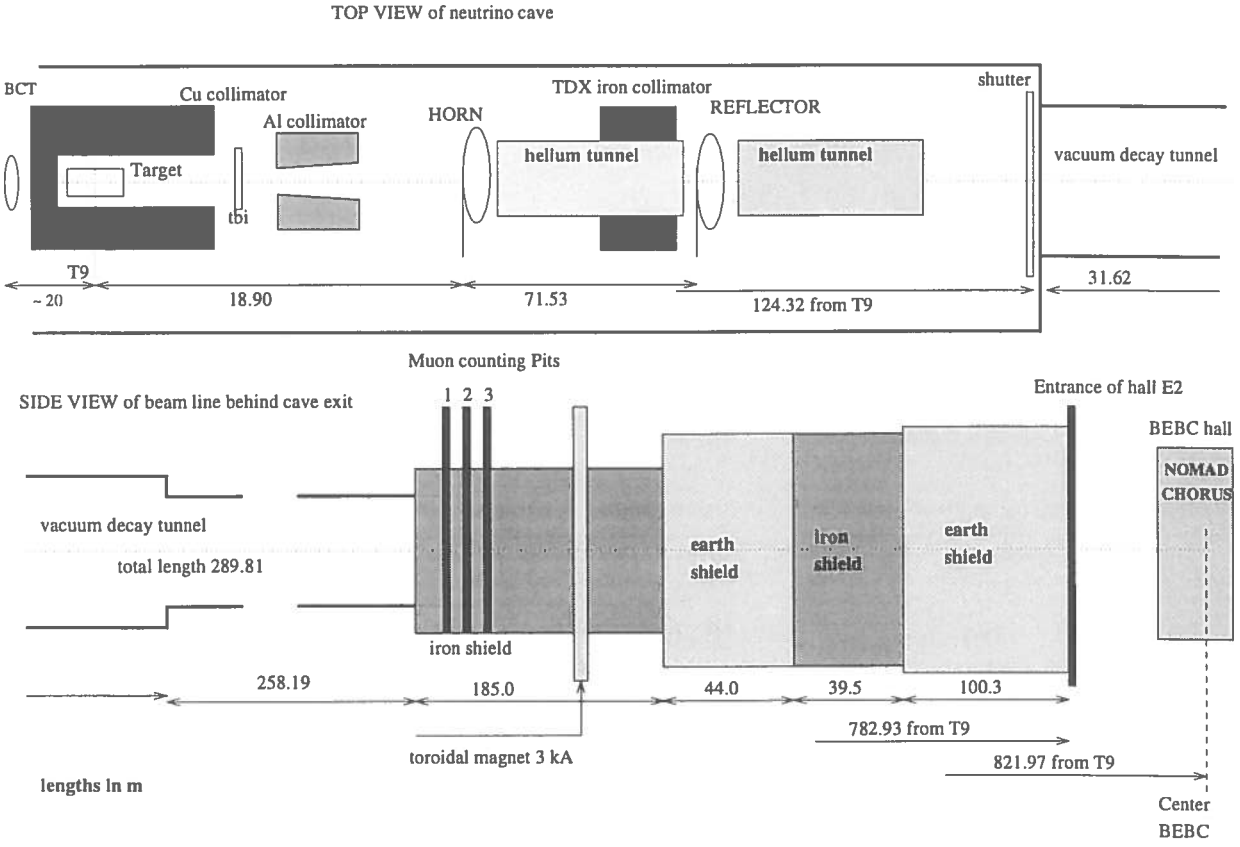

Fig. 3: Schematic layout of the CERN WANF beam line indicating its main elements (dimensions in metres)

Pions and kaons produced in the target, in the required energy band, are focused towards the detectors in an approximately parallel beam: two co-axial magnetic lenses, more familiarly known as horn and reflector, are used. These pions and kaons decay in flight to produce muons and muon neutrinos. The muons and remaining hadrons are stopped in a long iron and earth shield at the end of the decay path leaving only the neutrinos to continue to the detectors some 800 m from T9. In the WANF, the distance from the target to the beginning of the iron shield is $\sim$ 420 m. To minimize the number of 'parent' particles that interact in the air before their decay, the spaces between the focusing devices in the 120 m long cavern have large-diameter tubes filled with helium at atmospheric pressure. The final 300 m long decay tunnel is evacuated to 0.5 Torr.

Measuring the muon flux distributions at a number of monitoring gaps in the iron shielding has provided an invaluable diagnostic tool for understanding the neutrino flux and aligning the beam.

The last major upgrade of the WANF took place in 1992/93 in preparation for the CHORUS and NOMAD experiments which are now approaching the end of their data taking. These experiments aim at detecting evidence of non-zero neutrino mass, searching for neutrino oscillation, from ν_μ into ν_τ.

The SPS beam presently operating for CHORUS and NOMAD is a quasi-pure ν_μ wide-band beam with an average energy of 27 GeV, having a few per cent contamination of muon antineutrinos $\bar{\nu}_\mu$ and about 1% contamination of electron neutrinos ν_e. The contribution from ν_τ inherent in the beam, produced mainly by prompt τ decay of D_s^+ mesons, is expected in the charged current (CC) events in CHORUS at a level of 3×10^{-6} [36, 37].

Such a beam provides an excellent tool to search for oscillation of ν_μ. Both experiments are primarily performing a search for the appearance of ν_τ, aiming at the detection of τ^- leptons from CC ν_τ interactions. In addition, it is also possible to search for the appearance of ν_e via the detection of electrons from CC ν_e interactions, if the signal is significantly above the 1% background. Searches for disappearance of ν_μ are possible but less sensitive.

Significant improvements in the operation of the SPS as a neutrino source have been achieved and further progress is expected. The WANF has operated at unprecedented intensities, thanks to a better insight into the behaviour of the target and record performance of the SPS since 1995.

1.3 The Gran Sasso Laboratory (Laboratori Nazionali del Gran Sasso)

The Gran Sasso Laboratory (LNGS) [38] is located alongside the Gran Sasso tunnel, which is 10.4 km long, on the motorway connecting Teramo and Rome, about 6 km from the west entrance. This underground laboratory, founded by INFN in 1987 as a facility for cosmic ray and rare decay studies, is located at 963 m above sea level. The distance from CERN to Gran Sasso is 732 km, and its direction from CERN is:

- azimuth: 122.5° (w.r.t. geographic north)
- slope: −5.6% (w.r.t. the horizontal plane).

The LNGS is an INFN national laboratory with an International Scientific Committee, responsible for recommending the approval of the experiments. The experiments are conducted by international collaborations.

The LNGS underground laboratory consists of three experimental halls, conventionally named halls A, B and C, and of a series of connecting tunnels and service areas. The three experimental caverns are each more than 100 m long and about 18 m high and wide (see Fig. 4).

The Campo Imperatore region in the Gran Sasso massif is at an altitude of about 2000 m above sea level. In addition to the underground laboratories, this area houses a group of air shower detectors together with two geophysical experiments.

The position of the Campo Imperatore detectors and the presence of a nearby supporting laboratory provide a unique opportunity for combined studies between 'atmospheric' and underground detectors.

The support structure for the underground halls and the Campo Imperatore zone comprises a group of external buildings which house the LNGS headquarters with all the administrative offices, the computing centre, all the technical and engineering services, the electronic and chemical laboratories, the machine shop, stockroom, and a conference room.

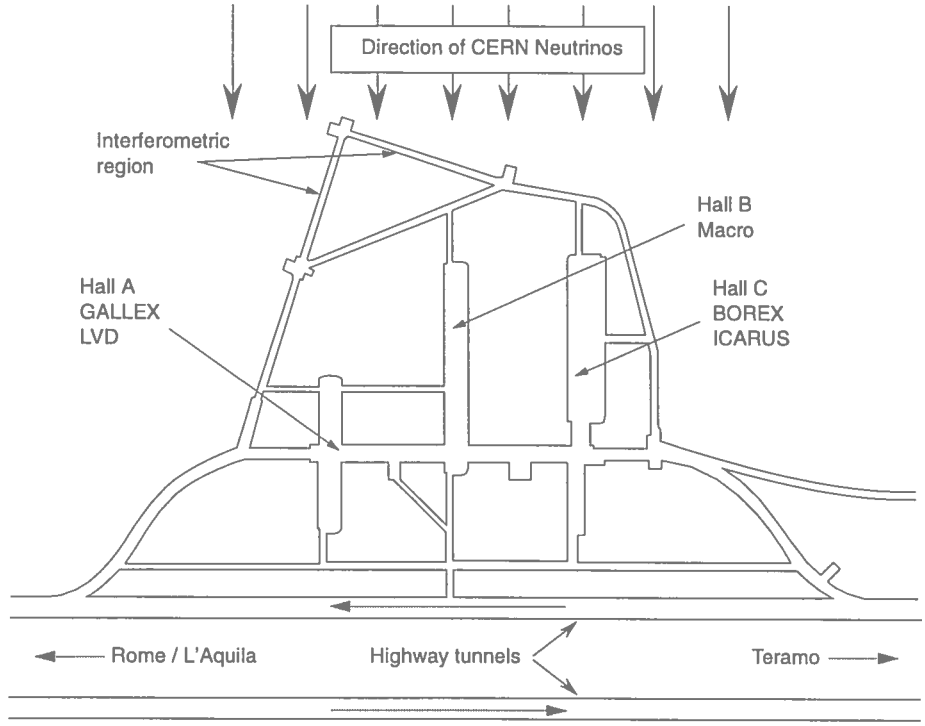

Fig. 4: Overview of the Gran Sasso underground laboratory, showing experiments which are presently running or approved for construction

The main justification for installing experiments in an underground laboratory like the LNGS is the shielding against cosmic rays. At Gran Sasso, the minimum thickness of the rock overburden, i.e. the shielding, is 1400 m, corresponding to 3800 m water equivalent. Only neutrinos and high-energy muons, among the known particles, can penetrate such a layer of rock. Owing to their low interaction probability, incoming neutrinos can filter through the rock independently of their energy, but among the muons that arrive on the Earth's surface (about $100\,\mathrm{m^{-2}\,s^{-1}}$) only those that have a sufficiently high energy, above 2 TeV, can reach the underground laboratory. Inside the Gran Sasso Laboratory, the remaining muon fluence rate is of about $1\,\mathrm{m^{-2}\,h^{-1}}$.

In addition to providing an efficient shield against cosmic rays, the Gran Sasso rock is characterized by a low rate of natural radioactivity. This results in a very low level of total radiation background. Therefore, the underground laboratory is an ideal place for delicate experiments which investigate rare events such as double beta decay and proton decay, as well as searches for magnetic monopoles and other exotic particles.

In the future, the intense neutrino flux of the NGS beam from CERN will provide another opportunity for a high quality experimental programme at Gran Sasso. Highly sensitive experiments will allow the detection of the source of the atmospheric neutrino anomaly, either by appearance or disappearance measurements.

1.4 Overview of the new facility

1.4.1 Layout of the NGS

Accelerator driven neutrino beams are generated from the decay of mesons, mostly π and K,

$$\pi^{+(-)} \rightarrow \mu^{+(-)} + \nu_\mu(\overline{\nu}_\mu)$$

$$K^{+(-)} \rightarrow \mu^{+(-)} + \nu_\mu(\overline{\nu}_\mu) \, .$$

These mesons are produced from a high-energy, high-intensity proton beam hitting a suitable target. The main ingredients of the proposed NGS are shown schematically in Fig. 5 and listed below. The layout is shown in Figs. 6 and 7.

- A proton beam with an energy up to 450 GeV (400 GeV nominal) extracted from the CERN SPS accelerator, transported and focused onto a small spot at the target.
- A target station consisting of a segmented graphite target, in which the secondary particles, π and K, etc., are produced.
- A two-stage focusing system, horn and reflector, which focuses a range of chosen π and K momenta into a parallel beam, pointing towards the Gran Sasso Laboratory.
- A 1000 m long decay tunnel, which allows a fraction of the π, K to decay in flight, producing a high-intensity ν_μ beam.
- A hadron stop, which absorbs the non-interacting primary protons as well as those secondary hadrons which have not decayed.
- A muon monitoring system, permitting on-line monitoring, tuning, and control of the beam and its alignment.
- The natural shielding provided by a long stretch of molasse (about 730 m) to absorb the muons from hadron decay upstream of the SBL detector.
- An underground experimental area allowing the installation of a short-baseline experiment.

The different components of the neutrino beam are briefly described in the following sections. A more detailed explanation is given in Sections 3 and 4 The underground experimental area for the SBL experiment is described in a forthcoming report.

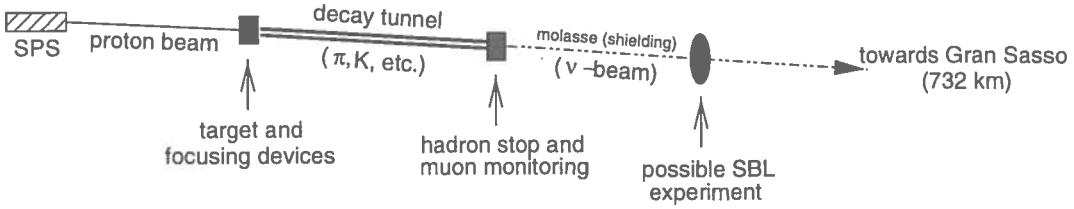

Fig. 5: Schematic layout of the new CERN neutrino facility

1.4.2 Implementation at and around CERN

The geographical layout of the NGS facility is shown in Figs. 6 and 7. The guiding principles for the implementation are the following:

- There should be no additional, permanent surface buildings, other than for the proposed SBL experimental area. This leads to the need for an 800 m long access tunnel from point 4 of the SPS to the NGS target cavern.
- The LHC project should not be hampered by the NGS implementation — a separate neutrino civil engineering shaft (PGCN) near point 4 of the SPS is thus required. This will be a temporary shaft to be closed once the construction is completed.
- The target cavern should be large enough to allow the possible installation, after a first generation of experiments, of a new target and/or a different focusing system, e.g. for a low-energy or a narrow-band neutrino beam.

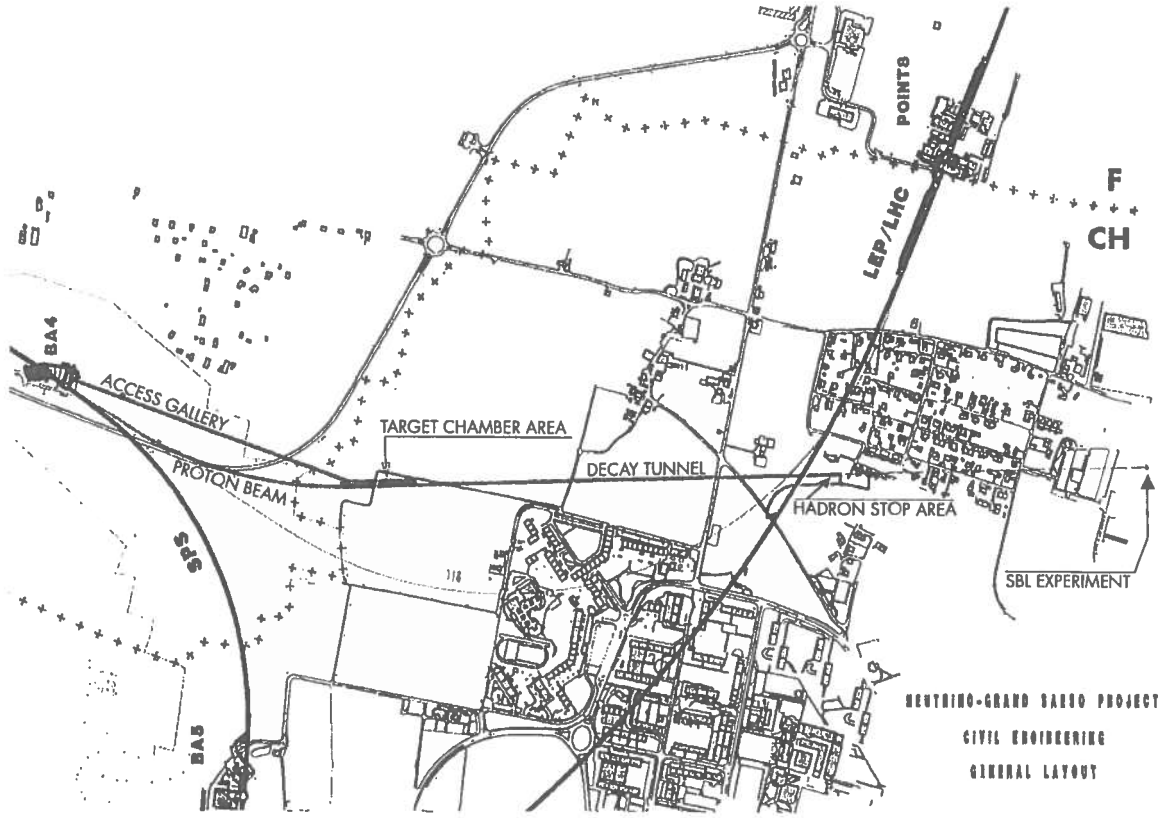

Fig. 6: Layout of the NGS at and around CERN

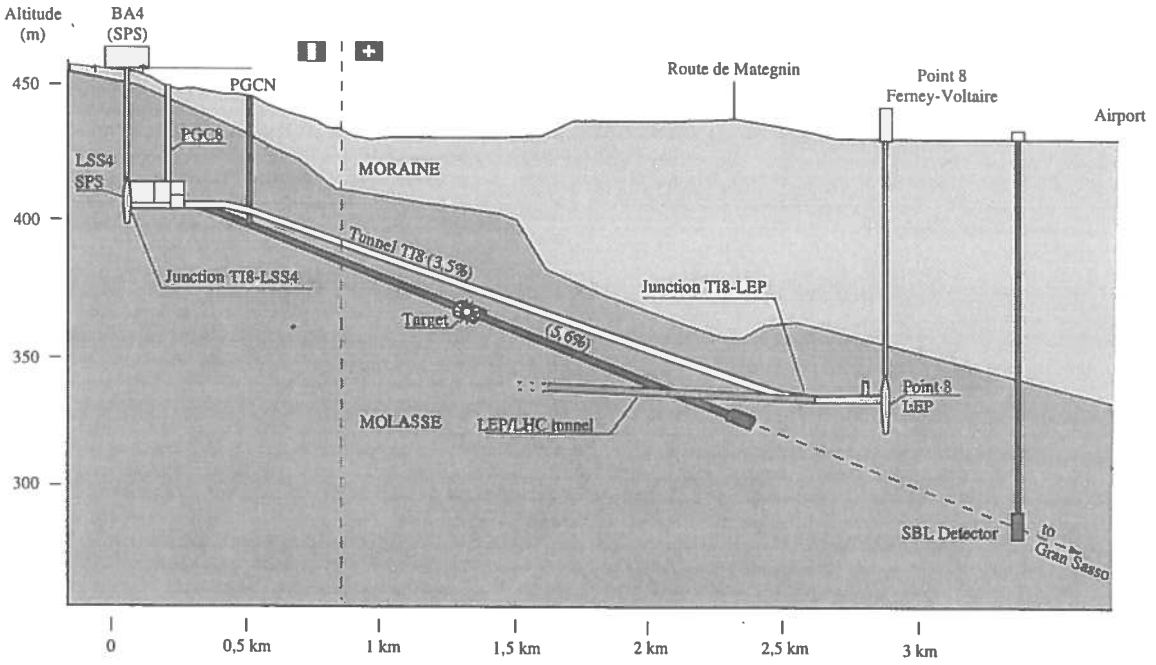

Fig. 7: Vertical cut showing the SPS and the main components of the NGS

- In order to protect equipment and to provide acceptable working conditions, a service gallery parallel to the target cavern, an enlargement of the cavern around the target, and a well-shielded radioactive storage area are foreseen.
- Access to two muon monitoring stations downstream of the hadron stop should be from the LEP/LHC tunnel.
- The minimal distance between the LEP tunnel and any other civil engineering should be about 10 m, to avoid disturbances to LEP operation.
- The short-baseline experimental area should be completely decoupled from the NGS beam construction. It should have its own access shaft and infrastructure in a suitable location.

1.4.3 Proton extraction from the SPS

The SPS accelerator is gradually being upgraded and modified for its new role as the LHC injector after the end of LEP operation, while continuing to deliver protons and ions for fixed-target physics. Details of the upgrade are described in Ref. [39]. For the purpose of the NGS, it is important that one of the extractions from the SPS towards the LHC, from LSS4, points roughly south. It was therefore earlier envisaged [40] to provide protons for a neutrino beam towards Gran Sasso. The extraction system foreseen for the LHC allows fast-extracted pulses (up to 20 μs) to be sent to the TI8 transfer line towards the LHC. With some modifications to allow two fast extractions per cycle, this system can also be used to extract protons on to the NGS target. The nominal cycle provides 3×10^{19} protons/year on target, assuming 200 days/year and an efficiency of 50%.

Note that the layout of the LSS4 extraction is designed such that it would in principle, though at substantial extra cost and only during a long shutdown of the SPS, allow the installation of a 'fast–slow' (resonant) extraction system, similar to the one currently used for the WANF.

1.4.4 Transport of the primary protons

The total length of the proton beam from the SPS to the NGS target is 830 m, and its maximum design momentum is 450 GeV/c, which is the maximum the SPS can provide. The beam branches off the TI8 beam after 110 m. The necessary deflection (horizontal and vertical) to reach the direction towards Gran Sasso is achieved by 73 conventional bending magnets.

Nothing in the current design of the extraction and proton beam line would prevent the future construction, if desired, of another neutrino beam (starting from the same SPS extraction) towards the deep-sea site of the NESTOR laboratory [41] presently under construction in the Ionian Sea off the south-west coast of the Peloponnese, Greece.

1.4.5 Production target

The target foreseen for the NGS is based on the successful design of the T9 target in the present WANF [42]. In a cast aluminium target container 11 rods of graphite, 10 cm long and 3 mm diameter each, form a 2 m long target array. The rods are cooled by a forced helium flow. The change from a beryllium target in the WANF to a graphite target has been mainly motivated by the change from fast–slow (6 ms) to fast (10 μs) proton beam extraction and by the better thermomechanical properties expected of graphite.

1.4.6 Secondary particle focusing system

The WANF experience is the origin of the choice for the focusing elements, namely horn and reflector which are two coaxial lenses, similar in shape but different in size. Their characteristics

are not very different from those used in the WANF [43]. The distances of horn and reflector from the target and the shape of the magnetic field provided by them are chosen to optimize a wide-band high-energy ν_μ beam.

1.4.7 Decay tunnel

In order to obtain a neutrino beam pointing towards Gran Sasso, the parent hadrons have to decay in flight while travelling in that direction. To avoid their interacting before they can decay, an evacuated decay path is necessary. Typical π decay lengths, 2.2 km at 40 GeV, imply that a long decay pipe is desirable; given the angular distribution of the parent hadrons which can produce neutrinos, a longer decay tunnel should also have a bigger diameter. For the NGS, a pipe of 2.45 m diameter and 1000 m length has been chosen.

1.4.8 Hadron absorber and muon shield

At the exit of the decay tunnel, a massive iron beam dump is needed to absorb the non-interacting primary protons as well as all secondary particles. Additional iron, beyond the 10 m typically needed for the beam dump, has to be added in order to protect the SBL cavern against high-energy muons.

It is foreseen to build a $18 \times 4 \times 4\,\mathrm{m}^3$ dump, assembled from iron blocks which can be recovered from the WANF. A 3 m long graphite insert at the upstream end provides a better distribution of the deposited heat. Under the most extreme assumptions (dedicated operation of the SPS at 450 GeV with 4.5×10^{13} protons on target every 6 s), a heat dissipation of about 50 kW has been estimated. A modest cooling system is thus sufficient to assure stable and relatively low temperatures in the hadron stop cavern.

1.4.9 Muon monitoring station

Most of the hadron decays produce a neutrino and a muon. Measuring the muon intensity and profile provides information on the intensity and profile of the neutrino beam. Measuring the muon signals induced in a set of thin silicon detectors allows an 'on-line' monitoring and tuning of the beam (steering of the proton beam on target, horn and reflector alignment, etc.).

The muon monitoring system consists of two arrays of silicon detectors measuring the intensity and profile of the muon flux penetrating (a) the hadron stop and (b) the hadron stop plus a 67 m thick region of molasse. The separation of the two planes, equivalent to 25 m of iron, allows a rough measurement of the muon energy spectrum. Moreover, some angular information on the beam is also available by using the information from the two measurement planes.

1.4.10 The short-baseline experimental area

Continued interest is being expressed for a next-generation, short-baseline, neutrino oscillation experiment at CERN [29], combining the assets of CHORUS and NOMAD. Naturally, such an experiment has to be located in the new beam towards Gran Sasso and thus forms a part of the NGS. Details of the experimental area as foreseen for this type of experiment will be discussed in a forthcoming report.

Present plans foresee the location of this SBL experimental area at a distance of about 1850 m from the NGS target, i.e. about 140 m underground just north of the Geneva airport (see Fig. 6). An underground cavern is accessed by a large shaft, containing personnel and material accesses. A modest surface building, access for trucks, and parking space is needed. The technical services (water, power, etc.) for this new experimental area are most likely to be connected to point 8 of the LEP/LHC.

1.5 Overview of the NGS beam performance

The expected performance of different neutrino beam configurations has been studied. The so-called 'reference beam', investigated in detail and discussed in Section 3, is considered a preliminary working hypothesis. Its conceptual design is guided by the requirements for long- and short-baseline ν_τ appearance experiments.

Simulations of the complete neutrino production process from 400 GeV SPS protons on a graphite target indicate that the expected fluences of ν_μ are about $4.4 \times 10^{-9}\,\mathrm{m}^{-2}$ per proton on target (pot) at the location of the LBL detector and $1.1 \times 10^{-3}\,\mathrm{m}^{-2}$ per pot at the SBL detector. The average energies of these ν_μ's are respectively 26.7 and 24.1 GeV. At both LBL and SBL locations a contamination of around 2% $\overline{\nu}_\mu$ and slightly less than 1% ν_e is expected. The ν_τ contamination is estimated to be of the order of 10^{-6} at the SBL detector location.

The rates of ν_μ CC interactions (events per proton per ton of detector material) are expected to be about 1.1×10^{-14} in an SBL detector and 4.7×10^{-20} in an LBL detector. While these numbers refer to the present working hypothesis, other options are under active study. The final beam will be designed according to the approved physics programme to be carried out with the NGS facility.

2 PHYSICS REQUIREMENTS AND NEUTRINO BEAM DESIGN CRITERIA

2.1 Beam criteria to meet physics requirements

The neutrino oscillation probability P in the standard two-flavour mixing scheme may be expressed in terms of the two oscillation parameters $\sin^2 2\theta$ (the so-called mixing parameter) and Δm^2 (namely the difference of the neutrino mass-squared):

$$P = \sin^2 2\theta \times \sin^2 (1.27 \times (L/E) \times \Delta m^2)\,,$$

where L is the mean distance of the detector from the neutrino source measured in kilometres, E is the average neutrino energy (in GeV) and Δm^2 is measured in eV^2.

From the above relation one finds that the oscillatory pattern of the probability has an amplitude $\sin^2 2\theta$ and an oscillation length $\lambda(\mathrm{km}) = 2.48 \times (E/\Delta m^2)$. Figure 8 shows the oscillation probability, as a function of L/E, for the case of $\Delta m^2 = 0.001\,\mathrm{eV}^2$.

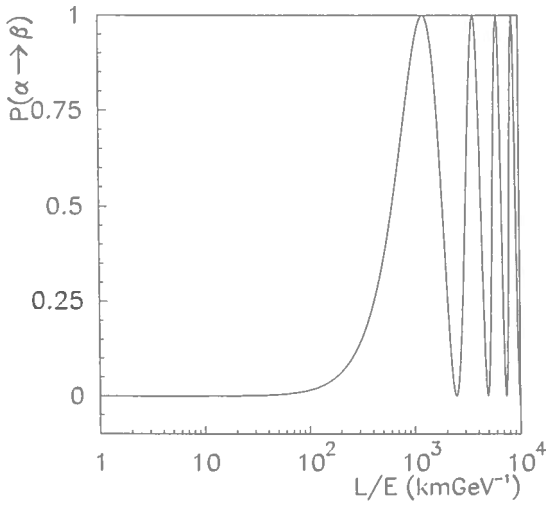

Fig. 8: Oscillation probability for the case of an LBL experiment

It follows that for large Δm^2 the oscillation probability no longer depends on L:

$$P = 1/2 \sin^2 2\theta \, .$$

On the other hand, the minimum Δm^2 to which the experiment is sensitive (for full mixing, i.e. $\sin^2 2\theta = 1$) is:

$$\Delta m^2(\mathrm{eV}^2) = \sqrt{P} \times E(\mathrm{GeV})/(1.27 \times L(\mathrm{km})) \, .$$

Therefore, the sensitivity in Δm^2 depends on the ratio E/L. For a typical accelerator neutrino energy $\mathcal{O}$ (10 GeV) we define short-baseline (SBL) experiments as those with $L \sim 1$ km, so mostly sensitive to $\Delta m^2 \sim 1$–$10\,\mathrm{eV}^2$, and long-baseline (LBL) experiments where $L \sim 1000$ km, required in order to access $\Delta m^2 \sim 10^{-2} - 10^{-3}\,\mathrm{eV}^2$.

Neutrino oscillation experiments can also be subdivided into disappearance and appearance searches. In the first case the main requirement is to have a beam with very well-known intensity. The flux of the main beam component (ν_μ in the case of the NGS) is measured at a given distance L from the source. The occurrence of neutrino oscillation can be detected as a reduction of the measured flux compared to the value expected in the absence of oscillation.

The sensitivity of disappearance experiments is limited by systematic uncertainties on the knowledge of the neutrino beam intensity. For this reason, the measurement of the flux can take advantage of another detector placed at a different position, i.e. L' smaller than L. One then names the latter a 'near detector'.

On the contrary, appearance experiments exploit beams consisting of predominantly one neutrino flavour and search for the 'appearance' of another flavour, which in principle is absent in the beam. The sensitivity of these experiments is obviously limited by the uncertainty in the contamination of the other neutrino flavours in the beam. In the case of the NGS the most interesting appearance search is for $\nu_\mu - \nu_\tau$ oscillation. The ν_τ contamination of the beam is at a very low level, which allows high-sensitivity explorations.

It is important to observe that since the appearance of a different neutrino flavour is detected through the interaction of this neutrino with the experimental target, the neutrino must be energetic enough to produce its corresponding charged lepton. This sets, for a given oscillation search, a lower limit to the energy of the neutrino. In particular, since the threshold to produce a τ lepton is ~ 3.5 GeV, a high-energy beam is preferred for a $\nu_\mu - \nu_\tau$ experiment.

Less stringent constraints apply to the neutrino energy for disappearance experiments. In that case, only the initially produced neutrino must have sufficient energy to produce its charged-lepton partner.

2.1.1 Long-baseline disappearance experiments

The class of experiments designed to test neutrino oscillation through the disappearence of the original flavour can also measure the values of the oscillating parameters, $\sin^2 2\theta$ and Δm^2.

In practice this is performed by extracting the characteristic oscillating pattern from the reconstructed neutrino spectrum; the period is directly related to the neutrino mass difference while the amplitude is related to the mixing angle. The oscillation pattern is reconstructed either by comparing the neutrino spectrum at the LBL detector with that obtained with a similar detector at a 'near' position, or by comparing the spectra obtained by means of charged-current events, sensitive to oscillation, and neutral-current events, insensitive to oscillation.

Without explaining details of the possible experiments, it is worth mentioning that disappearance experiments are based essentially on statistical methods. Hence very large detectors of several kilotons are required to minimize the statistical fluctuations; they have to be able

to measure accurately both the hadronic energy and the energy and direction of the outgoing lepton. This demands high granularity calorimeters equipped with a muon spectrometer.

This kind of measurement is best suited for large mixing angles and for Δm^2 values that fulfil the condition $1.27 \times (L/E) \times \Delta m^2 \simeq \pi/2$, where the disappearence effect is maximized. The beam requirements of this class of experiment follow directly from the above features. In order to maximize the disappearance effect for $\Delta m^2 \sim 10^{-2} - 10^{-3}\,\mathrm{eV}^2$ at 732 km, the optimum neutrino energy would be in the region of a few GeV. In addition, the best value has to be determined by taking into account the neutrino interaction rate which increases with energy, in order to maximize statistics. Moreover a wide-band beam is preferable because the higher energy events, where the oscillation is suppressed, are useful for normalization.

The ν_e contamination is not an important background as it is at the level of a few per cent, the systematic errors inherent to the disappearance method are estimated to be around 2–3%.

As already mentioned above, an accurate knowledge of the neutrino beam spectrum produced at the source is mandatory to perform a disappearance search. For this reason most of the proposed experiments based on this method require the presence of a 'near' detector to measure the neutrino beam with high statistics at the source. This is best performed if the near detector is using the same techniques as the far (LBL) detector, in order to avoid unpredictable systematic errors.

2.1.2 Long-baseline appearance experiments

As pointed out in the introduction, the combined result of Superkamiokande on atmospheric neutrinos and the null result of CHOOZ obtained with reactor neutrinos can be interpreted in terms of flavour oscillation, defining an allowed region in the oscillation parameters space only for the channel $\nu_\mu - \nu_\tau$. As a consequence, appearance searches in long-baseline experiments must be focused on the identification of the ν_τ signal, through the detection of the τ lepton.

There are, at present, two classes of proposed experiments aimed at ν_τ detection. One is based on the direct identification of the τ lepton, produced in CC interactions of ν_τ, by means of its decay pattern. The characteristic decay length, followed by a 'kink' due to the τ decay into one or more charged daughters plus neutrino(s) is a unique signature. In practice, since the τ decay length is only a few hundred microns this technique has to be based on emulsion as the active detector; this gives a granularity of the order of a micron. The τ detection efficiency may be relatively high, of the order of some tens of per cent. The CHORUS experiment makes use of this technique as does the envisaged OPERA detector at Gran Sasso.

Another class of experiment exploits the detector capability to measure the complete kinematics of the neutrino interaction. The extraction of the ν_τ signal is performed by defining sets of observables for which the ν_τ interaction is (at least partially) distinguishable from the ν_μ interaction. The τ detection efficiency depends on the cuts applied to separate the two samples and it is typically of the order of a few per cent. This is the technique adopted by the NOMAD experiment at CERN and by the already approved ICARUS experiment at Gran Sasso.

Both techniques require very specialized detectors to be built. As a consequence, the active mass cannot be very large, of the order of a kiloton or less for the experiments proposed for the Gran Sasso long-baseline experiments. Moreover, in both cases, the sensitivity is further reduced by the ν_τ CC cross-section, which gets smaller near the threshold (about 3.5 GeV) and slowly increases with energy, to reach asymptotically the value of the ν_μ CC cross-section at extremely high energy (above 100 GeV). This implies that, contrary to disappearance searches, in order to maximize the ν_τ detection probability (both in terms of interaction rate and detection efficiency) a higher energy neutrino beam is preferable.

To better quantify the above requirements, the number of ν_τ interactions in a given detector is determined by the following formula:

$$N_\tau = N_{\rm A} \times M_{\rm d} \times \int (\phi_{\nu_\mu}(E) \times P_{\nu_\mu - \nu_\tau}(E) \times \sigma_{\nu_\tau}(E) \times \epsilon(E) \times {\rm d}E) \, ,$$

where ϕ_{ν_μ} is the ν_μ flux at the detector site, $P_{\nu_\mu - \nu_\tau}$ is the oscillation probability between ν_μ and ν_τ, σ_{ν_τ} is the ν_τ CC interaction cross-section, ϵ is the τ detection efficiency, $N_{\rm A}$ is the Avogadro constant and $M_{\rm d}$ is the detector mass.

In case the condition $\Delta m^2 \times L/E \ll 1$ holds, the oscillation probability can be approximated as follows:

$$P = \sin^2 2\theta \times (1.27 \times (L/E) \times \Delta m^2)^2 \, .$$

Moreover, the ν_τ cross-section can be parametrized as:

$$\sigma_{\nu_\tau} = \sigma_0 \times E \times f_\tau(E)$$

where $\sigma_0 = 0.67 \times 10^{-38}$ cm^2. Then the number of ν_τ interactions may be expressed as:

$$N_\tau = N_{\rm A} \times M_{\rm d} \times \sin^2 2\theta \times (1.27 \times \Delta m^2 \times L)^2 \times \sigma_0 \times \int (\phi_{\nu_\mu}(E) \times f_\tau(E) \times \epsilon(E) \times {\rm d}E/E) \, .$$

In other words, the quantity to be maximized in order to take advantage of the long-baseline configuration is the average of $f_\tau(E) \times \epsilon(E)/E$ over the beam spectrum. To a first approximation a wide-band beam peaked around 20–25 GeV, similar to the present WANF, is the correct choice.

The $\nu_{\rm e}$ contamination in the beam has to be kept low because it can simulate the ν_τ signal mainly when using kinematic techniques. This requirement, as shown in the following paragraph, is even more relevant for SBL experiments. However, in this case a contamination of less than 1%, typical in most of the beam designs, is acceptable. Similar considerations hold for the $\overline{\nu}_\mu$ contamination: the typical level of a few per cent (see the following section) is low enough. To conclude, appearance experiments do not need, in principle, any near detector.

2.1.3 Short-baseline appearance experiments

The present SBL experiments on the WANF beam, CHORUS and NOMAD, have recently reported no evidence for $\nu_\mu - \nu_\tau$ oscillation at the level of $\sin^2 2\theta_{\mu\tau} \approx 3 \times 10^{-3}$ using a fraction of their available data [23, 24]. Finally they will reach a sensitivity of $\sin^2 2\theta_{\mu\tau} \approx 2 \times 10^{-4}$ for $\Delta m^2 \geq 100\,{\rm eV}^2$, corresponding to a ν_τ with a mass of about 10 eV. Their sensitivity to a lighter ν_τ, in the range of 1–5 eV is $\sin^2 2\theta_{\mu\tau} \approx 5 \times 10^{-2}$. This sensitivity can be greatly improved by a next-generation SBL experiment.

If oscillations occur at the present best limit, CHORUS and NOMAD would each record more than 50 events. Even if only a few τ^- candidates would be unambiguously detected, this would have profound implications on the understanding of the neutrino oscillation scenario. This would call for a new high-sensitivity exploration. Moreover, some phenomenological interpretations of the present data (see Section 2.1) suggest that $\nu_\mu(\nu_{\rm e}) - \nu_\tau$ oscillation may be found at a $\Delta m^2 \approx 1\,{\rm eV}^2$ and with small effective mixing angle.

The TOSCA Collaboration [29] has proposed to run a new SBL with improved sensitivity in the existing WANF beam, which would increase by more than one order of magnitude the sensitivity of CHORUS and NOMAD. For $\Delta m^2 \sim 1\,{\rm eV}^2$, it would detect about 20 τ^- candidates. TOSCA is expecting to run in the NGS facility at the SBL underground experimental area, near the Geneva airport. The infrastructure required for such an experiment is described in a forthcoming report.

The existence of neutrino oscillation is inferred from the occurrence of CC interactions of ν_τ in the emulsion target:

$$\nu_\tau \mathrm{N} \rightarrow \tau^- \mathrm{X} \, .$$

The τ^- is detected through its decay modes into muons, hadrons, and electrons. Its identification is carried out: by exploiting the characteristic decay topology; by the charge measurement of the decay products; by its distinct decay kinematics; and by the missing energy carried away by the neutrino(s) in the decay.

The main detector features reflect the need of a high-sensitivity SBL experiment, able to explore a parameter region in some respects complementary to that of an LBL experiment, namely with small mixing angle and relatively large Δm^2. The product of target mass, neutrino flux and τ detection efficiency has to be at least ten times larger than in the present searches. An increase of a factor of more than three in target mass and an increase of a similar factor in τ detection efficiency with respect to CHORUS is then required.

The first important criterion to be fulfilled by the NGS design is the high flux and the high neutrino energy: the sensitivity in the mixing angle improves linearly with the number of interacting neutrinos, which calls for high flux and, because of the linear dependence of the cross-section with the energy, for high-energy neutrinos. This can be obtained with a wide-band beam configuration.

However, the ν_τ contamination in the beam is the ultimate irreducible background for an appearance $\nu_\mu - \nu_\tau$ oscillation search with high sensitivity. The largest contribution to this background comes from the prompt tauonic decay of the $\mathrm{D_s}$ produced from proton interactions in the neutrino target, inside the shielding and in the beam dump. Estimates of such a background [36, 37] for a proton energy of 450 GeV and the CHORUS detector fiducial volume, agree on the ratio R of the number of ν_τ CC events to ν_μ CC events to be 3.0×10^{-6}.

This level of the prompt ν_τ background, comfortably below one event for the total duration of the CHORUS and NOMAD experiments, becomes more relevant for an experiment like TOSCA, aiming at improving the sensitivity by at least one order of magnitude. The dependence of this background on the energy makes a lower proton energy in principle preferable. However, a global optimization has to take into account the distance of the detector from the neutrino source. The prompt ν_τ may also be reduced by rejecting high-energy events [29].

The other physical backgrounds impose further constraints on the neutrino beam design. The most abundant events in the detector are inclusive CC interactions of ν_μ. They have a negative muon in the final state, which does not produce a decay topology, nor missing energy. Only those processes with special topology, such as charm production, may be misidentified as events with a τ in the final state.

As an example, charmed particles produced in ν_μ and ν_e CC interactions decay with a lifetime similar to the τ^-, but can be distinguished from the τ^- by their positive charge. Negative charmed particles are the most dangerous ones which can be produced in the CC interactions of $\overline{\nu}_\mu$ and $\overline{\nu}_\mathrm{e}$. The presence of a μ^+ or e^+ allows the rejection of these events. In the cases where the primary leptons are not identified, kinematical criteria may be exploited for further rejection.

The above considerations on the charm background lead to the need for a contamination as low as possible of $\overline{\nu}_\mu$, ν_e and $\overline{\nu}_\mathrm{e}$ in the main ν_μ beam.

2.2 Other considerations guiding the NGS design

2.2.1 The NGS as a general facility

The goal of this study is the design of the NGS as a general facility, which could be in use for many years to come and possibly house more than one generation of neutrino beams and experiments.

The study of neutrino physics in general and more specifically of neutrino oscillation is likely to be influenced by the results of a number of ongoing experiments. The results of first-generation experiments will dictate the aim and the design of the future neutrino beams and detectors. It seems impossible, today, to predict the long-term physics requirements for the NGS.

As discussed in Section 2.1, the requirements of the different experiments that are currently being proposed or discussed may imply different beam layouts. It is therefore mandatory to build a facility allowing the necessary flexibility. This principle guided several of the choices made for the civil engineering layout. They can be summarized as follows:

1. The length of the target and focusing hall was chosen to be 123 m, long enough to construct a high-energy beam of the WANF type, allowing the effective focusing of high-energy neutrino parents produced at small angles. Lower energy beams can easily be accommodated.
2. A high neutrino flux is vital to make both long- and short-baseline experimentation possible. The length of the decay tunnel was chosen to be about 1000 m, three times longer than in the WANF.
3. The closest possible location of the underground pit for an SBL experimental area was identified to be about 1850 m downstream of the proton target, below the boundary limits of the Geneva airport. On the surface, the region between the hadron stop and the airport is too densely populated to permit the installation of a deep experimental station and of the related infrastructures. Moreover, the solution chosen offers the additional possibility of using the existing molasse as a muon absorber, thus requiring less iron reinforcement.

Within these constraints, freedom is left to focus different energy slices of the secondary beam. The bulky and heavy power connections (strip-lines) are designed such that focusing elements can be positioned essentially anywhere in the 100 m length of the target chamber, downstream of the target itself.

It should be noted that focusing with the coaxial lenses (horn and reflector) permits antineutrino operation by simply switching the polarity of the devices, if this should be required at a later stage.

The reference beam described in detail in Section 3 corresponds to a particular choice of the positions, currents, and shapes of the horn and the reflector. Positions are respectively about 8 m and 80 m downstream of the target, the current is 120 kA for both. The shapes of the inner conductors of the two lenses are such that they can provide parallel focusing of pions and kaons of 50 and 85 GeV respectively.

2.2.2 Building on the CERN experience

CERN has accumulated a long and continuous experience in running neutrino beams since the early 1960s, first at the PS and later at the SPS. The present SPS neutrino facility, the WANF, has been, since its construction and even more today, the world's most powerful beam of high-energy neutrinos.

The history of the WANF is one of very high operational reliability, with minimal down-time, and ever increasing performance. Record yields of protons and neutrinos have been and are available to the ongoing physics programme carried out by CHORUS and NOMAD.

Unfortunately, the WANF cannot be used for LBL experimentation because it emerges from the SPS with an upward slope of about 43 mrad. The possibility of installing a detector on its axis exists only on the CERN site itself, where the beam reaches the ground level around 800 m downstream of the target — a suitable location for a SBL experiment. On the same beam axis one could possibly install a detector in the Jura mountains, about 17 km downstream of the target — this would be considered a 'medium-baseline' experiment. For LBL experiments using a neutrino beam from CERN, a new facility has to be constructed.

CERN has much experience in building tunnels and big caverns in the kind of rock (molasse) in which the new project has to be constructed. A total of 39 km of tunnels of various diameter and length exist, the longest one being the 27 km long LEP tunnel.

For the new NGS, the high energy of the SPS proton beam is one of the key elements that allows the production of high neutrino fluxes and interaction rates. It was decided, therefore, to design a facility capable of operating at the maximum (450 GeV) SPS proton energy. It is likely, however, that the facility will operate at a slightly lower energy, 400 GeV or so, where a higher number of protons per unit time can be delivered by the SPS.

The main improvement in the design of the new facility with respect to the WANF is of course its longer decay tunnel. Other improvements are being sought, however, in all areas of the design, for example: (1) In the search for an optimal focusing configuration, although the configuration adopted during the data taking of the CHARM II experiment (1986–91) is already very close to the requirements of the ν_τ appearance experiments that are being proposed. (2) In the choice of a target material different from the beryllium used in the WANF, a material which can sustain a larger number of protons per extraction and make full use of the protons that the SPS can deliver. (3) Shape and segmentation of the target are being studied to find ways to enhance the production from the target of secondary mesons capable of providing useful neutrinos within the acceptance of the detectors. (4) A gain in the number of neutrinos per proton is also expected from the larger acceptance of the focusing system envisaged in the new facility.

The beam tuning, monitoring, and trouble-shooting tools that have been developed for the WANF, particularly after its major reconstruction in 1992–93, have proved invaluable during the years of beam operation. Building on this experience, it is planned to equip the new facility with an upgraded control system. The requirements of beam alignment are indeed more severe than in the past and are being properly considered.

2.2.3 Other focusing systems considered

Quadrupole lenses have been considered but a narrow-band neutrino beam, using a spectrometer arrangement to give tight momentum selection, would not provide sufficient flux for the experiments that could be envisaged. However, there is sufficient space in the target chamber to install such a beam, similar to the N3 beam used in the WANF from 1977 to 1980, if required.

An on-axis, large-aperture, quadrupole triplet beam has been considered [44] and might provide a possible approach to a narrower energy band beam. However, there is no sign-of-charge selection and both neutrino and antineutrino parents are focused.

Plasma and lithium lenses have been considered and can, in theory, have advantages over 'conventional' horns. They usually have very limited angular acceptance and may not have the same, proven level of long-term reliability in operation.

2.3 Operation of the SPS

2.3.1 The future of the SPS physics programme

The physics programme of the SPS will most likely continue to maintain its proton fixed-target activities beyond 2002, the planned starting year of the NGS operation. This programme would include fixed-target experiments and detector test beams, particularly for the LHC experiments, in addition to the neutrino fixed-target programme discussed in this report. The approved COMPASS experiment and a possible continuation of the present NA48 experiment are in the fixed-target programme.

The first two of the above activities require a slow resonant extraction (SE) from the SPS while the neutrino programme will be served by a half-turn fast extraction (FE) of the circulating beam in two batches. Among the requirements of the SE physics is a supercycle providing an acceleration to 450 GeV/c and a long flat-top. The duration of this flat-top is presently 2.58 s, but owing to the time required for the second of the neutrino fast–slow extractions, the time available for the SE is 2.38 s, thus providing an effective duty-cycle of 16%.

A future SPS supercycle should be able to support the intensity requirements of the full proton fixed-target programme of physics experiments (SE and neutrino) and test beams running during the same period. Details of a proposal which satisfies the above requirements for the full fixed-target programme are given in Section 2.3.4.

2.3.2 The SPS as an LHC injector

The SPS will be the final machine in the injector chain for the LHC, accelerating protons of 26 GeV/c from the PS to 450 GeV/c before a fast extraction to the LHC via either the TI2 or TI8 transfer lines. A new fast-extraction channel, which also allows the extraction of protons for the NGS, will be constructed in the long straight section in LSS4. At this location the first part of the TI8 transfer line, required for the proton transfer from the SPS to the LHC anti-clockwise circulating ring, will also be constructed. A description of the extraction channel for the NGS and its relation to that of the LHC is given in Sections 4.1 and 4.3.

The protons in the SPS originate from the PS proton Linac II and are accelerated first in the PS Booster (PSB) and then in the PS itself. The SPS and PS operate on a cycle which is a multiple of 1.2 s, given by the repetition time of the PSB.

A number of modifications to the PSB and to the PS are foreseen to be implemented before the start-up of the LHC in an effort to double the brilliance (intensity/transverse emittance) required by the LHC. The NGS beam also takes advantage of these improvements. Among the upgrades planned is the injection of the protons from the PSB to the PS at 1.4 GeV instead of the present 1.0 GeV. This would reduce the space-charge effects during the time the beam spends on the 1.2 s PS injection plateau, resulting in potentially lower beam losses in the acceleration chain. This would enable the SPS to operate more comfortably at its present intensities of around 4.5×10^{13} protons per cycle and beyond.

Up to the middle of 2005 the SPS will be fully available for the fixed-target experiments including the neutrino experiments, except during the injection tests for the LHC in 2003 which will need a considerable fraction of the SPS time for two months. There is an option to continue the injection tests at the beginning of 2004 though this may conflict with the schedule of LHCb. The running-in of the LHC will start in the middle of 2005 probably requiring the injector chain to be dedicated to the LHC for a few days per week. It is expected that after this transition period in 2005 scheduled physics running will increasingly dominate the LHC running, which implies about two fills per day, each of them requiring the injector chain for about three hours. The remaining time, during which the LHC is in coast, would be available for fixed-target physics. This implies a reduction of total protons on target of about 25% per day. At a later

stage, the filling time will be reduced to two hours, reducing the loss for fixed-target operation to about 17% [45]. The SPS, serving in sequence the LHC and the fixed targets, must be capable of switching rapidly between the various supercycles, of different lengths and magnet cycling. A possible sequence of procedures would require three supercycle changes: from fixed-target physics to LHC pilot (a low-intensity test shot to check the injection process and the LHC machine parameters), from pilot to LHC filling supercycles, and finally back to the fixed-target supercycle.

At present, the switching time between different supercycles (as is the case between the proton and lead-ion supercycles) takes at least one hour, too long to run the complete physics programme efficiently. However, work is under way to modify the SPS control system so as to be able to change the supercycle on a cycle-to-cycle basis.

It is not inconceivable that at a later stage the LHC pilot cycles could be combined with the fixed-target supercycle in a longer supercyle in order to minimize the disruption of the fixed-target physics. The actual filling of the LHC always requires a dedicated cycle minimizing the time the beam has to dwell in the LHC at injection energy.

It has to be pointed out that the operation of the LHC with ions for ALICE precludes the SPS operation of protons. This also entails a reduction in the number of protons available for the fixed-target experiments except for the case where the total SPS operation time would be increased by the time required for ALICE (about four weeks) beyond the 200 days per year assumed for fixed-target proton running.

2.3.3 Intensity limitations from the SPS and from the neutrino target

As a working hypothesis, the maximum number of protons per SPS cycle is assumed to be 4.5×10^{13}, a value which has been safely reached and even surpassed in 1997. Given the above improvements in the SPS and PS complex for the LHC, it is likely that the maximum achievable intensity will further increase so that 4.5×10^{13} protons could be safely assumed for normal SPS operation.

The maximum proton intensity per burst onto a neutrino target is governed by the choice of target material and geometry and by the beam parameters. The limit imposed by the target material stems from an equivalent stress which must not be exceeded. Stresses in targets result mostly from the thermal shock produced by the impinging protons (see Appendix C).

With the purpose of calculating the maximum permissible intensity onto the neutrino target, detailed one-dimensional analytical calculations have been performed for both beryllium and graphite targets and a proton beam from two FEs of 10 μs duration separated by 50 ms. The results indicate that a graphite target is superior to a beryllium target as it is able to withstand about twice as many protons as beryllium under the same conditions.

A summary of the intensity limits on a graphite target versus the burst duration is given in Table 1 for 450 and 400 GeV/c. To a good approximation, the allowed proton intensities scale with the inverse of the incident proton energy.

2.3.4 Proposed SPS acceleration cycle and expected proton intensity on target

A number of operation modes of the SPS have been investigated where the number of protons on target per year has served as an important parameter in defining these schemes. Since the impact of LHC commissioning and operation is not taken into account, the following numbers refer to the years 2002 to 2004. The proposed SPS cycle configuration is presented below, optimized for the NGS and for the users of the SPS requiring an SE spill structure.

Table 1: Intensity limitations for a graphite target at 450 GeV/c and 400 GeV/c incident proton momentum

Burst duration (μs)	Maximum intensity ($\times 10^{13}$ protons/extraction)	
	450 GeV/c	400 GeV/c
6 (3 extractions)	1.8	2.0
10 (2 extractions)	2.0	2.2
20 (1 extraction)	2.1	2.4

The following assumptions have been used as input for the definition of a future SPS supercycle:

- Since the NGS will commence operation only after the termination of LEP, the current LEP cycles (2.4 s total duration) will no longer be required.
- The average SPS power dissipation over the duration of the supercycle should respect the limit of 33 MW.
- The SPS should be able to provide an SE at 450 GeV/c with a duty cycle around the present 16%. Obviously, although the number of protons per SE remains constant, the integrated intensity per year for the SE depends on the duration of the supercycle.
- The combination of an FE with an SE in one cycle seems to be very difficult, and no solution exists at present. An FE before an SE would imply the extraction of one or more proton bunch trains, leaving a large gap in the azimuthal beam distribution, which is unacceptable to the clients of the SE beam. An FE following the SE implies that the beam must stay bunched during the SE in order to maintain the gap for the kicker risetime. A spill of a bunched beam at 200 MHz is, however, not acceptable to the SE users.

Although not yet thoroughly tested, the injection of three pulses could be feasible leading to the following azimuthal beam distribution in the SPS: 3 × (1.4 μs gaps and 6.3 μs beam). Hence this study is considering up to three FEs per SPS cycle, always respecting the machine and target intensity limits. In order to accommodate the risetime of the extraction kicker, the injection from the PS must create as many bunch trains in the SPS as there are extractions per cycle with gaps of about 1 μs between them. This implies that the number of PS injection pulses must be equal to the number of FEs per cycle.

It has been decided to restrict the SPS supercycle types to those consisting of two PS injections as in the present operation of the SPS. Two PS injections are sufficient to maximize the intensity for both the neutrino and SE physics without needing to lengthen the cycle duration by 1.2 s as would be the case if an additional PS injection were used.

Figure 9 shows the proposed SPS supercycle which could be used to provide protons for the shared mode of FE and SE physics. The supercycle consists of separate cycles for the SE physics and for the FE neutrino programme, thus decoupling the parameters (e.g. incident proton momenta) requested by the two communities. The proton momentum range considered for the neutrino cycles is 350 GeV/c to 450 GeV/c while 450 GeV/c has been chosen for the SE, being identical to the present SPS operation. The lower value for the neutrino cycles is attractive as it suppresses the prompt ν_τ irreducible background to a short-baseline experiment while the upper value is preferred for a higher neutrino production (see Section 2.1.3).

Table 2 gives the total number of protons per year for the neutrino cycles normalized to a run of 200 days. A somewhat conservative global machine efficiency ϵ of 50% has been assumed, being the product of two, about equal factors of 70%. The first is the combined availability of the PS/SPS complex (in 1997 this was 78.3%), and the second takes into account that the

maximum intensity is not always available. For comparison, the corresponding global machine efficiency for 1997 was 58%.

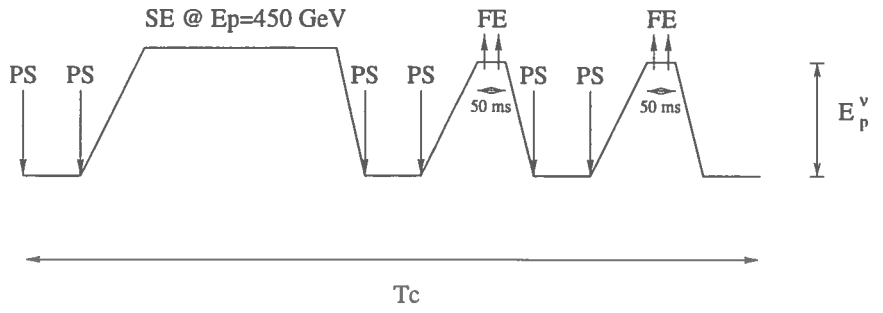

Fig. 9: The proposed SPS supercycle. The parameter E_p^ν is the incident proton momentum for the neutrino cycles and has been studied for all the values given in Table 2

Table 2: SPS operation parameters

Supercycle type	E_p^ν (GeV)	T_c (s)	ν pot/year ($\times 10^{19}$)
A	350	22.8	3.41
B	360	22.8	3.41
C	370	22.8	3.41
D	380	24.0	3.24
E	390	26.4	2.95
F	400	26.4	2.95
G	410	27.6	2.75
H	420	28.8	2.57
I	430	31.2	2.32
J	440	32.4	2.18
K	450	34.8	1.99

Figure 10 illustrates the variation in the proton intensity limits per cycle and per year (200 days and $\epsilon = 50\%$) coming from the machine and target. For comparison, the target limit from a beryllium target is plotted, illustrating the inferiority of such a target in relation to a graphite one. It can be seen that the number of protons per year from the two limits coincides at an incident proton momentum of 400 GeV/c (supercycle type F) as expected since at this momentum the limit from both factors is 4.5×10^{13} protons per cycle.

The favoured supercycle type F respects the duty cycle requirements for the SE (around 16%). It should be noted that in this scenario the first of the cycles is dedicated to the SE, without any reduction to the flat-top duration from a neutrino extraction as is the case at present.

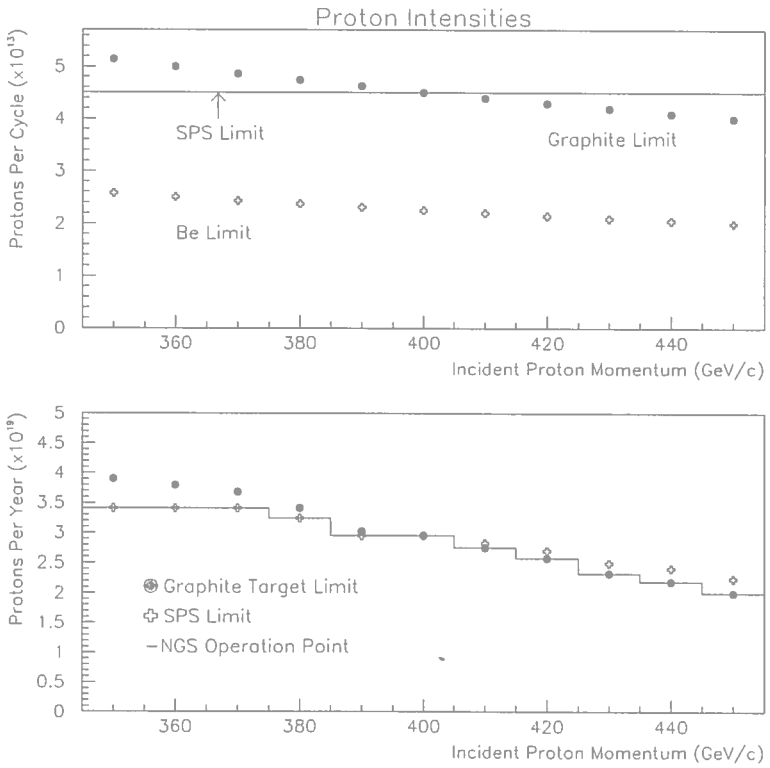

Fig. 10: The upper limits from target and SPS considerations (a) per cycle and (b) per year

The corresponding integrated number of protons per year for the SE shown in Table 3, which assumes 2.0×10^{13} protons per SE cycle, is about the same as was provided in 1997 to the targets other than the WANF neutrino target (0.5×10^{19} per year). The numbers in Table 3 can also be compared to the required number of protons per year quoted in the present NA48 proposal (0.36×10^{19}), in the COMPASS proposal (0.60×10^{19}), and the number required for the T1 and T2 targets together (0.24×10^{19}) used mainly for LHC test beams. A total of about 1.2×10^{19} protons seems to be required. The numbers in the last column of Table 3 take into account a global efficiency of 50%.

The SE proton deficit between what is requested and what could be supplied by supercycle type F could be recovered by increasing the proton intensity during the SE cycle. Since the flat-top time would be longer (4.15 s versus the present 2.38 s effective time), the intensity could be increased in the ratio of flat-top times so that the instantaneous proton intensity does not change from the present one[1]. This would provide 1.1×10^{19} protons per year, close to the present SE performance.

Finally, for comparison, Fig. 11 and Table 4 give the configuration and performance of a dedicated neutrino cycle. Obviously, the gains for the NGS are substantial, but at the expense of the SE programme. However, given that such a neutrino mode of operation is relatively inexpensive in terms of electrical power, due to the absence of an extended flat-top, the neutrino beam could be foreseen for periods extending beyond the normal SPS proton fixed-target operation.

[1]It should be remembered that the current machine limit is 4.5×10^{13} protons for any cycle.

Table 3: SPS and SE physics parameters

Supercycle type	E_p^ν (GeV)	T_c (s)	Flat-top (s)	SE pot/year ($\times 10^{19}$)
A	350	22.8	3.78	0.76
B	360	22.8	3.68	0.76
C	370	22.8	3.55	0.76
D	380	24.0	3.78	0.72
E	390	26.4	4.35	0.65
F	400	26.4	4.18	0.65
G	410	27.6	4.36	0.63
H	420	28.8	4.51	0.60
I	430	31.2	5.00	0.55
J	440	32.4	5.07	0.53
K	450	34.8	5.41	0.50

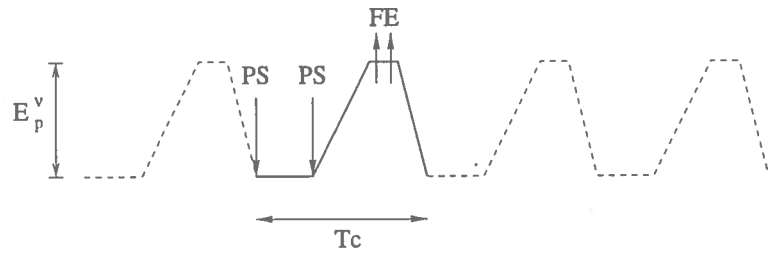

Fig. 11: The dedicated neutrino operation mode of the SPS

Table 4: SPS parameters for dedicated neutrino operation

Supercycle Type	E_p^ν (GeV)	T_c (s)	pot/year ($\times 10^{19}$)
A	350	6.0	6.5
B	360	6.0	6.5
C	370	6.0	6.5
D	380	6.0	6.5
E	390	7.2	5.4
F	400	7.2	5.4
G	410	7.2	5.4
H	420	7.2	5.4
I	430	7.2	5.4
J	440	7.2	5.4

Obviously, once LHC commissioning and operation starts in parallel with the fixed-target operation, the expected number of protons on target per day in all the modes (FE and SE) will be decreased by about 25%. Whether this has an impact on the number of protons per year depends on the scheduling.

3 THE NEUTRINO BEAM

The final detailed parameters of the first beam to operate in the NGS need to be defined by the end of 1999[2], in order to allow sufficient time for manufacturing and testing of the horn and reflector. This assumes a beam starting date of spring 2002. Work has to continue for some time to optimize the target configuration and the coaxial lenses for the initial physics requirements. In parallel, results from different simulation packages are being compared. However, in order to proceed with other aspects of the NGS design and to provide a basis for comparison, parameters of a 'reference beam' have been defined: this beam, which should be considered a preliminary variant, is intended to match the requirements for long- and short-baseline ν_τ appearance experiments given in Section 2

A schematic overview of the beam elements is given in Fig. 12, the list of parameters can be found in Appendix A. An indication of possible improvements and variants to the 'reference beam' is given at the end of this section.

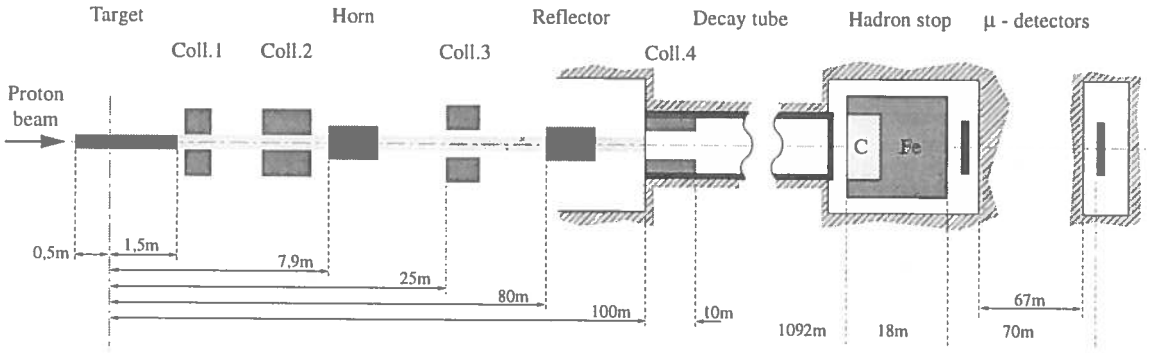

Fig. 12: Components of the proposed neutrino beam

3.1 Beam simulation and production spectra

A full Monte Carlo simulation of the beam has been made using several different computer programs. Two differing hadron production models have been used: the version of FLUKA92 [46] integrated into GEANT 3.21 and the code FLUKA97 [47]. The hadronic interaction and particle production models have been extensively improved with respect to the version available in GEANT [48] in the last few years. Preliminary comparisons [49] with the NA56 (SPY) experiment [50] show an overall good agreement for the current model, while problems show up for the version embedded into GEANT [51]. It is worth taking note, however, that this latest version of FLUKA has a softer fragmentation function, hence the predicted ν_μ flux is about 20% less, and the beam energy somewhat lower, than the FLUKA92 version used in GEANT 3.21. The corresponding differences in the calculation of the fraction of unwanted neutrino types should stay within a factor of 2, according to the comparisons carried out for the present report and to those performed for the WANF beam [51].

In addition to the comparison of hadron production models, different particle transmission codes with complex geometry and materials have been used: the well-known GEANT 3.21 in the form developed by CHORUS and NOMAD with a new geometry to describe the NGS beam [52], and a completely new application, written for the NGS, using the stand-alone FLUKA97 package. Moreover, a fast tracking version with precomputed particle production tables based

[2]This date assumes that the requested currents in horn and reflector are not higher than 120 kA, allowing the use of a design as described in this report.

on FLUKA97 has been used [53]. In all cases the neutrino parents are tracked in detail to their point of decay. Realistic values for material thicknesses, magnetic field strengths etc. have been used wherever possible. The use of several independent packages, which allows the comparison of production models and different tracking results lends much confidence in the results presented in this report. As the FLUKA97 package shows the best consistency with the experimental results of the SPY [50] experiment, this has been used in the plots showing neutrino fluxes and event rates.

In order to optimize the integrated neutrino event rates, a proton beam energy of 400 GeV is assumed, as described in detail in Section 2.3

3.2 Decay kinematics

The ratio of π to K produced in the target is roughly 10:1. The mean free path of π before decay is 55 m/GeV and for K is 7.5 m/GeV. The maximum energy of ν_μ from π decay is $\approx 43\%$ of the parent π energy. The two-body decay of K gives ν_μ of up to 96% of the parent energy. This leads to two superimposed parts of the overall neutrino spectrum, dominated by the π-generated component at lower energies and a smaller K component at higher energy. For a neutrino beam of mean energy ≈ 25 GeV it is necessary to collect neutrinos up to 55 GeV, this implies decays of K of up to 60 GeV and π up to 120 GeV.

3.3 Target configuration

The target should be dimensioned such that almost all incident protons interact but, at the same time, cause as little absorption or scattering of the secondary (neutrino parent) particles as possible.

In order to minimize the interactions of secondaries produced at large angles, it is required that the diameter of the target should not be larger than that required to contain the incident proton beam. The 400 GeV beam has a size of less than 2 mm ($\pm 2\sigma$) at its focal point, so that, allowing for small beam instabilities and scattering in the target material, a target diameter of 3 mm is chosen as for the WANF.

The length of the target is ~ 3 interaction lengths, ensuring that 95% of the protons interact. For particles produced at small angles which have a longer path length in the target, a material of low atomic number is chosen: 'diluting' the target can further reduce absorption by having discrete elements of target material separated by air gaps.

However, increasing the target length gives an extended source for the secondary beam optics which can become significant with respect to the focal lengths of the focusing system. A compromise has to be found.

Pure beryllium targets have been used in most CERN PS and SPS neutrino beams to date but evaluations on the use of graphite as a target material look promising in view of operation with short, intense proton spills in a fast extracted beam. A detailed discussion of the thermal and mechanical properties under these conditions is given in Appendix C. Particle production from the two materials is similar and detailed optimization of the positions and lengths of the target elements has still to be carried out together with the final choice of the beam optics layout.

For the 'reference beam' calculations, the target layout is identical to that presently used in the WANF except that graphite (density 1.81 g/cm^3) is assumed: it consists of 11 cylindrical rods of 10 cm length and 3 mm diameter supported on the beam axis by thin disks: the spacing between rods is 9 cm, giving an overall target length of 2 m. A schematic view of the target region is shown in Fig. 13.

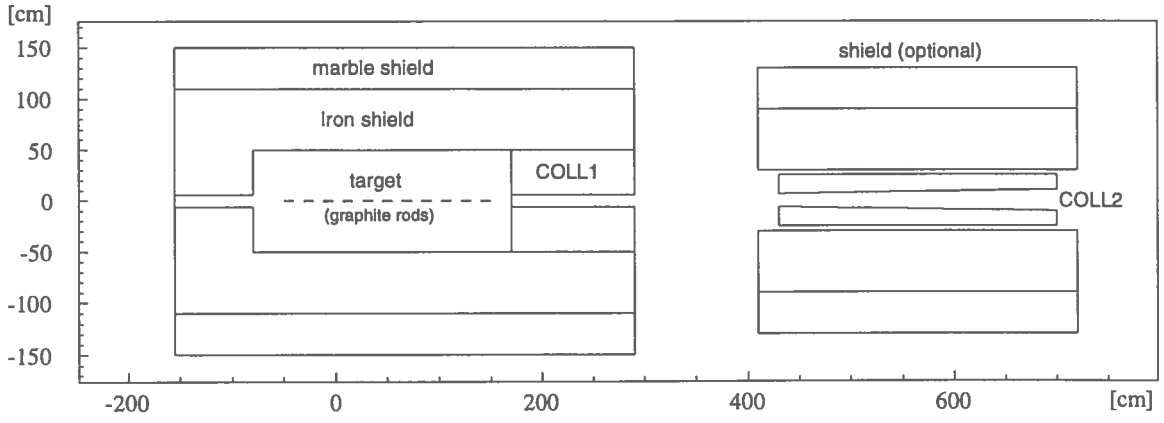

Fig. 13: Schematic view of the target configuration and the first two collimators

3.4 Focusing system

Coaxial magnetic lenses are chosen since they give higher angular and momentum acceptance than other focusing systems. They can be made to withstand high radiation levels, have cylindrical symmetry, and also give some sign selection, enabling both neutrino and antineutrino beams to be produced.

A toroidal magnetic field is produced in the volume between two tubular coaxial conductors when a high current flows along the inner conductor and back through the outer. The strength of the field B (Tesla) at any point is given by $B = I/(50 \times R)$ where I is the current (kA) and R is the radius (cm). There is no field inside the inner conductor or outside the outer conductor which is usually cylindrical.

In a magnetic **horn**, the inner conductor is shaped so that particles coming from the target, with a given energy but with a wide angular spread, traverse an integrated magnetic field which will focus them into a parallel beam. Particles of the opposite polarity will, of course, be defocused. The inner conductor is made as thin as possible to minimize absorption but must withstand the high current density needed and the radial forces induced by the magnetic field.

A magnetic **reflector**, downstream of the horn, works in the same way. It has a large central aperture to allow the particles which are already well-focused to pass undisturbed, but provides additional focusing for particles of different energies which have been underfocused or overfocused in the horn. In this way the energy band which is focused by the system is broadened. Several reflectors can be used but the potential gain in flux and bandwidth is usually offset by losses from additional absorption.

Cross-sections of horn and reflector are schematically shown in Fig. 14. A few selected rays tracked through the system are illustrated in Fig. 15, showing the focusing/defocusing effect of these coaxial lenses.

The beam for ν_τ appearance experiments should have the highest possible flux, with an energy band which is substantially above the threshold for ν_τ charged-current interactions. The choice of 25 GeV as the nominal neutrino energy is a compromise between the requirements for high flux and high energy. The sensitivity of the different detectors to neutrino oscillation, which is energy-dependent, will also need to be considered at a later stage.

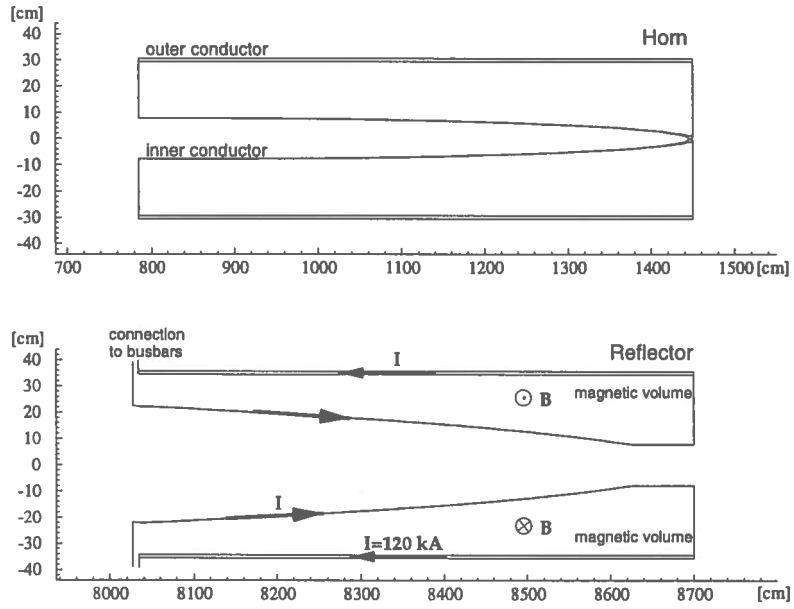

Fig. 14: Cross-section of horn and reflector. The current and magnetic fields are indicated schematically for the latter

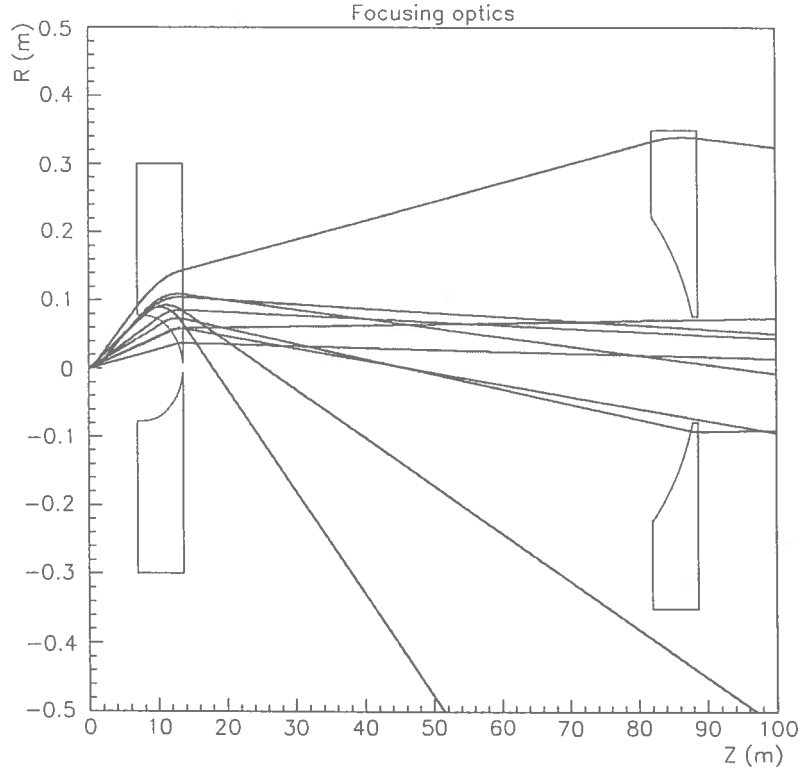

Fig. 15: Particles emerging from the target, deviated in the fields of horn and reflector

The overall physical lengths of the horn and reflector are ≈ 7 m, giving an optical length of 6.65 m. The design is extrapolated from the CHARM II beam used in the WANF from 1986 to 1991, which had characteristics similar to those required for the NGS. In order to achieve a higher neutrino flux, the horn and reflector have been moved closer to the target to increase the angular acceptance. As a fast extraction is used, the current pulse length needed in the lenses is shorter and the peak current can be increased to 120 kA for the same integrated current density. To a first approximation, the angular acceptance of the horn is proportional to the square root of the current and the inverse distance from the source.

The parameters of the horn and reflector are given in Table 5. Positions along the beam axis (Z) are referred to the focal point of the proton beam in the target. The dimensions given are those of the magnetic field region: D refers to the conductor nominal diameter, T to the conductor thickness. The horn is designed to focus π and K of 50 GeV nominal energy into a parallel beam and has an acceptance of almost 10 mrad. The reflector focuses π and K of 85 GeV after they have left the horn but will also refocus particles of lower energy which have been strongly overfocused.

The current in the horn and the reflector can be reversed so that negative mesons are focused in order to produce antineutrinos, should this be required.

Table 5: Reference beam: horn and reflector positions and conductor coordinates are given

Current Start coordinate Length		Horn 120 kA 7.85 m 6.65 m			Reflector 120 kA 80.35 m 6.65 m	
Inner conductor	Z [cm]	D [cm]	T [mm]	Z [cm]	D [cm]	T [mm]
	0.0	15.5	2	0.0	44.3	2
	77.7	15.5	2	6.4	44.3	2
	171.1	15.3	2	55.2	42.9	2
	264.5	14.7	2	175.0	38.8	2
	355.0	13.7	2	284.2	34.5	2
	439.6	12.2	2	381.4	30.1	2
	515.1	10.4	2	465.8	25.4	2
	578.0	8.2	2	536.3	20.5	2
	627.5	5.6	2	592.0	15.5	2
	655.0	2.9	5	665.0	15.5	2
	659.8	1.5	9			
Outer conductor	Z [cm]	D [cm]	T [mm]	Z [cm]	D [cm]	T [mm]
	0.0	60.0	12	0.0	70.0	12

3.5 Decay tunnel, helium cylinders, collimators

Collecting neutrinos up to 55 GeV for a beam of mean energy ≈ 25 GeV implies decays of K of up to 60 GeV and π up to 120 GeV with mean free paths of 450 and 6600 m respectively. With the proposed decay path from the target to the hadron stop of 1100 m, essentially all K will decay. It should be noted that a large fraction will already decay in the first 100 m of the target cavern, so absorption in this region should be minimized. A smaller fraction of π will have decayed in 1100 m, a longer decay path would therefore clearly increase the neutrino flux.

For the LBL detector, the effect of a longer decay tunnel, up to 1400 m in length, is shown in Fig. 16 and a cumulative plot in Fig. 17. These plots show the distribution of the points of origin, i.e. the decay points of parent mesons, as a function of the longitudinal distance from

the target, for all ν_μ events occurring in the detector. The contribution to the number of ν_μ CC events from a unit section of evacuated tunnel decreases linearly with its distance from the target. The cumulative gain with increasing length becomes modest at lengths more than 1000 m.

The effect for the SBL detector is presented in Fig. 18, and the cumulative plot in Fig. 19. These plots show that event rate would greatly benefit from a longer decay tunnel. The contribution to the flux of ν_μ from an additional unit section of evacuated tunnel increases very rapidly due to the increase in the solid angle. In the NGS layout, the possible SBL location is fixed. A longer decay tunnel would imply less molasse, but the shortened length of molasse shielding would no longer be able to absorb all the muons before they reach the SBL detector and would have to be compensated for by an extended iron shielding.

The decay tunnel length chosen, 1000 m, is therefore a compromise between intensity and the high cost involved in extending the evacuated decay tunnel and reinforcing the iron shielding. It should also be noted [44] that a longer decay path does have some additional unwanted consequences: the proportion of ν_e in the beam increases as more of the μ produced in π and K decay can themselves decay.

The effect of increasing the diameter of the decay tunnel was also studied. Figure 20, and the corresponding cumulative plot Fig. 21, show the distribution of the radial distance of the point of origin from the beam axis for all ν_μ CC events occurring at the LBL detector. The distribution for the SBL detector is very similar. It appears that most of the decays leading to useful ν_μ CC events are well contained within the proposed radius of 1.225 m from the beam axis. The gain in flux from an increased diameter would not be substantial.

However, if a lower energy neutrino beam were later required, this could benefit from a larger decay tunnel radius [44]. The diameter of 2.45 m was therefore a reasonable compromise adopted for the NGS.

The vacuum pressure in the decay tunnel should be below 5 mbar. At this pressure, the absorption in the 2 mm titanium window at the beginning of the tunnel is comparable to that in the residual air over the 1000 m, each being 0.007 interaction lengths. The expected loss in neutrino flux due to this material is 1.4% [3]. The vacuum system has been designed to reach a pressure of 1 mbar in 3 days, see Section 4.8.2.

Having a vacuum in the target cavern is not practical as access is needed to the target station and to the horn and reflector. However, the air in the cavern represents about a 10% loss of flux by absorption. If the air is replaced by helium at atmospheric pressure over two-thirds of the 100 m path length, this loss can be halved. As has been done in the WANF, it is foreseen to install a large diameter helium tube between the horn and reflector, see Section 4.5.3. Losses in its two 0.3 mm titanium windows are less than 0.2%.

It is essential to stop all unwanted particles as early as possible in order to:

i) concentrate induced radioactivity in well-defined areas;

ii) avoid the propagation of defocused particles that could decay and produce background in the beam.

[3] Note that the loss of neutrino flux would be about 75%, if the decay tube is left at atmospheric air pressure, and about 20% with 1 atm helium.

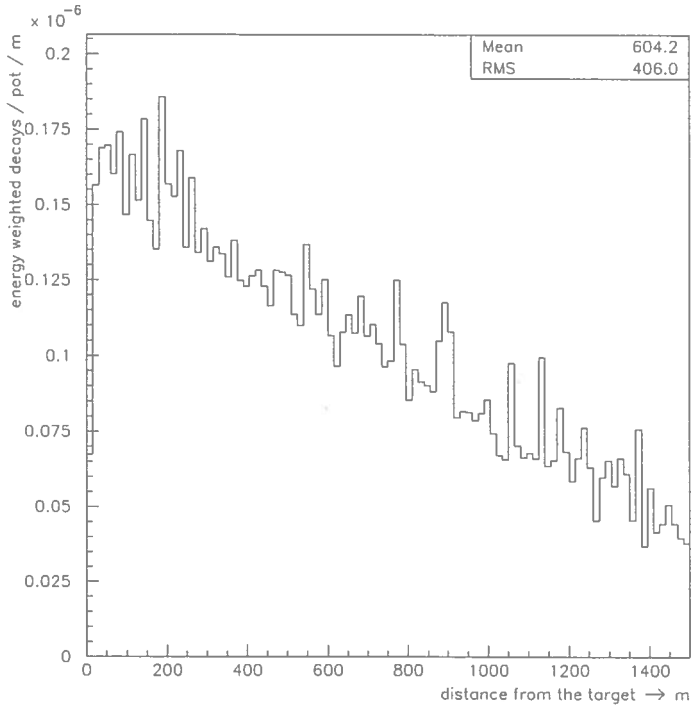

Fig. 16: Longitudinal distribution of the decay-point of parents of ν_μ CC events in the LBL detector

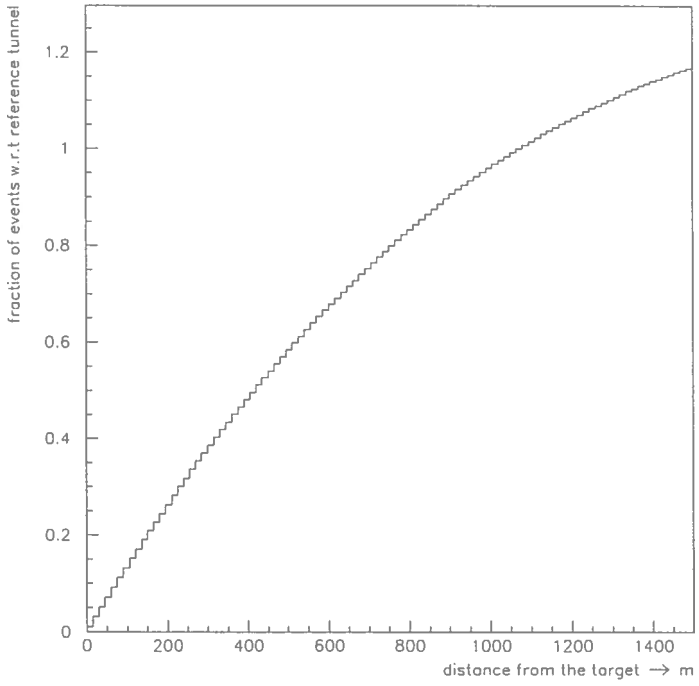

Fig. 17: Cumulative distribution of the decay-point of parents of ν_μ CC events in the LBL detector, normalized to $d = 1100\,\mathrm{m}$

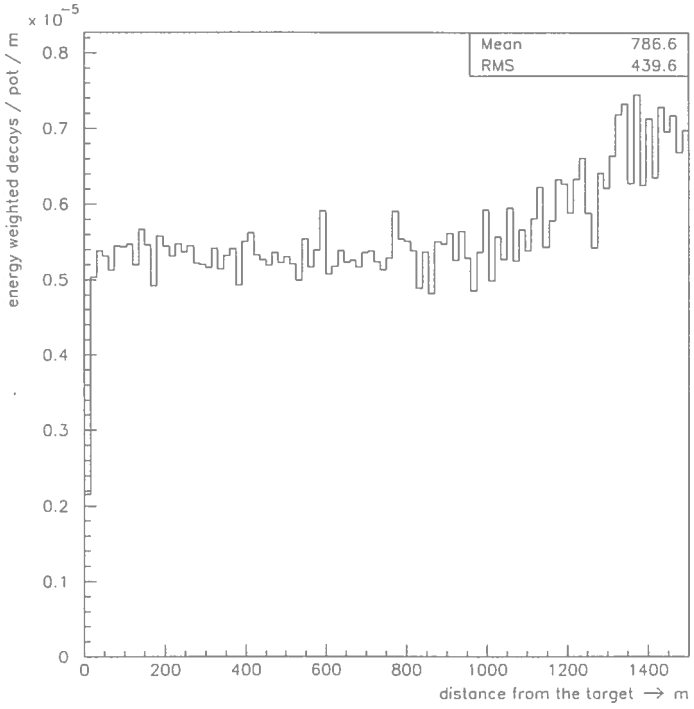

Fig. 18: Longitudinal distribution of the decay-point of parents of ν_μ CC events in the SBL detector

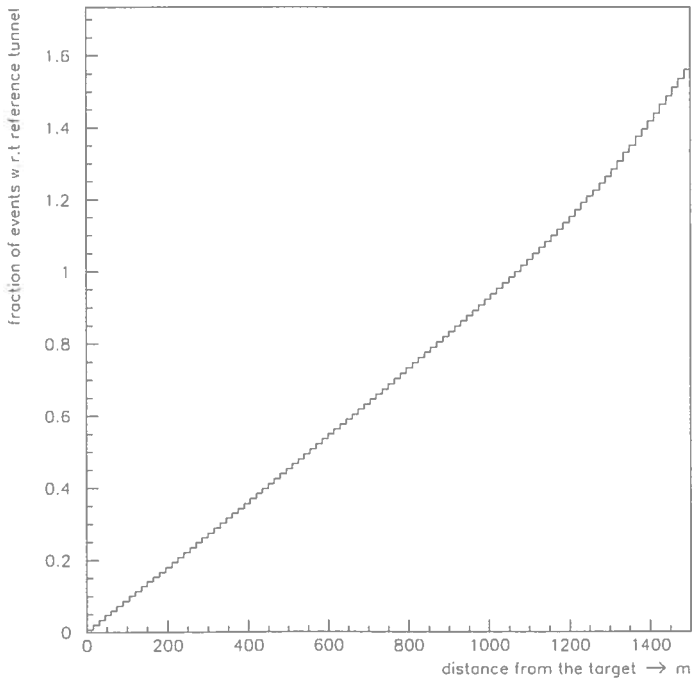

Fig. 19: Cumulative distribution of the decay-point of parents of ν_μ CC events in the SBL detector, normalized to $d = 1100\,\mathrm{m}$

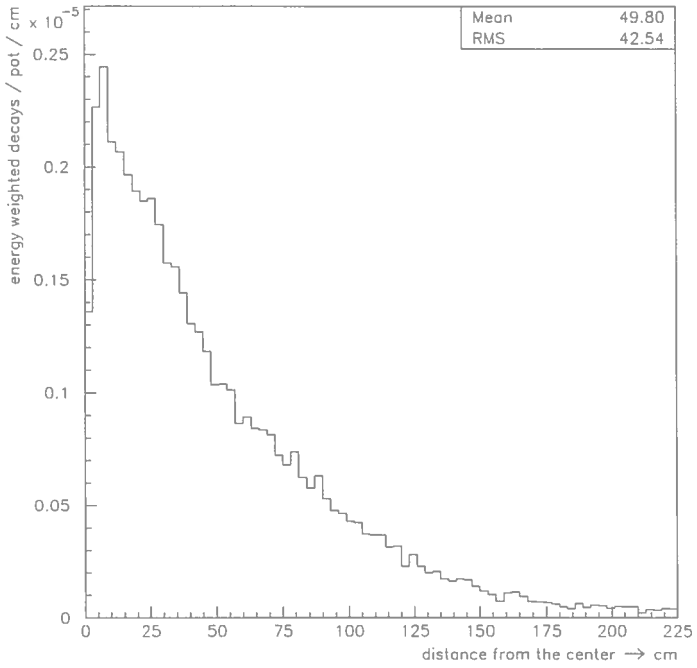

Fig. 20: Radial distribution of the decay point of parents of ν_μ CC events in the LBL detector

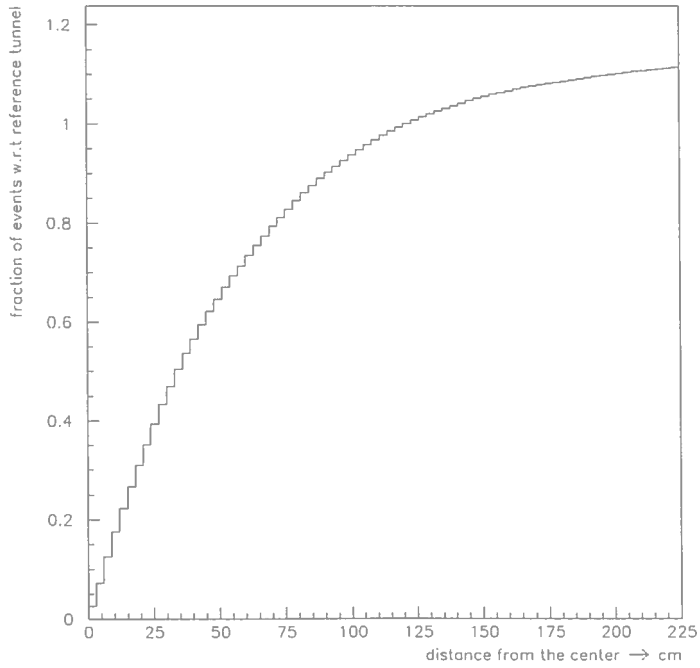

Fig. 21: Cumulative radial distribution of the decay point of parents of ν_μ CC events in the LBL detector, normalized to $R = 122.5\,\mathrm{cm}$

The positions, dimensions and material of the collimators are given in Appendix A. The function of the collimators are as follows:

- Collimator 1 can be considered as part of the target shielding. With eight interaction lengths of material, it absorbs all particles emerging from the target outside of a cone with a ± 20 mrad opening angle.
- Collimator 2 is placed between the target station and the horn. Its function is also to limit the angular acceptance of particles reaching the horn. In the 'reference beam', the design acceptance of the horn is 10 mrad at the nominal energy of 50 GeV. However, particles with lower energy at higher angles can possibly be focused and therefore an acceptance cone of 15 mrad has been chosen. Collimator 2 can be exchanged more easily than collimator 1 and can therefore be tailored to different beam requirements in the future.
- Collimator 3 is made of steel blocks with a rectangular aperture, installed between the horn and reflector. Its function is to absorb all particles which are outside the acceptance of the reflector and therefore do not contribute to the neutrino beam: in particular it absorbs particles of opposite polarity which are defocused by the horn. It is effective in reducing the ν_e background in the beam absorbing unwanted mesons: these can decay to produce μ which can straggle into the decay tunnel and in turn decay to ν_e.
- Collimator 4 is a cylindrical collar at the entrance of the decay tunnel. Its function is to limit the acceptance of the decay tunnel and minimize the number of hadrons reaching the steel tube of the vacuum pipe. Its inner diameter is determined by the cone from the reflector outer conductor to the end of the decay tunnel; the outer diameter is the same as that of the vacuum pipe. An additional function is to absorb particles defocused by the reflector.

3.6 Beam spectra and event rates for the reference beam

The energy distribution of the ν_μ for the 'reference beam' is shown in Fig. 22 for an LBL experiment and in Fig. 23 for an SBL detector.

These calculations, especially for an LBL detector, are very time consuming. Primary 400 GeV protons and all the secondaries produced are tracked in each run through the entire beam line from the target until they interact, decay, or escape. The detailed description of the geometry of the 'reference beam' materials and magnetic field is implemented in each of the beam simulation programs used. The neutrinos coming from secondaries produced in reinteractions are included in the neutrino spectrum.

In order to collect sufficient events, in particular for the LBL detector, 80 to 100 decays are generated for each neutrino parent that reaches its decay point before interacting or escaping. A statistical accuracy of 1% or better is thus achieved at the price of some increase in local statistical fluctuations.

Neutrinos from the decays are scored at an LBL detector if they hit a circular area of 100 m radius. This is significantly larger than any conceivable detector and it is used only to collect higher statistics. It was verified that the results of the calculation change less than the fluctuations from run to run, if smaller detector surfaces are used. The sensitive area of an SBL detector is taken to be that of the proposed TOSCA detector, about $2\,\mathrm{m}^2$ (1.44 m lateral size).

These and other results of the calculations are summarized in Table 6. Event rates for CC deep inelastic neutrino interactions are quoted, per proton and per ton of target detector material, assuming a linear dependence of the interaction cross-section on energy using the measured slope ($0.67 \times 10^{-42}\,\mathrm{cm}^2/\mathrm{GeV}$). The production of CC events by neutrinos different from the main ν_μ component are given as a percentage of the ν_μ content.

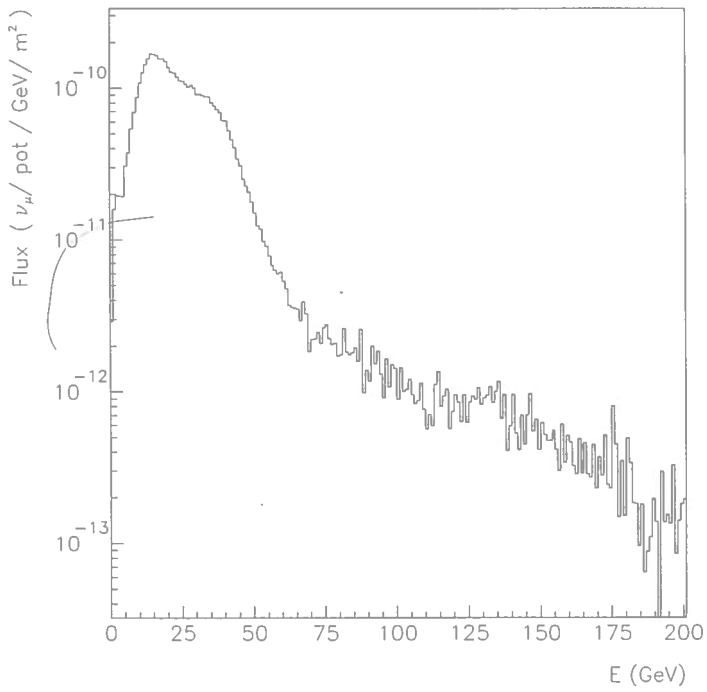

Fig. 22: Energy distribution of the ν_μ flux at the LBL (732 km) detector

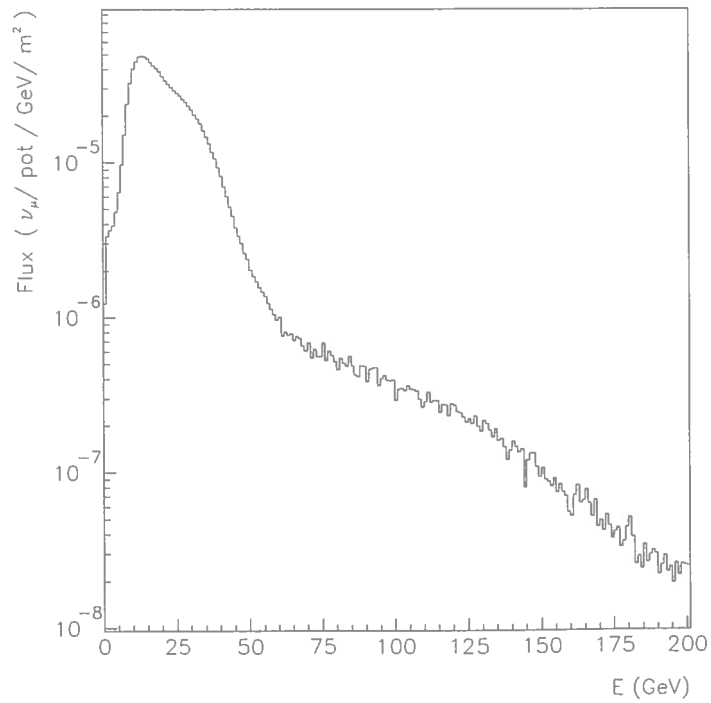

Fig. 23: Energy distribution of the ν_μ flux at the SBL (1.85 km) detector

Table 6: Predicted performance of the NGS 'reference beam'. The statistical accuracy of the Monte Carlo simulations is indicated for the ν_μ component of the beam

	LBL detector	SBL detector
ν_μ [m^{-2}/pot]	4.39×10^{-9} (0.7%)	1.09×10^{-3} (0.3%)
Mean ν_μ energy [GeV]	26.7	24.1
ν_μ CC events/pot/ton	4.73×10^{-20} (1.0%)	1.06×10^{-14} (0.4%)
ν_μ CC events/year/ton	1.40	3.13 10^5
Fraction of other neutrino events:		
ν_e/ν_μ	0.8%	0.9%
$\overline{\nu}_\mu/\nu_\mu$	2.2%	2.0%
$\overline{\nu}_e/\nu_\mu$	0.08%	0.07%
σ_τ/σ_μ	0.50	0.47

The CC interaction cross-section of ν_τ increases slowly with energy above its 3.5 GeV threshold and reaches the universal linear dependence only above energies of about 100 GeV or so. The average value of the ratio (σ_τ/σ_μ) of the CC interaction cross-section weighted with the neutrino energy spectrum is also quoted in Table 6. This is a decisive factor for ν_μ–ν_τ oscillation experiments. Together with the fact that the ν_τ detection efficiency typically also increases slowly with energy, it gives a clear preference for ν_τ appearance experiments to operate in a high-energy neutrino beam. The energy distribution of CC neutrino interactions is shown in Fig. 24 for an LBL detector and in Fig. 25 for an SBL detector. The transverse distribution of ν_μ is shown in Fig. 26 for an LBL detector and in Fig. 27 for an SBL experiment.

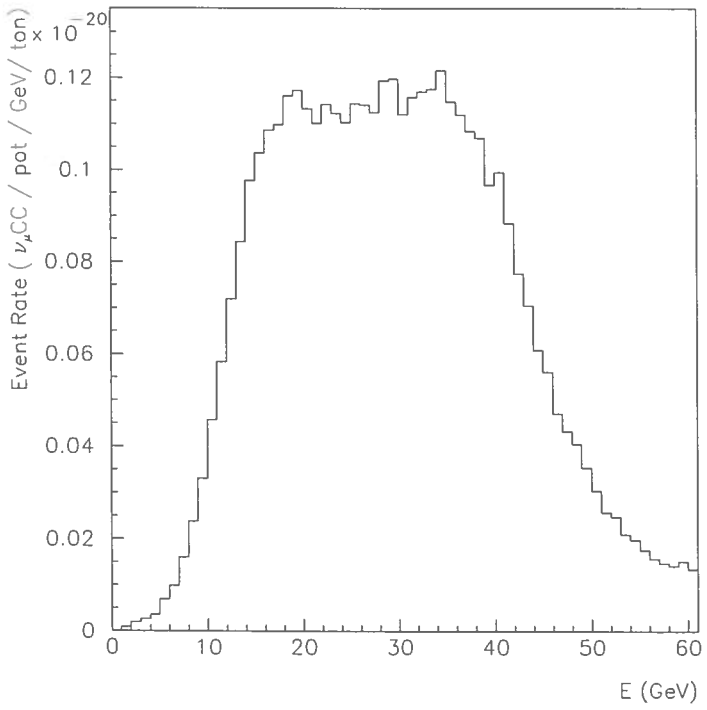

Fig. 24: Energy distribution of CC ν_μ interactions at the LBL (732 km) detector

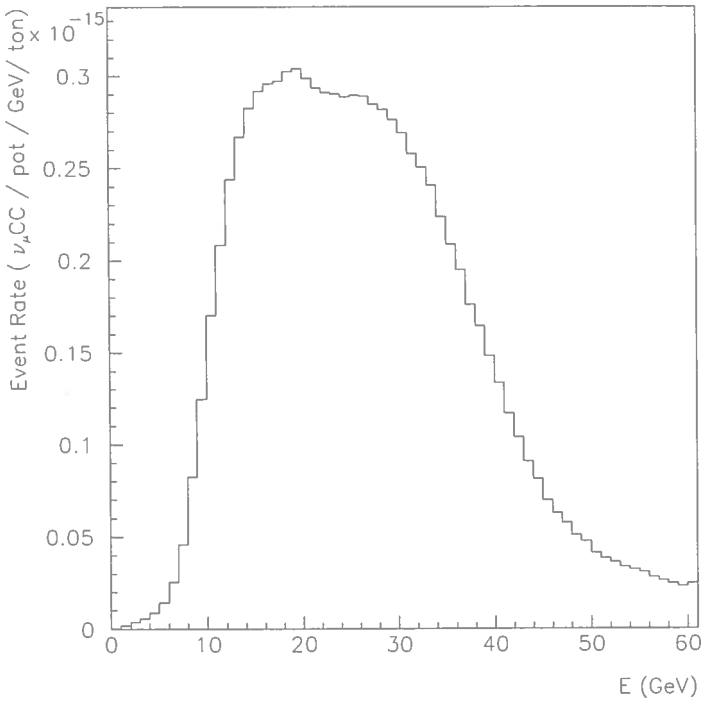

Fig. 25: Energy distribution of ν_μ CC interactions at the SBL (1.85 km) detector

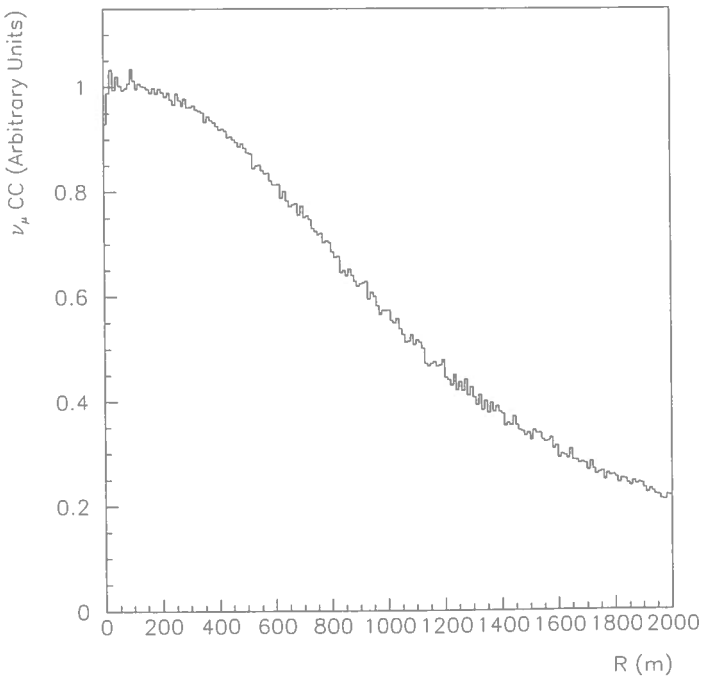

Fig. 26: Radial distribution of ν_μ CC events at the LBL (732 km) detector

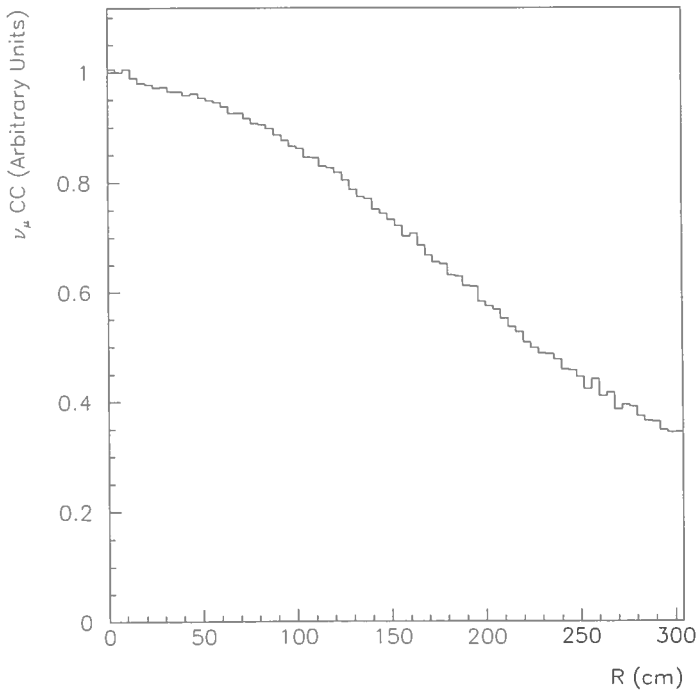

Fig. 27: Radial distribution of ν_μ CC events at the SBL (1.85 km) detector

The standard deviation of the radial ν_μ distribution at an LBL detector is about 850 m. At an SBL detector it is 1.9 m, flatter than in the present WANF where most of the decay tunnel has a smaller diameter (1.2 m) than the one adopted here (2.45 m).

The number of ν_μ CC events in both the short- and long-baseline experiments is rather similar for proton momenta between 360 and 440 GeV/c if the difference, due to the SPS cycle, in the allowed number of protons on target is taken into account. For the 'reference beam' simulations, a few examples of rates are shown in Table 7. The reference proton beam momentum has been chosen to be 400 GeV/c. For example, operating at 360 GeV/c yields slightly less neutrino events at the detectors than at 400 GeV/c but has the advantage of a lower energy consumption, of a shorter supercycle length, and of a reduced prompt ν_τ background for the SBL experiment.

Table 7: Predicted ν_μ CC event rates for different primary proton beam energies

Energy	pot/year	LBL detector		SBL detector	
(GeV)	(see Table 2)	CC/pot/ton	CC/ton/year	CC/pot/ton	CC/ton/year
360	3.41×10^{19}	3.88×10^{-20}	1.32	8.78×10^{-15}	2.99×10^{5}
400	2.95×10^{19}	4.73×10^{-20}	1.40	1.06×10^{-14}	3.13×10^{5}
440	2.18×10^{19}	5.61×10^{-20}	1.22	1.27×10^{-14}	2.77×10^{5}

3.7 Muon background at the SBL experimental area

There are two kinds of muon background that must be considered at the SBL experiment:

- muons coming from the neutrino-induced reactions in the material in front of the detector;

– muons coming from hadrons decaying in the the decay tunnel and punching through, or multiple scattering around the shielding material in front of the detector.

The first case is an irreducible background that cannot be avoided. Adding or taking away material makes little difference as the neutrino interactions and muon fluence are in equilibrium. The intrinsically high p_t of the muons does have some effect, but only with large distances of air in front of the detector, i.e. 20 to 30 m. The size of the background can, however, be reliably calculated from the knowledge of neutrino interactions and the estimated neutrino flux at the detector. Taking into account the expected neutrino flux and its radial distribution, neutrino interactions are generated in a large volume of molasse in front of the SBL cavern. The volume used is a cylinder along the beam axis of diameter 30 m and a length of 200 m. The material used is molasse, with a density of 2.4 g/cm^3. It is not necessary to consider a longer cylinder, as 200 m of molasse is sufficient to range out almost all produced muons. All muons are tracked, with multiple scattering and energy loss to the SBL cavern, and the number crossing a typical detector of $2 \times 2 \times 6\,\mathrm{m}^3$ is calculated. For an incident proton beam of 450 GeV a background of 10 muons per 10^{13} protons on target is found, corresponding to about 2.5 muons per m^2. Not surprisingly 95% of the muons that reach the detector come from the last 40 m of molasse.

The second background is more difficult to estimate. Ideally, the punch-through muons should give a background flux less than the local production of muons from neutrino interactions. Unlike the shielding of the WANF beam (see Section 1.2), which was very inhomogeneous and lacked any rotational symmetry about the beam axis, the NGS beam is completely and uniformly imbedded in molasse. Hence a simple geometrical description of the shielding and a two-dimensional calculation can be made. The total material in the hadron stop and the molasse up to the nominal SBL cavern position is 186.0 kg/cm^2. In reality, there may be up to 20 m of molasse less, in order to fit the surface buildings and access pit on the rather restricted site. The real stopping power may be only 182.0 kg/cm^2.

If all energy loss mechanisms: ionization, bremsstrahlung, pair production, and nuclear interactions are taken into account, the mean energy loss, and penetration, as calculated in Refs. [54] and [55] for a 450 GeV/c muon in the 'reference beam' shielding would be 145.8 and 141.9 kg/cm^2, respectively. These values show satisfactory agreement, however, as the authors of Ref. [55] write, "It is important to realise that at high muon energies the stochastic nature of the energy loss makes it inappropriate or even misleading for detailed designs to be based on a single mean value".

The problem is to estimate the penetration to greater depths of material due to the stochastic processes, i.e. the straggling of the muons. Unfortunately, if all the processes except ionization loss, with some low delta-ray energy cut-off, are arbitrarily switched off, the mean penetration is of the order of 191.0 kg/cm^2, rather more than the stopping power available with the present geometry. Hence there is no simple Yes/No answer and a full Monte Carlo simulation of the neutrino beam and the muon penetration of the shield has to be attempted.

The result of the simulation for a 450 GeV/c proton beam on a WANF type beryllium target is shown in Fig. 28. The program used is described in Ref. [47] and the features of the 'reference beam' have been fully simulated to give a realistic hadron and final muon spectrum. The figure shows the muon flux density in a radial section, out to 20 m against the distance from the front face of the hadron stop to the position of the SBL cavern. Although there is substantial straggling of the muons well beyond the mean value, fortunately there still seems to be a margin of safety before an SBL detector. The results predict that there should be an incident muon rate on the SBL of less than 0.25 m^{-2} per 10^{13} protons on target.

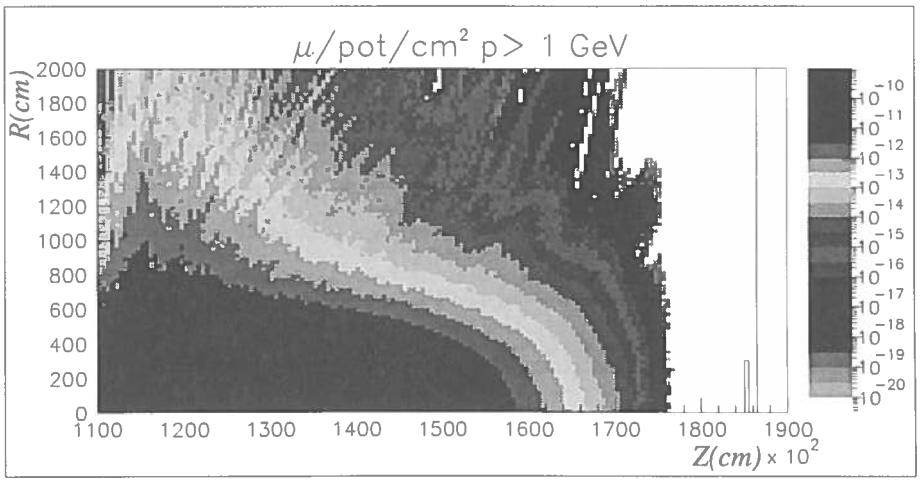

Fig. 28: Radial section of muon flux in the molasse between the front of the hadron stop and an SBL detector

3.8 Improved neutrino beam design

The design of the optimal beam configuration in the NGS facility has only just begun. It should be stressed again that the 'reference beam' option presented above should be considered as a starting point for the overall design and costing of the facility. The final beam design will be dictated by, and optimized to give the best possible performance for, the approved scientific programme. Changes in the details of the target layout, the focusing system and of other elements in the target chamber are therefore to be expected. The necessary flexibility has been built into the target chamber design to make this possible.

The results of the beam calculations are also influenced by the improved version of the FLUKA hadronic interaction generator [47] which has been used, and which is a closer match to the SPY data [50] on yields of neutrino parents from the target. Using FLUKA97 results in a somewhat lower, but more realistic prediction of the neutrino flux.

A number of different beam optics have already been tried and various beam configurations more favourable than the 'reference beam' for ν_τ appearance experiments have been identified. This work is far from complete. Possible alternative configurations which could be to considered are a beam of higher neutrino energy, with a horn focusing π and K of 70 GeV and a reflector focusing π and K of 120 GeV. This could give a comparable ν_μ fluence at a higher energy, and a correspondingly better position above the ν_τ threshold for ν_τ appearance experiments.

Above all, it is of great importance to reduce as much as possible, consistent with reliability, the amount of material in the path of the secondary hadrons in the first stages of the beam. Comparison of the ν_μ flux calculations, with and without material in the beamline, show that for the 'reference beam' design almost half of the useful π and K are absorbed or interact before they can decay.

3.9 Possibility of a lower energy neutrino beam

The option of a neutrino beam of considerably lower energy has been the subject of some discussion. Such a beam has been considered in view of ν_μ disappearance experiments, operating in an energy region where detection of ν_τ CC interactions is strongly suppressed. The aim of this type of experiment would be to explore a region of lower neutrino mass differences, hardly accessible with neutrino beams like the NGS 'reference beam' described above.

A low energy beam would restrict the $\nu_\mu - \nu_\tau$ study to disappearance measurements. Furthermore, in order to collect a sufficient number of events, a low-energy beam would require a proton intensity which may not be compatible with the possibilities of the existing CERN facilities nor with the foreseen physics programme of CERN. For these reasons, the low-energy beam option is not discussed further in this report. It should eventually become the subject of a separate study, along the lines of Ref. [44].

3.10 Comparison with the Fermilab NuMI and KEK K2K projects

3.10.1 NuMI in the U.S.A.

A new neutrino facility, Neutrinos at the Main Injector (NuMI) [56], is being planned using protons of 120 GeV/c from the Fermilab Main Injector to produce a neutrino beam intended for experiments located on the Fermilab site and 730 km away at the Soudan mine in Minnesota. The long-baseline experiment MINOS will consist of two detectors — a near detector situated about 1.3 km from the target and a far detector at 730 km.

As for the NGS, the neutrino beam at NuMI described in Ref. [56] is a wide-band beam. The mean ν_μ CC event energy at the NuMI LBL experiment is given as 17.6 GeV. The secondary π and K resulting from the primary proton interactions with the nuclei of a graphite target are focused by a set of three magnetic horns in the direction of the detectors. The horn system is pulsed in coincidence with the Main Injector proton spill over 1 ms at 170 kA. The decay pipe at the end of the focusing region provides an evacuated space of 750 m length for the secondary particles to decay. All hadrons, including the primary protons which did not interact in the graphite target, are absorbed in the hadron stopper — a water-cooled core of aluminium and copper surrounded by steel of dimensions $3 \times 3\,\mathrm{m}^2$ and 4.9 m long.

The flux, position, and momentum of the muons originating (primarily) in the secondary particle decays which produce the neutrinos are monitored by muon detectors placed in a number of pits constructed in the dolomite downstream of the hadron absorber. The choice of the number of slots and their location is being optimized.

Tables 8 and 9 compare the expected parameters for the incident proton beam and for the neutrinos at the NGS and at NuMI. While FLUKA97 has been used to calculate the NGS neutrino beam, the numbers for NuMI where obtained with GNUMI[4]. For both facilities, a 'year' is normalized to a period of 200 days with an assumed global machine efficiency of 50%. Thanks to the higher repetition time of the Main Injector (1.9 s compared to 26.4 s), NuMI is expected to provide about six times as many protons per year compared to the NGS. However, the higher incident proton momentum at the SPS (400 GeV/c compared to 120 GeV/c) will result in an increased production of neutrinos at the NGS. For the LBL experiment this partially compensates for the difference in the two projects arising from the number of protons on target (pot). For the case of a possible SBL experiment the difference in pot is somewhat compensated by the larger distance between the target and an SBL experiment in the NGS (1.85 km in the NGS compared to about 1 km at NuMI). Furthermore, for a ν_μ–ν_τ oscillation search an additional factor of at least two in favour of the NGS (SBL and LBL) comes from the reduced ν_τ interaction probability at the lower NuMI neutrino energies.

As outlined in Section 2.3, the NGS operating parameters are those demonstrated to be possible at the present SPS. The various improvements envisaged for the SPS will enable it to operate at even higher intensities. Together with an improved secondary beam, as discussed in Section 3.8, the NGS will increase its proton and neutrino intensities. To conclude, the NGS performance compares well with that of NuMI.

[4]GNUMI is a Monte Carlo beam simulation program based on GEANT, developed at Fermilab by J. Hylen and A. Para, see also [56], Appendix B.

Table 8: Incident proton parameters for the NGS and NuMI. A 'year' is assumed to allow 200 days of accelerator operation with 50% overall efficiency

Protons	NGS	NuMI
Momentum (GeV/c)	400	120
Cycle length [s]	26.4	1.9
Protons per cycle	9×10^{13}	4×10^{13}
Protons per s	3.4×10^{12}	2.1×10^{13}
Total protons per year	2.95×10^{19}	1.84×10^{20}

Table 9: Neutrino beam parameters for the NGS and NuMI. A 'year' is defined in Table 8. It is now known that the FLUKA97 code gives 20% less flux compared to simulations based on GEANT, such as GNuMI

Neutrinos	NGS SBL	NGS LBL	NuMI SBL	NuMI LBL
Simulation	FLUKA97	FLUKA97	GNuMI	GNuMI
ν_μ fluence $[\mathrm{m}^{-2}\,(\mathrm{pot})^{-1}]$	1.09×10^{-3}	4.39×10^{-9}	1.90×10^{-3}	1.72×10^{-9}
ν_μ CC events $[(\mathrm{ton})^{-1}\,(\mathrm{pot})^{-1}]$	1.06×10^{-14}	4.73×10^{-20}	1.01×10^{-14}	1.04×10^{-20}
ν_μ CC events $[(\mathrm{ton})^{-1}\,(\mathrm{year})^{-1}]$	3.13×10^{5}	1.40	1.82×10^{6}	1.89

3.10.2 K2K in Japan

The Japanese neutrino project KEK-to-Kamioka (K2K) [57], currently under construction, will search for oscillation on a long baseline by sending a neutrino beam from KEK to Superkamiokande, 250 km away. Its primary aim is to probe the region of the atmospheric neutrino anomaly with a Δm^2 between 10^{-2} to 10^{-3}.

The K2K project is based on the KEK-PS which operates at 12 GeV and is expected to eventually accelerate up to 6×10^{12} protons per cycle with a repetition time of 2.1 s.

The detection of the neutrino events will be performed by two near detectors situated about 300 m from the target: the fine-grain detector and a one-kiloton water Cerenkov detector similar to Superkamiokande. The far detector is Superkamiokande itself. The secondary π and K from the interactions of the primary protons with an aluminium target will be focused towards the experimental detectors by a system of two magnetic horns pulsed for about 1 ms at 250 kA in coincidence with the proton spill. A decay tunnel of 200 m length and located 20 m downstream of the target will provide the space for these secondary particles to decay. At the end of the decay tunnel, a beam dump will be constructed to act as the hadron absorber. The dump will consist of a 3.5 m thick iron layer and a 2 m thick concrete shielding behind which muon chambers will be instrumented to monitor the muon profile and hence the neutrino spatial distribution.

K2K will study $\nu_\mu - \nu_e$ oscillation with a search for the appearance of an excess of electrons above the background in the far detector, while the $\nu_\mu - \nu_\tau$ channel will be studied by measuring the disappearance rate between the near and far detectors. Owing to the low average neutrino energy (1.4 GeV at the near detector), the direct observation of the ν_τ is not possible at K2K.

A three-year run commencing in April 1999 is expected to result in 10^{20} protons on target, yielding about 400 ν_μ CC events in the 22.5 kton fiducial volume of Superkamiokande.

4 CONCEPTUAL TECHNICAL DESIGN

4.1 Civil engineering

4.1.1 Introduction

The preliminary design of the underground structures making up the NGS project has been drawn up. The requirements considered for this preliminary design were:

- As short a work schedule as possible, taking into account the project dates specified (see Section 6).
- The greatest possible degree of independence between the NGS and LHC-TI8 projects, with a choice of compatible systems.
- The choice of technically economical systems without compromising the durability of the structure.

The status of the project as described here is the one defined in November 1997 by the CERN–INFN Technical Committee. This made it possible to initiate civil engineering design studies by a consortium of two outside consultants, who will produce the technical documents required for the Call for Tender. These documents are due in April 1998.

The project is approached in this section from two distinct viewpoints: first, a description of the various parts is given which contains the main geometrical parameters. Then, an account of the working methods is provided including various items of equipment to be used to complete the project successfully.

4.1.2 Description of the project

General The civil engineering project is divided into five underground structures:

i) the primary proton beam tunnel,
ii) the target chamber and its ancillary structures,
iii) the equipment and personnel access tunnel to the target chamber, including the access shaft,
iv) the decay tunnel,
v) the hadron stop chamber, the muon detector chambers and their connecting tunnels with the LHC.

Towards the SPS accelerator, these structures are connected to the existing hall ECA4 via the access gallery (see Fig. 29), and, at the level of the chamber TJ8, to the LHC injection tunnel TI8. On the side of the LEP/LHC accelerator, a connection is foreseen from the hadron stop area of the NGS to the electrical alcove cavern RE88.

The structures have to be excavated almost entirely from rock, which is Léman basin molasse. This rock consists of variable-quality strata ranging from relatively soft marls to extremely hard sandstones. The methods and means of excavation and support have been matched to this type of rock, as described below.

The sole exception is the access tunnel shaft via which all the civil engineering work is done. Its upper part passes through about 15 m of moraine.

It has been decided to provide access to the work site for the NGS project and to this shaft from the French side of the border for two main reasons:

- the location of this work site area together with that of the LHC-TI8 tunnel is on land already available to CERN;
- on the Swiss side, the land above the target chamber is environmentally protected.

Generally, a cylindrical shape for all the underground structures has been chosen, as it is economically the best choice for this type of ground. The values given in the following description are the final internal dimensions which define the actual available space. To obtain the excavation diameters, the dimensions given in the report must be increased by 0.60 to 1 m to allow for the thicknesses of the temporary support and the final lining.

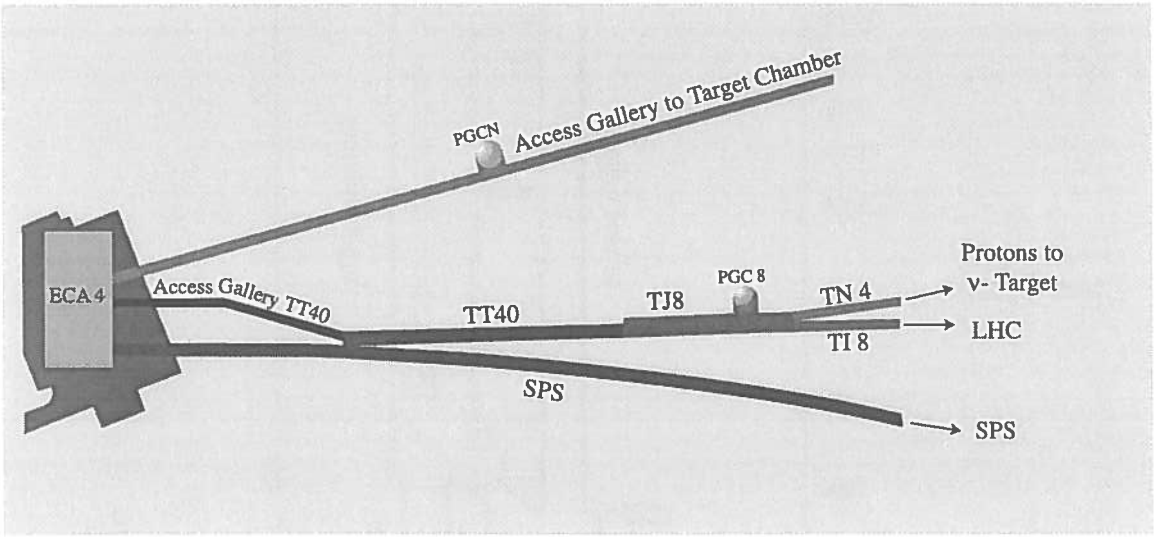

Fig. 29: Schematic view of the tunnels around point 4 of the SPS

Proton beam tunnel From its connection to a stub-tunnel at the junction with chamber TJ8 to the first structure of the target area facilities, i.e. the junction tunnel, the proton beam tunnel is 590 m long. Its diameter is 3.10 m over its entire length[5], except for the last 20 m before the target chamber, where it is 3.50 m. The width of the tunnel floor slab is 2.24 m, with a height at the crown of the arch of 2.50 m. Its radius of curvature in the horizontal plane is about 1 km.

This tunnel has a central main drain buried in the floor slab. The walls and vaults of this tunnel are of concrete cast *in situ*. Its overall slope is 3.50%.

Target chamber and ancillary facilities The target chamber and the surrounding facilities are shown schematically in Fig. 30, the detailed civil engineering layout is shown in Appendix B.

The target chamber itself is a cylindrical cavern 115 m long with a diameter of 6.50 m. At its head is a junction tunnel providing a connection to the access and proton beam tunnels. The length of this structure is 8 m and its diameter 9 m.

This chamber is widened on the south side near the targets to a diameter of 8.50 m over a length of 15 m. It is fitted over its entire length with a 10 ton capacity overhead travelling crane running on steel tracks.

Upstream of the tunnel junction are the following:

- a storage chamber 20 m long and 3.10 m in diameter;

[5]Considering the usual tolerances in alignment and construction, a usable diameter of 3.00 m should be assumed.

– a cavern 15 m long and 9 m in diameter to house the ventilating and cooling equipment, which is fitted on to a 2.70 m high platform providing a passage beneath it.

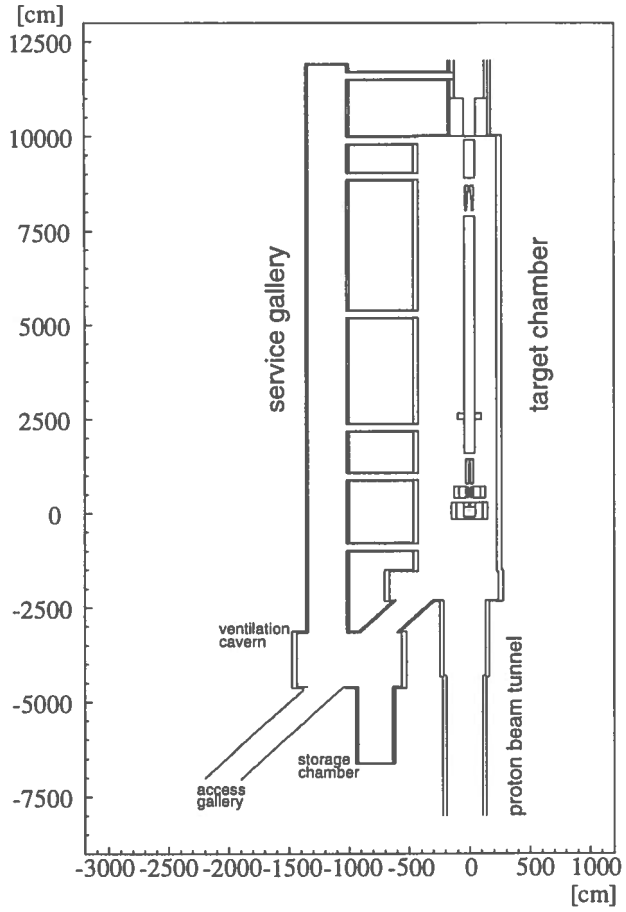

Fig. 30: Schematic top view of the NGS target area

The storage chamber is connected to this cavern on the side opposite the target chamber and on the same side as the access tunnel connection. The ventilation equipment cavern is connected to the target chamber by a tunnel 8.50 m long with the same cross-section as the access tunnel. These ancillary structures are aligned horizontally.

Parallel to the target chamber there is to be a service tunnel 3.40 m in diameter with a total length of 148 m. It is directly connected to the ventilation equipment cavern at one end, and to the decay tunnel at the other, via a perpendicular tunnel 1.80 m in diameter to allow the connection of the vacuum equipment.

At the downstream end of the service tunnel there is a sump of 30 m^3 in volume to take the water draining from all the upstream structures, as well as water from any leaks of the cooling circuit. The sump is fitted with a pumping system to take the collected water to ECA4.

In addition, the target chamber and service tunnel are interconnected by six transverse tunnels 1.80 m in diameter providing access for people and supply connections. The floors, walls, and vaults of these structures are of concrete cast *in situ* except for those of the service tunnel, which have only a shotcrete[6] lining. The overall slope of these structures is 5.62%.

[6]Shotcrete is a concrete without large aggregates, sprayed at high pressure in layers against excavated rock sur-

Access tunnel and civil engineering shaft The access tunnel provides access for personnel and equipment from the existing chamber ECA4 at point 4 of the SPS accelerator to the target chamber via the junction tunnel. It is straight, 768.80 m long and 3.10 m in diameter. The floor slab has a width of 2.36 m in which the pipes for drainage and for discharging the water from the target chamber sump are embedded. The maximum headroom is 2.55 m. The overall slope of the structure is 2.20%. Its walls and vaults are shotcreted over the entire length.

The shaft from the surface providing access for all construction work is at 130 m from the existing chamber ECA4. It is 57 m deep with a diameter of 8 m and is connected and centred on the access tunnel at its base.

This structure is for temporary use only and therefore its walls are protected only by shotcrete and rockbolts. Once the entire project has been completed, this shaft will be covered at the surface by a reinforced concrete slab and the local environment restored to its original state as far as possible.

Decay tunnel The decay tunnel is located between the downstream end of the target chamber and the upstream end of the hadron stop chamber. It contains the steel pipe in which a vacuum of 1 mbar is created so that the secondary particles can decay in flight, undergoing only little interaction or multiple scattering. The tunnel is 994 m long and its inside diameter is 3.10 m. After the passage of the tunnel boring machine, the walls and vaults are shotcreted. The base of this tunnel consists of prefabricated segments for use as a track for carrying the iron blocks to the hadron stop and fitting the steel pipe.

The inside diameter of the steel pipe, which is of the same length as the tunnel, is 2.45 m (96″). It is made of 6 m sections welded *in situ*. The space between the steel pipe and the tunnel is filled with concrete.

The overall slope of this tunnel is 5.62%. It passes 9.80 m below the LEP/LHC tunnel, shortly before reaching the hadron stop.

Hadron stop chamber, muon detector chambers and linking tunnels The general layout of the hadron stop and the surrounding area is shown in Fig. 31, the details of the civil engineering in this region are given in Appendix B. The total length of the hadron stop chamber itself is 26 m with a diameter of 6 m. It is mainly intended to contain a volume of $4 \times 4 \times 18\,\mathrm{m}^3$ of steel blocks, graphite, and aluminium elements to stop the hadrons. The decay pipe projects into this chamber over a length of 2.50 m. The widened section thus provided around the end of the decay tunnel is intended to allow the steel blocks forming the hadron stop to be handled. The walls of this chamber are of concrete cast *in situ*. The spaces between them and the steel blocks of the hadron stop are filled with concrete. The last 5 m long downstream section of the hadron stop chamber houses muon detector No. 1.

There is a perpendicular tunnel section 20 m long and 3.10 m in diameter on the south side of the region of muon chamber No. 1. At the end of this tunnel section there is a connecting chamber 10 m long and 4 m in diameter for the passage of detector equipment and to house the electronic and ventilation/cooling equipment. This chamber is itself connected to the end of the existing alcove RE88 of the LEP/LHC tunnel via a tunnel 224 m long and 3.10 m in diameter for access and various connections. This tunnel consists of a straight and a curved section. Their slopes are respectively 5.64% and 10.80%.

A second muon chamber 6 m in diameter and 3.50 m long is located at 67 m from the first one on the beam axis, housing muon detector No. 2. It is linked to the connecting chamber

faces. It is required to provide immediate protection and stabilization of the rock around the foreseen underground structures.

mentioned previously via a tunnel 104 m long and 3.10 m in diameter. This tunnel consists of two straight sections at an angle of 75° connected by a curved section. Its overall slope is 3.76%.

The walls and vaults of all the connecting tunnels and chambers are shotcreted, while those of the muon detector chambers are of concrete cast *in situ*.

Each of the muon detector chambers is equipped with a sump for collecting drainage water.

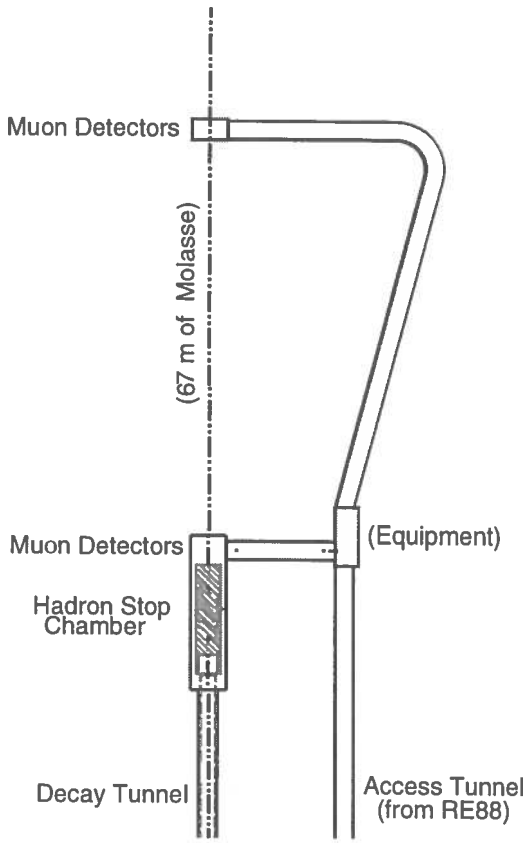

Fig. 31: Schematic layout of the hadron stop chamber, the muon chambers, and their access tunnels

4.1.3 Working methods

General The civil engineering for the project is based on two essential conditions:

- The dates when the various underground structures have to be available for the installation of the equipment (see Section 6). These dates in turn depend on the objective to obtain the first neutrino beam in May 2002, despite the fact that the first proton beams for the LHC will not use the tunnel TI8 until October 2003. Generally speaking, these deadlines require a very rapid construction as shown in the project planning (see Section 6).
- The desired independence of the two projects: NGS and LHC-TI8. This entails provision of separate access shafts and separate means for performing the work for the NGS.

It should be noted that the work on the LHC-TI8 project has to be speeded up over the initial LHC programme to make it compatible with that of the NGS project.

These two parameters have of course affected the choice of equipment and working methods, as shown below.

Material resources The material resources to be used by the contractor for this work should be:

- For excavating the access shaft: traditional, using explosives and a rock breaker.
- For excavating the standard cross-section of all the tunnels (except, possibly, for the proton beam tunnel and part of the access tunnel): a single-shield Tunnel Boring Machine (TBM) with a diameter of about 3.50 m.
- For excavating the chambers and tunnels not made using the TBM: point-action machines (roadheaders) of various gauges, dumpers and rock breakers.
- For the concrete lining: several heavy-duty shotcreting machines (for temporary and permanent walling) and a set of curved shuttering with trains or pumps for transporting the concrete.

The means of transport over the entire run (underground and surface) for the spoil in one direction and concrete in the other also have to be provided.

By and large, all the equipment described above is that required in the specification of the call for tenders. Bidders are free to propose similar equipment which is more available to them, or more fitted to their own working methods, constrained by the proposed time schedule.

Performance sequence of the work

Excavation The performance sequences for the excavation work designed to meet the required schedules are:

1. Excavation of the access shaft and a chamber at the shaft foot (see Section 3.2).
2. Lowering the tunnelling machine into and assembling it in this chamber.
3. Using the TBM to excavate successively and without interruption:
   - the access tunnel,
   - the connecting tunnel and the target chamber (to the actual diameter of the TBM),
   - the decay tunnel,
   - the hadron stop chamber up to its end (to the actual diameter of the TBM).
4. At the same time excavation of the access tunnel section from the shaft to chamber ECA4 using a roadheader.
5. Also at the same time and depending on compatibility with the removal of the spoil from the TBM, widening the various upstream chambers to their final dimensions using a roadheader. The same applies to the structures not directly located on the TBM run, e.g. the service tunnel or the storage chamber.
6. There are two options once the TBM has finished this excavation: either the TBM is dismantled, transported to and removed via the PGCN shaft, implying that the proton beam tunnel is excavated with a roadheader, or the TBM is dismantled, carried to the target chamber and reinstalled in the opposite direction in order to excavate the proton beam tunnel.
7. At the same time as the above work with the TBM is being carried out, all the remaining excavation work can be performed using a roadheader: widening the hadron stop chamber and detector chamber No. 1 to their final dimensions, excavating the access tunnel to the muon detector chamber No. 2 and the chamber itself, completing the connecting tunnel to the existing LEP/LHC compartment RE88, in compliance with the radiation protection requirements (and taking advantage of the LEP annual shutdown). Where appropriate, the excavation work on the ancillary chambers and structures near the target chamber can also be completed with a roadheader.

Concreting The concrete lining of the structures will be carried out as follows:

1. For the access and service tunnels, shotcreting should be applied as the excavation progresses. It is very important to protect the molasse walls quickly as the rock deteriorates very rapidly in contact with air and may give rise to dangerous swelling, cracking and rockfalls. A flat floor should be laid using prefabricated concrete segments or concrete cast *in situ* once the excavation has been completed.
2. For the other structures of the project except for the decay tunnel, the vault should be made by slabbing and walling using concrete cast *in situ* and the usual finishing work. The steel track beams for the overhead travelling crane in the target chamber should be secured on anchored metal supports or on curved steel profiles embedded in the concrete of the vault.
3. Concerning the decay tunnel, the metal pipe should be taken to the point of work via the shaft and access tunnel in 6 m long sections. The sections, after careful wedging and alignment, are welded *in situ* and inspected. The annular space between the pipe and the excavation is filled with 'non-shrink' concrete as each section is installed.
4. For the hadron stop chamber 'non-shrink' concrete is to be used around the cast iron blocks after their installation.

Deadlines and comments According to present planning, the civil engineering work, except for the fitting of the metal pipe in the decay tunnel, is to be completed in December 2000, or February 2001 allowing for the clearing of the work site. The fitting of the metal pipe is to be completed in January 2002.

The working rates needed to make it possible to attain these difficult objectives necessitate the use of highly competent and reliable contractors who have *ad hoc* human and material resources available.

A rigorous selection procedure must be set up, drawing heavily on the experience gained in civil engineering for the LHC project, to ensure that these goals are met.

4.2 Geodesy and metrology

4.2.1 Introduction

Directing a neutrino beam to a remote detector at 732 km distance is a long-range sighting problem, the parameters of which are expressed in terms of absolute positions of the origin and of the target. This permits the deduction of the related azimuth and slope of the vector. All computations must, of course, be made in a common coordinate system but they must also take into account some physical aspects of the Earth, i.e. gravity field anomalies and their effects.

The divergence of the neutrino beam and the resulting distribution at the Gran Sasso Laboratory can be roughly estimated from the typical transverse momentum of ν_μ from π decay (30 MeV/c) and from the typical pion momentum in the reference beam (50 GeV/c). The resulting order of magnitude is 0.6 mrad for the divergence, thus 450 m for the beam size at Gran Sasso. Simulations of the reference beam yield a transverse beam size of about 850 m (1σ, see Fig. 26). For the purpose discussed here, a maximum offset of 100 m from the ideal beam position at Gran Sasso is therefore assumed to be sufficiently accurate.

This maximum offset has been adopted as a goal, and the geodetic process must therefore try to comply with final r.m.s. errors of ± 37 m, as far as random errors alone are concerned. This corresponds to $\pm 5 \times 10^{-5}$ rad r.m.s., i.e. 10 arcsec. Such a specification for the geodetic process is not easy, but is achievable. Nevertheless, other uncertainties and various error sources may affect the direction and the slope of the beam during operation, like geomechanical forces

on the constructed structures, thermal expansion and mechanical constraints on the critical components, etc.

Another crucial point is the length of the sighting baseline and its stability during the running period. From this point of view and referring to the above specification ($\pm 5 \times 10^{-5}$ rad r.m.s.), the baseline can hardly be thought of as the magnetic horn alone: How to guarantee such an angular accuracy and stability on its magnetic axis at all stages of the installation and operation?

Supposing now that this stability condition is given and try to solve the alignment problem upstream of the horn: the criticality would therefore lay on the last straight segment of free trajectory, i.e. between the last horizontal/vertical corrector and the axis of the horn. Knowing that the possible deformations and movements can progressively reach millimetres, it becomes a monitoring problem, complicated by the hostile radiation level of the area.

The NGS project foresees a muon detector station at the end of the decay tunnel after the hadron stop, and the reference segment for the final alignment has therefore its origin at the exit axis of the horn and its end at the centre of the muon detector. This is the only way to provide a checking of the beam set-up and stability during operation. The following study and discussion for the geodesy and metrology of the project is based on this 1 km long baseline.

4.2.2 Geodetic parameters

Preliminary data As usual, the preliminary data were either coarse geographic coordinates (latitude ϕ and longitude λ) interpolated from cartographic maps or, more precisely, issued from transformations between national and global systems. Then these ellipsoidal data were transformed into isometric coordinates on a sphere, in order to solve the 'position' triangle by the means of spherical trigonometry and to obtain the initial data of the line: azimuth, slope and distance. Nevertheless, it is well known that our cartographic systems are based on old (historical) data and are subject to various discrepancies and distortions, which depend on the ellipsoid chosen as the mathematical model, the deflection of the vertical at the datum (origin) and across the geodetic network, the cumulation of measurement errors, the bridge distance between astrogeodetic control points, etc. The resulting errors can reach the order of metres across large national networks, they can be much more between systems (one arc second error in ϕ or λ leads to an error of 31 m in position).

Final parameters All these old problems are now perfectly mastered by modern spatial geodesy. The techniques used for continental/intercontinental links are Very Long Base Interferometry (VLBI) by correlation of signals from quasars, Satellite Laser Ranging (SLR) by very accurate timing of the flight time of ultrashort pulses, and Global Positioning System (GPS) used in a sophisticated differential ('interferometric') way, with measurements of the phase differences on the two carriers, at 1.2 and 1.5 GHz. This latter technique can reach an accuracy of 10^{-8}, or even better at the permanent stations used for orbitography and for intercontinental measurements.

The link between CERN and Gran Sasso does not need to be so accurate in terms of relative positioning, but the orientation parameters remain critical. Horizontally, the precise knowledge of the azimuth depends only on the angular differences between the local system and the GPS satellite system(s). Vertically, the precise knowledge of the slope is additionally affected by that of a reference equipotential surface, called 'geoid' and defined at a presupposed zero level of the coordinate system. This is a consequence of a physical fact: altitudes (i.e. elevations above zero level) are measured by levelling techniques, which refer to gravity, whilst the GPS Z coordinates are orthogonal heights above the reference ellipsoid, called GRS80. The

general problem is therefore to 'map' the geoid and its undulations with respect to the GRS80 surface, used for geometrical computations [58]. Such undulations of our level 'zero' relate to gravity anomalies and deflections of the vertical: the induced vertical discrepancies can reach regionally 60 m between mountains and seas, and up to 140 m from hollows to bumps in the global geocentric model! In the limited area of CERN, with the effect of the Jura mountains, a precise study of the local geoid has been made for the construction of LEP, by means of mass models and accurate astrogeodetic measurements, and it has shown a maximum local distortion of about 14 cm over 10 km [59]. This is not at all negligible, but due to the good knowledge (to a few millimetre accuracy) of the local undulations around CERN, the only remaining uncertainty is in the slope of the CERN local geoid with respect to the GPS satellite system(s), in the direction of the beam line.

All these orientation and slope parameters can be obtained from careful GPS measurements of some stable points of the CERN geodetic network, linked to national and/or international reference GPS points (i.e. permanent stations), expressed in a common computational system: World Geodetic Reference System 1984 (WGS84) in a first stage, and then European Reference Frame (EUREF) for refined data. For the Gran Sasso side, simple differential GPS measurements at both ends of the tunnel and a connection of these new points to the surveying data of the underground laboratory would be sufficient [60]. Nevertheless, the precise assessment of the parameters of the CERN local geoid with respect to national and international (geocentric) models is not a trivial problem, and this may leave more uncertainty on the slope.

4.2.3 Successive stages of the geodetic process

In accordance with the schedule of the final construction design, and in order to ensure the optimal set-up of the geodetic parameters along the beam lines (mainly along the last straight segment under control), the geodetic process consists of the following:

1. Differential GPS measurement of two points at Gran Sasso (already made) and a link to reliable survey data, in order to locate correctly the theoretical target point. Errors of a few metres would not be significant when considering the rather large divergence of the neutrino beam.
2. First GPS campaign at CERN (required for the LHC) in March/April 1998.
3. First refinement of the geodetic parameters of the neutrino beam line, by reworking all preliminary computations with coherent data, recently measured and expressed in the WGS84 system — in order to provide checked values for civil engineering.
4. Second GPS campaign at CERN, limited to the primary geodetic network, in collaboration with the Laboratoire de Recherche en Géodésie (LAREG, Paris) and the Institut Fédéral de Topographie (L+T, Berne). This accurate measurement creates the links to some national and/or international reference GPS points in France and in Switzerland, in order to enlarge the span of the comparison between tridimensional systems and to reduce the errors in the resulting transformation parameters over the CERN area. It mainly allows a study of the dual assessment of the geoid, from both sides, according to the models adopted in each country [61],[62]. Final conclusions are drawn for expressing the best transformation parameters of the 'local' geoid used in the CERN coordinate system.
5. Last refinement of the geodetic parameters of the neutrino beam line, from coherent GPS data expressed in the EUREF system and with the optimal transformation parameters between all useful coordinate systems and reference surfaces, including a sufficient knowledge of the local and global geoids. This provides the final theoretical data for the positioning of beam components.

6. New calibrations of the gyrotheodolite, on the primary geodetic network, for expressing its measured azimuths in the EUREF system, along with measurements in the tunnels.

The details of the geodetic metrology of the underground beam line, starting from the SPS extraction region and ending at the muon detector pits, is described in Appendix D.

4.3 Proton beamline TN4

The general layout of the primary proton beam line, to be called TN4, is shown in Figs. 6 and 7. The primary proton beam for the NGS uses the new fast extraction system of the SPS and the first part (called TT40) of the beam transfer line TI8 from the SPS to the LHC [39], [45]. The LHC proton beam fills 3/11 of the SPS ring (23 μs $\times$ c in circumference) so that the rise time of the existing extraction kicker system is largely sufficient for this application. The proton beam for the NGS facility, on the contrary, consists of two batches, 10.5 μs long and separated by 1.05 μs. The rise and fall times of the kicker system are about 15% too long. It is planned to reduce them to the required values by shortening the length of the magnets. The corresponding loss of deflection strength is then compensated by an additional magnet. The two batches are extracted successively with an interval of 50 ms towards the NGS target.

4.3.1 Beam optics and magnetic structure

After 110 m a set of eight dipoles is used as a switch to branch off the TN4 proton beam from TI8. These switch magnets together with their power supply and vacuum chambers will be recovered from the existing WANF. They give a total deflection of 25 mrad. The rest of the primary proton beam line essentially consists of a 580 m long arc to bend the beam in the direction of Gran Sasso, followed by a 90 m long focusing section to obtain the desired beam size on target. The arc must provide a horizontal deflection of 33° and a final vertical slope of 5.6%. This is achieved by using 73 new 6.3 m long dipoles, each of them deflecting by 8 mrad. These magnets are enlarged versions (37 mm gap height) of the dipoles used in TI8. The required vertical aperture for these magnets can be estimated using the formula:

$$A/2 = (n \times \sigma + D \times \Delta p/p) \times k_\beta + C.O.,$$

where D is the dispersion function, k_β the optical mismatch factor (taken to be 1.1), $\Delta p/p$ the momentum spread (actually 0.12%), $\sigma = \sqrt{\beta\epsilon}$ the betatronic r.m.s. beam size and $C.O.$ the deviation from the ideal beam trajectory. A normalized emittance of $12\pi \times$ mm $\times$ mrad is assumed in both transverse planes ($0.028\pi \times$ mm $\times$ mrad physical emittance at 400 GeV/c). Table 10 contains the different contributions which have to be accommodated in the gap height of the main bending magnets.

The maximum vertical dispersion is 1.1 m and a peak trajectory excursion of $C.O. = 4$ mm is assumed, as in the case of TI8 [63]. With these assumptions, space is left for $\pm 5\sigma$ transverse beam dimension in the magnets[7]. This includes the beam size as such, the kicker and power supply ripple, and the SPS closed-orbit imperfections.

The magnetic field of the main dipoles is 1.9 T at 450 GeV and 1.7 T at 400 GeV. A careful choice of the parameters for these magnets makes it possible to use the same power supply as for TI8, because filling the LHC and sending a proton beam to the NGS target at the same time is not possible. This option has been retained to reduce the cost of this project. In any case, the required vertical direction is obtained by tilting 32 of the magnets along the beam axis by 12.8°.

[7]Note that $\pm 6\sigma$ are foreseen for the transfer lines to the LHC. In the final NGS design, a scheme with more correction elements for the beam trajectory might have to be used in order to reduce the contribution of $C.O.$

Table 10: Physical vertical aperture of the main dipoles in the TN4 line

Item	Size [mm]
Nominal gap height	37
Vacuum tube wall thickness (including tolerances and and insulating foil)	2×1.5
Sagitta	±0.5
Magnet misalignment ($\pm 2\sigma$, $\sigma = 0.2$ mm)	0.8
Mechanical tolerances	±0.2
Remaining full physical aperture	31.8

The common part (TT40) and the first two quadrupoles in the line are used to match the optics parameters of the SPS to the FODO lattice of the neutrino line. The arc is made of seven cells of this FODO lattice ending with five shortened cells to cancel the horizontal dispersion by means of individually powered quadrupoles. The half-cell has a length of 31.3 m and is made up of a quadrupole followed by a short straight section and four dipoles. The short straight section offers space for a monitor and a steering dipole to adjust the beam trajectory. The shortened half-cell includes only three dipoles. The quadrupoles are an enlarged version of the ones used in TI8, their length is 2.2 m and the inscribed diameter is 45 mm. The nominal gradient of these quadrupoles, of which 21 have to be built, is 40 T/m. The arc quadrupoles are powered by power supplies recovered from LEP. The final focus consists of three quadrupolar lenses. The first one is a single magnet which increases the horizontal dimension of the beam. Then follows a doublet which focuses the beam onto the target to achieve a final spot size of 2 mm in both directions at 400 GeV ($\sigma \approx 0.3$ mm). The first lens of the doublet is made of three quadrupoles powered in series and the last one of two such magnets. Both the magnets and the power supplies for this section are salvaged from existing CERN facilities (SPS West Area and LEP). The optical functions for the beam line are shown in Figs. 32 and 33.

Beam steering along the beam line still has to be studied. Using a scheme comparable to TI8 would imply around 12 new steering dipoles. Four recovered dipoles have to be added to allow an orthogonal steering in both directions onto the target. The new steering dipoles would be powered with small ($\sim$ 3 A) power supplies. As for TI8, the cores would be recovered from LEP correctors and appropriate pole pieces would have to be added.

4.3.2 Beam monitoring

The beam steering of the TN4 line uses the information from beam-position monitors (pick-up devices), as foreseen for TI8. The monitoring of the proton beam at the target and of the secondary hadron beam is performed by a system comprising one or more Beam Current Transformers (BCTs) upstream of the target and by Secondary Emission Monitors (SEMs).

The BCTs, located immediately upstream of the neutrino target, measure the number of protons per spill impinging on the target. Experience from the WANF shows that the BCTs can provide a very accurate determination for the absolute proton intensity with fast-extracted beams of the order of 1%.

The proton intensity is also measured by the SEM foils situated in front of the target. SEMs work on the principle that a traversing charged particle liberates electrons from the surface of a metal foil, thereby providing a current which is proportional to the incoming beam intensity.

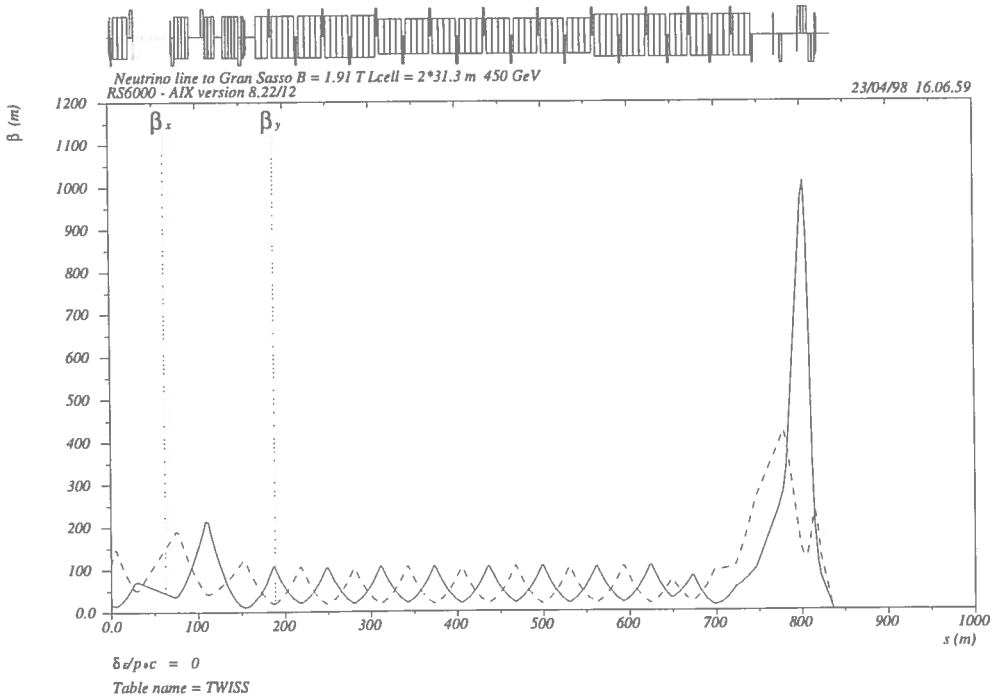

Fig. 32: TN4 proton beam optics (horizontal and vertical β-functions)

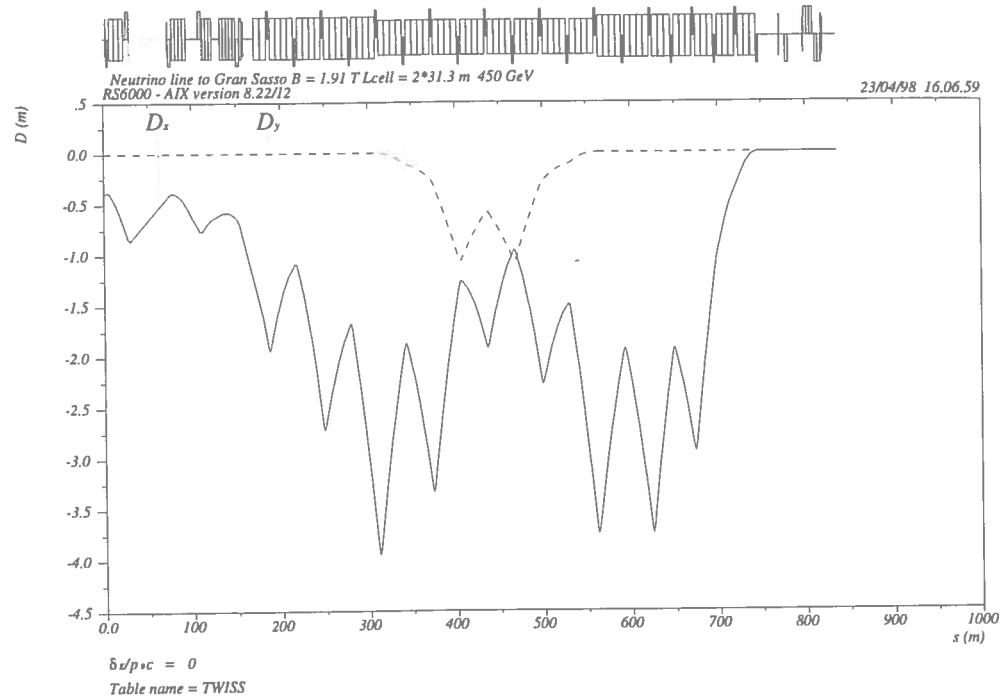

Fig. 33: TN4 proton beam optics (dispersions)

SEMs are typically made from metallic foils, e.g. aluminium or (more recently) titanium, but have been found to be less accurate than the BCTs. However, they are required for the steering of the proton beam onto the target. The ratio of currents measured in SEMs located immediately downstream and upstream of the neutrino target provides an estimate of the multiplicity of secondary particles produced from the target. For correct steering this multiplicity value should be maximized. In addition, by using SEM grids oriented either vertically or horizontally, a measurement of the proton beam position and size is obtained.

4.4 Target station

4.4.1 Target station design

The heart of the target station is the target box: 11 graphite or beryllium thin cylindrical rods are aligned in a cast aluminium box. They are cooled by helium gas in a closed circuit with the flow adjusted to each rod. The box is motorized horizontally and vertically at both ends, to remotely optimize the secondary particle production by aligning the target with the incident proton beam. Radiation protection around the station is guaranteed by about 300 tons of shielding material: iron, copper, marble, and concrete. A schematic view of the target station is shown in Fig. 13, detailed drawings can be found in Appendix B.

Target box The cast aluminium box is designed to receive either graphite or beryllium rods: 11 rods of 3 mm diameter by 10 cm long, spaced every 9 cm. Each one is supported by two thin (2 mm) hollowed-out disks of the same material, which ensure its lateral positional precision and a certain axial freedom. The two disks are fixed to a U-shaped aluminium support, and the supports are aligned by a channel milled in the bottom of the box. The alignment precision of the rods is ± 0.03 mm. Three longitudinal conduits, cast into the structure, ensure the circulation of the coolant gas; they are extended upstream by stainless steel flexible tubes which traverse the shielding. The inlet conduits terminate with 22 stainless steel jets, disposed in opposing pairs either side of each rod.

The box is sealed by a bolted aluminium cover, and by two titanium beam windows of 60 mm diameter and 0.1 mm thickness. The horizontal and vertical displacement (± 20 mm) of each end of the box is achieved by mechanisms driven by DC motors located under the box and protected from radiation by a thick shielding plate which transmits the movement. The target box, the mechanisms, the motors, and the shielding plate are considered as a unique assembly, which should only be pre-positioned (± 0.5 mm) during the first installation and subsequent replacements, the final alignment being refined by a few iterative beam efficiency optimizations, as was successfully, rapidly, and cheaply done at the WANF [64].

The experience gained during the last years of neutrino beam operation at the WANF shows that, after only a few months, movable equipment near the target becomes unreliable due to radiation damage. However, experience also shows that these few months of operation are sufficient to perform the necessary target-box position adjustments. After the target alignment, the motors are electrically disconnected to prevent accidental movements of the target box.

The target box assembly defined above (box, mechanisms, motors, and shielding plate) is taken out of the front end of the station by removing at the same time the upstream collimator and monitor (TBIU); this is done after having disconnected the three helium flexible tubes, plus 6.7 m of upstream vacuum chamber (see Figs. B.4, and B.5 in Appendix B). All these operations, as well as the reverse ones, should be performed quickly and safely, with minimum irradiation of personnel, by means of automatic or semi-automatic procedures which still have to be technically finalized.

Helium cooling Helium flow from each pair of jets is calibrated experimentally, by means of diaphragms of differing diameters positioned at their entries. Flow is maximal on the second rod (about 50 l/s), and diminishes progressively to the last one (about 10 l/s). The gas flow is provided by a 1465 turns/min Roots pump housed in the service gallery, delivering 2000 m^3/h at atmospheric pressure to the target box, via two water-cooled heat exchangers and over 20 m of flexible piping. This circuit, fitted with numerous joints, is not perfectly tight (which would be unnecessary and expensive); consequently, the helium system should be purged twice per week during periods of operation, and once per week otherwise; an automatic procedure could easily be implemented, if required. The heat transfer coefficient between rod and helium (about 500 W/m^2 °C for the first rod) was measured in a similar laboratory test installation, with 'silver steel' rods of the same dimensions.

Helium gas is an excellent medium for protecting the target rods (especially graphite) from oxidation. Acquired experience demonstrated that helium cooling is efficient, safe, inexpensive, and does not need any additional cooling like water or air: interior air ventilation initially provided for the WANF was rapidly removed because of irradiated dust inside the station.

Shielding and handling An iron shielding encloses the target box assembly; it ensures the lowest possible radiation dose to maintenance personnel compatible with restricted access areas. The shielding base supports two lateral fixed walls and two collimators: the upstream collimator (60 mm diameter) is movable to allow the exchange of the target, the downstream copper collimator (85 mm diameter) is cooled by six independent water circuits. This 'sarcophagus' is closed by a fixed cover, surmounted by 20 cm thick concrete plates. The two lateral sides are protected by an additional 40 cm of marble. The shielding elements are handled by an overhead travelling 10 ton crane. The iron elements and the copper collimator are shaped to respect this weight limitation. At the same time, the design avoids leaks in the shielding by means of overlapping edges (see Fig. B.7 in Appendix B).

Appropriate dismantling facilities are foreseen, anticipating among other scenarios a possible crane immobilization; this is one of the reasons why a sufficiently large lateral passage is required on each side of the target station. These facilities will be refined with the help of a wooden model, and video films will be made during the first installation for later training of the maintenance teams.

4.4.2 Summary of the thermomechanical analysis

The maximum thermal and mechanical constraints that a target can safely accept depends on its geometry, on the material that it is made of, and on the beam characteristics: energy, intensity, proton beam spot size and divergence, burst duration, and repetition rate. The parameters used to estimate the thermo-mechanical stresses of the target are shown in Table 11.

In order to maximize the safely acceptable ultimate beam intensity on target, the appropriate target material and rod length have to be chosen. A 1-D analytical method of thermomechanical analysis [65], which proved to be in good agreement with the classical 2-D finite-element method [66], allows an easier optimization of target length as a function of beam intensity and burst duration. Details of the calculations, performed for beryllium and isotropic graphite rods, can be found in Appendix C. A summary is given here.

Detailed FLUKA simulations of the energy deposited in the target rods show that the highest energy density is found in the first rod. Therefore, for the thermomechanical analysis, only this rod is considered. The 1-D analytical calculations for this first rod provide the theoretical beam intensity limitations for different rod lengths and FE burst duration as summarized in Table 12.

Table 11: Parameter values investigated in the thermomechanical analysis of the NGS target. Bold values are those assumed for dedicated SPS operation (see Section 2.3)

Target diameter	3 mm
Proton beam energy	$\leq$ 450 GeV
Intensity	$\leq 5\times10^{13}$ protons/elementary SPS cycle
Spot diameter ($\pm2\sigma$)	2 mm
Divergence	$\approx$ 0 mrad
FE duration	6, **10** or 20 μs
Bursts per cycle	1, **2** or 3 bursts
Repetition time	6, **7.2** or 8.4 s

Table 12: Maximum allowed intensity per burst for a 450 GeV FE beam on beryllium and graphite targets, in units of 10^{13} protons

	Beryllium			Graphite		
Burst duration (μs)	6	10	20	6	10	20
Rod length $2L$ (mm)						
60	0.96	1.19	1.32	1.83	1.95	2.12
70	0.84	1.16	1.30	1.83	1.95	2.12
80	0.78	1.13	1.20	1.83	1.95	2.12
90	0.78	1.06	1.17	1.83	1.95	2.12
100	0.78	0.97	1.24	1.83	1.95	2.12
110	0.78	0.90	1.23	1.83	1.95	2.12
120	0.78	0.83	1.22	1.83	1.95	2.12

It is found that graphite can resist the thermomechanical shock of 10 μs FE proton beam bursts at about twice the intensity compared to beryllium. Moreover, the length $2L$ of the graphite rods is no longer correlated to maximum intensity at relatively low values (i.e. already from $2L = c_s \times t_0 = 23.2$ mm for a 10 μs FE burst duration, see Appendix C).

4.4.3 Work outstanding

The present working hypothesis for the NGS target is to use a structure of 11 graphite rods, as described above. However, several issues still need to be carefully addressed:

- The final optimization of rod geometry and spacing for graphite, strongly related to the optimization of the neutrino beam optics.
- A search for a commercial graphite and beryllium with the best mechanical properties.
- A sample test of a graphite rod under realistic FE conditions using the WANF facilities, if possible.
- A 3-D estimation of off-axis beam effects. These will most likely lead to more constraints on beam steering accuracy rather than on intensity limitation.
- The technical study of target box handling facilities.

4.5 Secondary beam elements (horn and reflector, helium tank, collimators)

The secondary beam line equipment located behind the target down to the entrance window of the decay tunnel includes:

- A pulsed horn (Figs. 34 and 35) and a pulsed reflector. These magnetic elements produce toroidal magnetic fields along the beam axis. They consist of two cylindrically symmetric thin aluminium alloy current sheets properly shaped as described in Section 3.4, to focus the pions and kaons emitted from the target into a nearly parallel beam. This maximizes the neutrino flux seen by the detector for a wide-band neutrino momentum distribution.

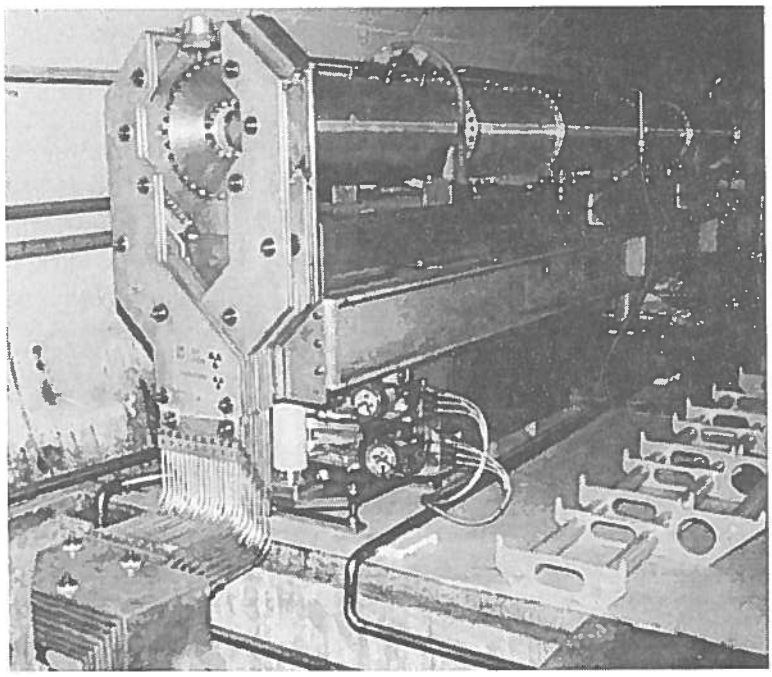

Fig. 34: Photograph of the WANF magnetic horn

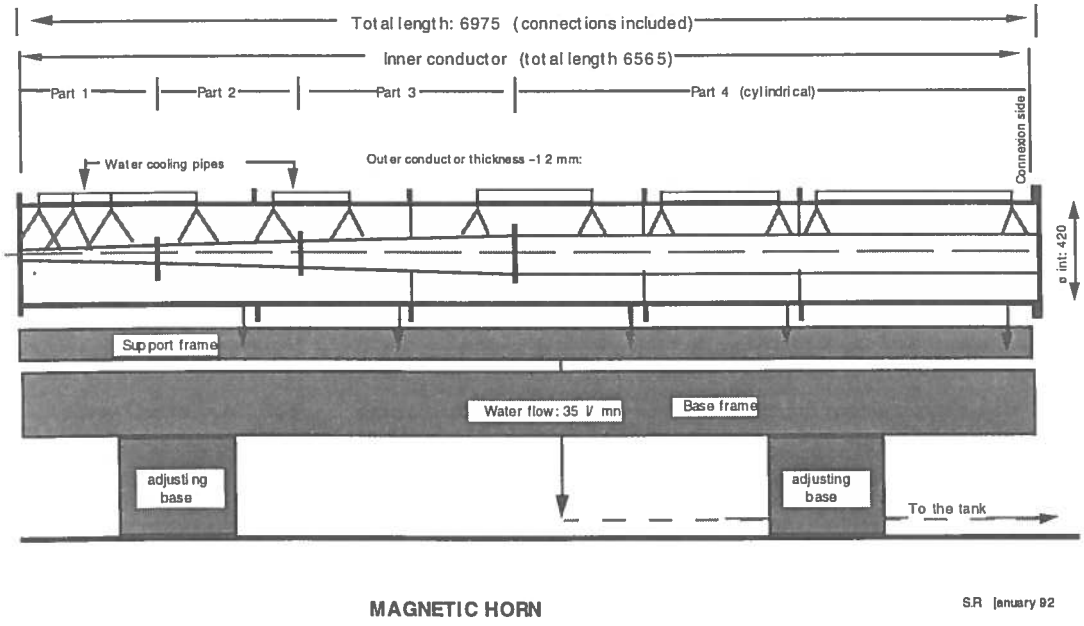

Fig. 35: Schematic view of the general assembly of the magnetic horn (dimensions in millimetres)

- A helium gas tank at a slight overpressure, reducing the absorption effect of the neutrino parents. This tank fills the useful decay volume between horn and reflector.
- Massive collimators COLL2 and COLL3 whose aim is to collimate the hadrons in order to reduce the number of neutrinos of the wrong sign and to reduce the activation of the walls of the target chamber and decay tunnel.

For the design and construction of these elements, the WANF experience is a valuable guideline. Details of the present WANF secondary beam elements are described in Ref. [43].

4.5.1 Horn and reflector mechanical systems

Design principles

- Apart from their inner and outer conductor shaping, the horn and reflector systems are conceptually identical. We have chosen two independent systems for reasons of flexibility.
- Since the horn and reflector are highly irradiated, organic insulation material has to be avoided: the use of an adapting pulse power transformer with low voltage on the horn/reflector solves this problem since the use of glass–mica compounds becomes possible.
- A maximum of components have to be kept outside the target chamber and are located in the service gallery.
- The inner conductor, end plates and, to a smaller extent, the outer conductor have to be as thin as possible to minimize the absorption losses of secondary particles.
- Higher currents lead to higher cone angles of the inner conductor, so reducing the path and the corresponding absorption of the secondary particles through the aluminium walls.
- The horn and reflector are electrically pulsed. Therefore, the structure is submitted to dynamic repetitive forces inducing fatigue effects. The inner conductor is, in first approximation, forced into traction when pulsed. The design goal is to provide full reliability over at least 10^7 current pulses.
- Precise centring of inner and outer conductors and accurate azimuthal thickness of the wall are very important since electromagnetic forces tend to pull the conductor into the centre line, thus creating alternate flexion.
- The degree of revolution symmetry of the magnetic field distribution has to be as high as possible, especially on the current feeding side of the magnetic volume: a basic condition to be fulfilled is that the currents in the feeding strip-lines be equal.
- The horn and reflector need to be water-cooled (the possibility to cool the reflector with air is envisaged). The high radiation level contributes to the production of a highly corrosive atmosphere. Metal surface treatment needs to be carefully studied.
- Quality and reliability of the electrical contacts is a particularly critical issue. One should keep in mind that contact pressure must not vanish when pulsing.
- Precise displacement of the remotely controlled horn and reflector is crucial in order to tune the beam position and angle at the muon counters (and thus at Gran Sasso).
- Easy exchange of horn or reflector with minimal human intervention is compulsory. An overhead crane with remote control and video camera is proposed, complemented with special tools for connection/disconnection from the feeding strip-lines.

Horn and reflector currents The operational currents retained are $I_H = 120\,kA$ and $I_R = 120\,kA$. Fatigue effects caused by 10 million alternate tractions are taken into account when considering the mechanical stress limit. Stress calculations and experimental results from

the WANF beam operation confirm that the expected lifetime of 10^7 pulses, corresponding to typically four years of operation, is realistic.

General mechanical concept The magnetic horn for the present WANF as seen from the electrical connection side is shown in Fig. 34. The construction of the NGS horn and reflector is very similar. The attachments to the flexible copper grids connected to the feeding strip-lines are visible. The flexibility of these grids allows the horn or the reflector to be moved in the up/down and left/right directions as required during the alignment procedure. The copper grids are made of 16 flexible copper cables (50 mm^2 section each) soldered with tin into the copper connection bars. Each grid assembly is then silver-plated (flush of 10 μm).

Mechanical construction

General assembly:

Figure 35 shows the general assembly of the horn station and its overall dimensions. The horn is screwed onto a support frame. This assembly is picked up by two hooks, transported and precisely placed in position by means of the overhead crane onto a base frame. The positioning is ensured by special vertical girders so that the support frame comes accurately into place when deposited.

Remote alignment on the beam:

The base frame is itself attached to two adjusting bases each equipped with one vertical and one horizontal DC motor with corresponding position sensors. Remote horizontal and vertical adjustments are possible for the beam entrance and exit part of the horn. The movement ranges are ± 5 mm for each direction with a precision of 0.01 mm.

Inner conductor:

It is made of four pieces. The neck region is machined out of Perunal, an aluminium alloy. The remaining part is an assembly of three parts screwed together, each one made out of Anticorrodal 100 (1.7 mm thick metal sheets rolled and welded). The properties of these aluminium alloys can be found in Ref. [43].

Outer conductor:

This conductor is cylindrical with a wall thickness of 12 mm and is an assembly of five parts screwed together, each one made out of Anticorrodal 100. The inner diameter of the outer conductor is machined with a maximum ovality default of 0.2 mm. Inner/outer concentricity is 0.1 mm. Centring of the inner conductor is achieved with adjustable centring appliances using stainless steel cables to hold and precisely centre the inner conductor with respect to the outer conductor. Insulation of the cables with respect to the outer and the inner conductor is obtained by means of Arclex M glass–mica compound spacers.

Water cooling:

The cooling systems of horn and reflector are identical (unless air cooling can be retained for the reflector). The water circuit is open, with the pump sucking the water from the recuperation tank of the magnetic element and spraying it continuously onto the inner conductor. The sprinklers are distributed along two external pipes located on the upper part of the outer conductor. The water is collected by gravity into the tank located in the strip-line trench. The total amount of cooling water is 35 l/min for both horn and reflector. The flow is monitored with an electronic flowmeter showing the analog flow-value. As additional safety, the water circuit includes a digital flowmeter with an open contact when the flow falls below a predefined threshold. Both flowmeters cut the power supply in case of insufficient flow. The water level in the tank is measured and triggers a warning to refill. It cuts the pump and the power supply when limits are reached. The

water is cooled through a heat exchanger located, with the pump and all auxiliaries, in the service tunnel.

4.5.2 Horn and reflector electrical systems

The electrical circuits for horn and reflector are identical. The technical requirement is to produce a stable, reproducible field in both focusing elements during the two fast extractions (10 μs each). The precision required is 0.1%. A detailed description of the electrical system is given in Appendix E.

4.5.3 Helium tank

To reduce particle absorption in air, a 'helium tank' fills the useful secondary beam volume between horn and reflector (approximative length 60 m). The absorption length is $\lambda = 800$ m for air and $\lambda = 2500$ m for helium. Both ends of the tank are closed by a titanium window 0.3 mm thick. The helium tube is an assembly of 14 cylindrical aluminium alloy elements (5 mm thick) and of the same inner diameter 80 cm (see Fig. 36). Each element is bolted to the other and has two welded flanges with machined grooves for metallic O-ring seals. All equipment, except for the tank, is located in the service tunnel. The helium is contained in the tube at a positive differential pressure of less than 20 mbar. An oxygen analyser controls the helium concentration; the exhaust minimum flow rate, to ensure the measurement of the helium concentration with precision, is about 30 l/h. The helium flow is controlled and adjusted by a flowmeter equipped with a needle valve.

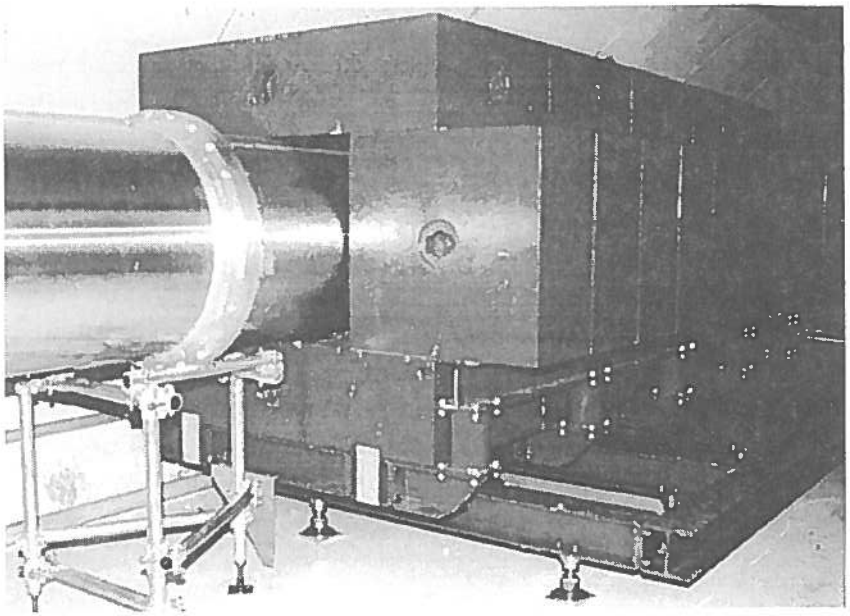

Fig. 36: Photograph of the WANF iron collimator, equivalent to COLL3 in this project. The helium tube, passing through it, can be seen in the foreground

4.5.4 Aluminium collimator

The aluminium collimator COLL2, located downstream of the target, precisely limits the opening angle for the secondary particles. It is a machined round bar of 2850 mm length and outer diameter 490 mm; its total weight is about 1400 kg.

On its longitudinal axis, a bored beam hole ($\varnothing = 88.8\,\text{mm}$) partly cylindrical and partly conical results in the average requested opening angle Appendix A. The collimator is centred along the slope of the beam axis. It is placed on a manual adjustable base frame supported by a specially equipped CERN standard iron shielding block.

Support, collimator, and base frame are autocentring and can easily be removed. The collimator is water-cooled by two separate drilled circuits, one at each end, both cooling circuits being connected in parallel. The cooling circuit of the aluminium collimator COLL2 is connected to the same closed circuit as the copper collimator COLL1. The corresponding pump station is located in the service tunnel with a heat exchanger cooled by the primary beam transport demineralized water circuit. The total water flow is $1.5\,\text{m}^3/\text{h}$ with $\Delta p = 3\,\text{bar}$ resulting in a mean temperature of 60°C measured on the outer circumference at the middle of the collimator, when the total SPS intensity is 3.0×10^{13} protons for the two spills of the SPS 6.4 s supercycle.

4.5.5 Iron collimator

The overall dimensions of the iron collimator COLL3 (4 m length) correspond to the arrangement of the WANF TDX collimator (see Fig. 36). The assembly is built up with $80 \times 80 \times 40\,\text{cm}^3$ standard iron blocks.

4.6 Hadron stop

The hadron stop is placed at the end of the decay tunnel. The purpose of this object is to absorb the energy deposition of the primary and secondary particles arriving at the end of the decay region. The design is based on the following requirements:

1. There must be a high density and potentially demountable region where the energy deposition of the primary and secondary hadrons from the intense production at the target are absorbed. The cascade of these particles interacting in the dump has to be contained, as there must be minimal deposition of radioactivity in the molasse.
2. The hadron stop must be considerably larger than any protection required to absorb the hadrons as there is a need to provide additional material for muon attenuation at the SBL detector to give a direct muon background less than the irreducible background induced by neutrino interactions in the molasse in front of the detector. The evaluation of the amount of material required was discussed in Section 3.7.
3. In order to steer the beam towards the Gran Sasso Laboratory, accurately positioned detectors must be placed behind the hadron stop. In practice, experience has shown that at least two detector pits are required to provide angular and very rough energy information to control any misalignment of the horn and reflector with respect to the target. The two pits should be separated by sufficient material to give an energy difference of the muons sampled of about 40 GeV.

4.6.1 Hadron stop design

Unlike the WANF system it is evident that because of its insulation against heat loss, buried deep underground in a bed of poorly conductive molasse, the hadron stop has to be actively cooled. Preliminary calculations, discussed in the next section, indicate that after 200 days of running with 5×10^{12} protons per second at 400 GeV/c, parts of a simple iron dump could reach several hundred degrees Celsius (≈ 700°C). These high temperatures would risk destroying the concrete supporting structures, excluding further access to the muon detector pits. Several heat flow calculations [67] with different conditions have been made, indicating that the dump should be actively cooled. Also, it is clearly advantageous to have a lower density insert at the start

of the dump to diffuse the hadronic cascade over a larger volume to improve the heat flow and minimize exceptional hot spots due to non-interacting primary protons on the beam axis.

The design requirements for a cooled hadron stop are listed below:

1. The total power deposited on the hadron stop in the worst case of continuous dedicated running is about 50 kW. Half of this deposition comes from non-interacting protons, and is highly localized in the centre of the dump. The rest, coming from secondary hadrons, is relatively diffused over a region of 2.6 m in diameter.
2. The back end of the hadron stop needs to be at a reasonable, constant temperature, 20–25°C, in order to allow stable operation of the solid-state detectors and electronics.
3. Water cooling must be demineralized in a closed circuit and be very robust. It should be designed for a 20-year lifetime with no intervention to the heat sink required.
4. A monitoring system of the water flow and temperature is necessary. This has to be designed with appropriate redundancy, considering the mechanical and thermal stresses expected in the hadron stop region.

The general layout of the civil engineering of the hadron stop area is shown in Fig. 31. Access to the area is evidently very limited. It is only possible when neither the LHC nor the NGS is running. Access is possible via pit 8, about 1.5 km around the machine tunnel, to the RE88 service area, then down 200 m of sloping gallery to the first muon pit area. The second muon pit area is a further 67 m downstream. This distance of molasse gives the required attenuation of 40 GeV. Access to this pit is via another 100 m gallery. It is initially slightly angled away from the detector so that any muons in this region see only an additional 10 m of air gap. The hadron stop is installed in a cavern 6.5 m in diameter and 26 m long. A preliminary design of the hadron stop is shown in Fig. 37. The decay tunnel pipe is terminated by a substantial steel plate welded to the 96 inch gas piping used as the actual evacuated decay tunnel. An insulating air gap, 20 to 25 cm, is left to separate the plate from the hadron stop and to minimize the heating of the end plate by the dump. Once installed this region is completely sealed from the galleries and muon pits.

The first component of the stop is a block of graphite $2.6 \times 2.6 \times 3.0\,\mathrm{m}^3$ which is used to diffuse the hadron cascade over a large volume to reduce the temperature gradient in the dump and take advantage of the better heat conductivity. The graphite block is enclosed in an aluminium box, with a wall thickness of 10 cm. This box ensures a good heat conductivity over the whole surface to the heat sink on which the box sits. This heat sink of $280 \times 20\,\mathrm{cm}^2$ cross section and 5 m long is water-cooled by 12 independent circuits, each of 4 cm diameter mild steel pipes leading to the back of the hadron stop. Each circuit is independently attached to a general manifold and can be turned off in case of internal leaks or breakage. A schematic drawing of the heat sink is shown in Fig. 38.

The whole water-cooled module is encased in standard CERN steel blocks, see Fig. 39, and all gaps to the cavern walls filled with concrete.

As it is impossible to transport the aluminium box filled with graphite as a complete structure down to the cavern, one possibility is to build it in five 60 cm segments, each weighing about 10 tons. These segments are bolted together *in situ*, as shown in Fig. 40. The water-cooled module is followed by a mass of $240\,\mathrm{m}^3$ of iron blocks. The cross section of $4 \times 4\,\mathrm{m}^2$ is sufficient to attenuate any muons that would multiple-scatter around the hadron stop, and the length of 15 m along the beam axis should provide enough attenuation to give a safety margin to prevent muons from reaching the SBL detector. The heat sink is 5 m long, 2 m longer than the graphite. This provides some continuity of cooling to the final mass of iron. The water cooling is provided by closed-circuit pumps and a heat exchanger situated in the equipment chamber at the hadron stop, see Fig. 31. Power and cold water requirements are discussed in Section 4.8.1.

The total amount of iron needed for the hadron stop can be found by recovering standard sized blocks from the WANF system. In the WANF beam line at the end of the West Area, 105 m^3 of $80 \times 80 \times 160$ and $40 \times 80 \times 160$ blocks can be found. The remaining blocks can be recovered from the 4700 tons of blocks buried outside the West Area, between the hall and the CERN fence.

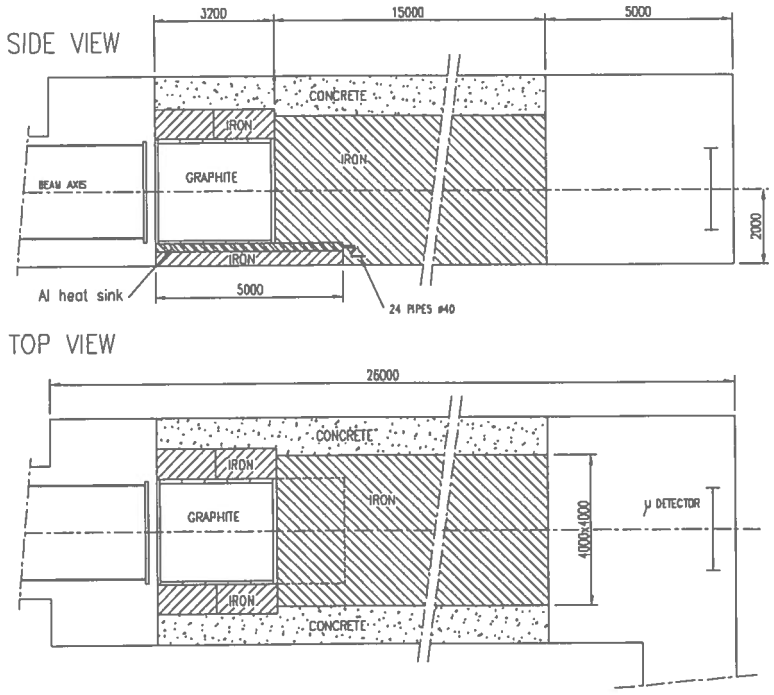

Fig. 37: Elevation and plane views of the hadron stop cavern (dimensions in millimetres)

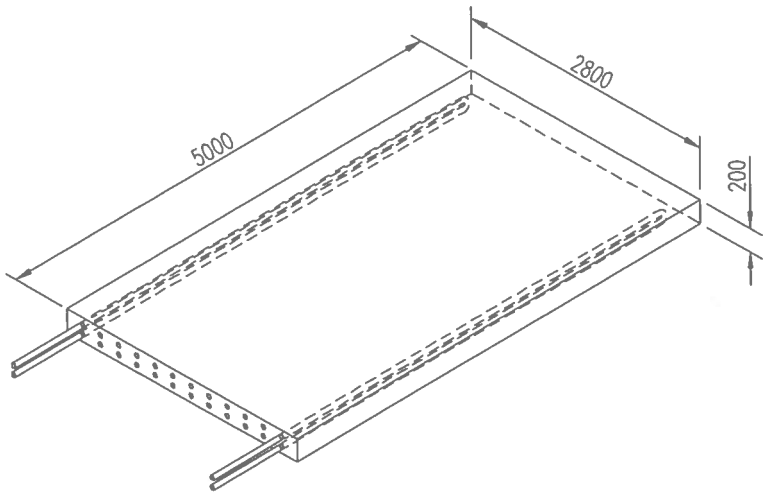

Fig. 38: Illustration of a preliminary heatsink design (dimensions in millimetres)

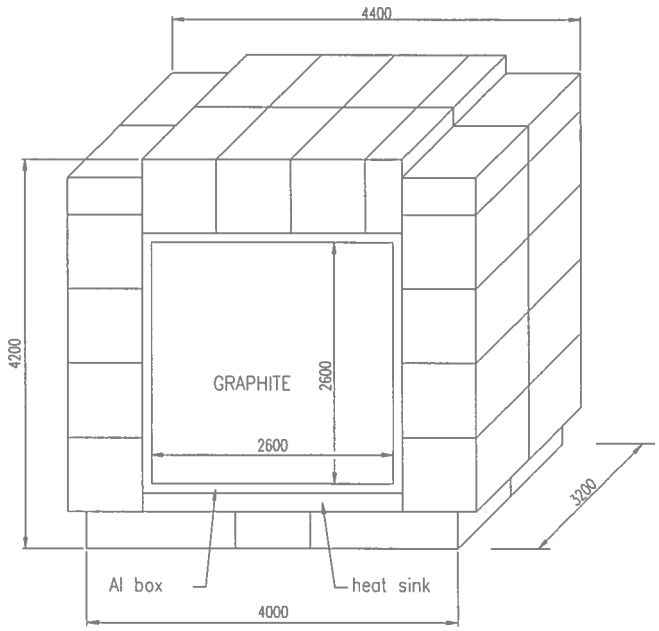

Fig. 39: Beam view of the upstream end of the hadron stop (dimensions in millimetres)

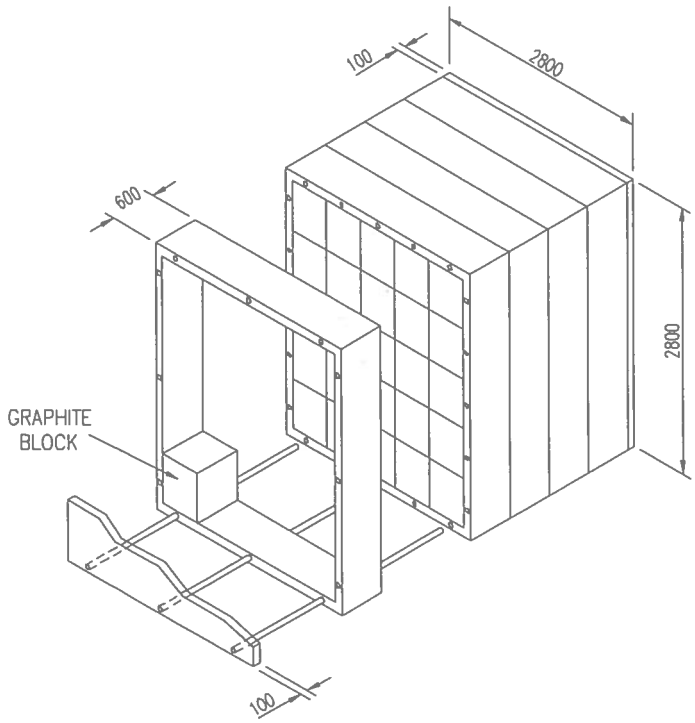

Fig. 40: Schematic view of a possible assembly of the graphite inserts (dimensions in millimetres)

4.6.2 Heating of the hadron stop

Some preliminary calculations have been made of the heat flow and final temperatures in the hadron stop, though no final optimization of all the possible parameters has been made. These calculations have, however, given indications of what could be a reasonable, safe design that would satisfy the required conditions. The proposed design is described in the following section.

The calculation of the heat flow in the hadron stop was performed in two steps. First the FLUKA program [47] was used to calculate the average energy deposition in the hadron stop by a fully simulated reference neutrino beam, including primary protons not interacting in the target. The output from this simulation was used as the input to the dynamic heat transfer calculation in the hadron stop.

Several simplifying assumptions were made to ease the calculation problem. A rotational symmetry was assumed to allow a faster first round of calculations, e.g. the heat sink was taken as a 3 m long cylinder of aluminium with an inside radius of 1.46 m and a thickness of 10 cm. To compensate for this global coverage of the heat sink, which is in reality only at the bottom of the hadron stop (see Fig. 37), the cooling power was reduced to a quarter of the expected one, i.e. to 12.5 kW. Boundary conditions in the molasse surrounding the hadron stop were fixed at 14°C at a reasonable distance of 20 m.

The temperature profile due to the impact of the hadron cascade along the beam axis is shown in Fig. 41, for the hottest region after 200 days of beam on target. The maximum temperature on axis in the hadron stop, after 200 days continuous running, rises to 160°C, partly due to non-interacting protons[8]. The peak in temperature at 3 m is reduced with the foreseen longer heat sink of 5 m. The maximum temperature at the end of the dump is still fairly high, about 55°C, but can be easily reduced with some air gap and insulation, or with additional water cooling.

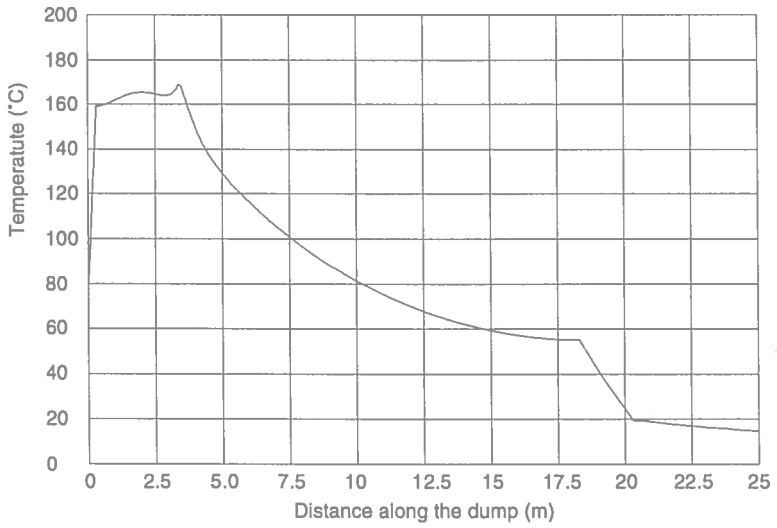

Fig. 41: Temperature profile along the hadron stop (with cooling)

The time development of the maximum temperature on axis, in the worst case of continuous running is shown in Fig. 42. Note that in the simulations, the cooling of the dump is assumed to stop when the beam is stopped, after 200 days of operation. In the case of complete

[8]This could be reduced with the use of a longer target in the proton beam.

loss of water-cooling, the same time response is shown in Fig. 43. At the hottest spot in the dump, just at the end of the 3 m long heat sink, the temperature at a lateral distance of 2 m can rise to about 140°C. This is also reduced with a longer heat sink of 5 m. Further calculations indicate that with a modest increase of the water-cooling power, these temperatures can be reduced considerably.

4.7 Muon monitoring station

Muon counters in the form of silicon diode detectors (SSDs) are used as in past experiments [68, 69] to monitor the intensity and distribution of the muon flux after the iron of the hadron stop. These counters are installed in two chambers, chamber 1 is immediately downstream of the hadron stop in a small cavern $4 \times 4 \times 5\,\mathrm{m}^3$. Chamber 2 is a smaller cavern $3 \times 3 \times 3.5\,\mathrm{m}^3$, on the beam axis 67 m downstream, reached by a gallery 100 m long, see Fig. 31. Each chamber is equipped with a free-standing support holding 19 fixed SSDs arranged as shown in Fig. 44. The central position on the beam axis is equipped with three SSDs, to allow checks and provide some redundancy. These fixed detectors have a point-to-point spacing of 30 cm. An additional set of five SSDs, (CALBOX), in each chamber, is mounted on a moveable arm, such that the group of detectors may be remotely scanned, horizontally and vertically over the useful $2 \times 2\,\mathrm{m}^2$ area. The precision of movement of this arm is fairly critical, a position accuracy of 0.2 mm is required. These sets of detectors are used to provide a relative calibration between the fixed detectors and also to provide precision scans of the muon profiles. Note that the whole support structure has to be tilted by 5.6% so that it is perpendicular to the beam axis. During data taking the CALBOX is put in a far off-axis, garage position, as the presence of the CALBOX in front of a fixed SSD counter affects the detector response.

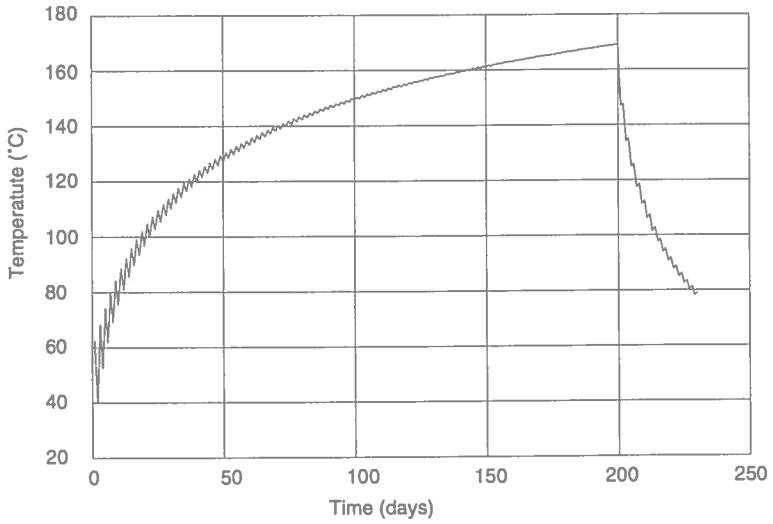

Fig. 42: Temperature evolution with time at the hottest point of the hadron stop (with cooling)

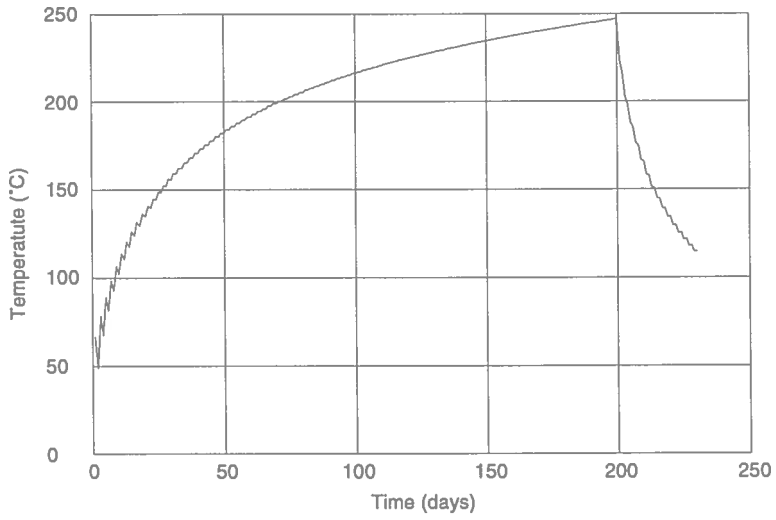

Fig. 43: Temperature evolution with time at the hottest point of the hadron stop (without cooling)

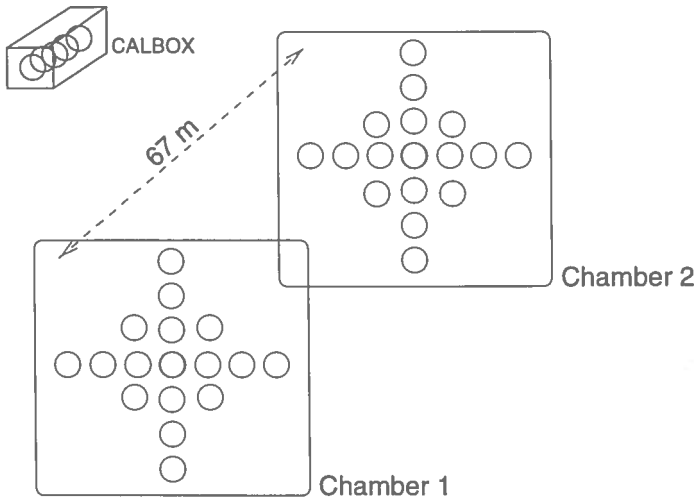

Fig. 44: Layout of the counters in the two muon chambers. Each chamber is equipped with a moveable CALBOX containing five SSDs

In the WANF muon monitoring system an additional set of five SSDs (REFBOX) was used to intercalibrate the different chambers. Experience and calculations have shown that the detector response, particularly the e/μ ratio is very sensitive to the physical environment in the chambers, i.e. the material and distance of the chamber walls. In view of the recent developments in the speed and accuracy of automatic scanning of nuclear emulsion plates, it is proposed to calibrate each CALBOX detector with emulsion plates, thus avoiding the additional complexity of a REFBOX system. The disadvantage of this process is that a few hours of dedicated SPS time are required to reduce the proton beam intensity in the SPS — in this way, an exposure of the emulsions can be made with a sufficiently low μ intensity so that the plates can be scanned.

The movement control and DAQ electronics for the SSDs is placed in the hadron stop annex. A few racks of low-power CAMAC or VME crates are required, less than a kilowatt, but some water cooling should be foreseen. Electrical power and water is supplied from the 'stub-tunnel' RE88. The control and data acquisition system should be connected via an optical fibre link to the SL data connection channel to provide connection to BA4 or, if that is considered undesirable, an optical fibre connection could be made to point 8 of the LEP/LHC.

4.8 Infrastructure

4.8.1 Cooling and ventilation

This section describes the ventilation and fluid systems for cooling (by water) as well as the fire extinguishing system for the different zones in the NGS underground areas. A schematic overview of the technical concept for the ventilation system of the target chamber and the tunnels is given in Fig. 45. The hadron stop and muon detector area, which can only be accessed from the LEP/LHC tunnel, is treated in a separate paragraph at the end of this section.

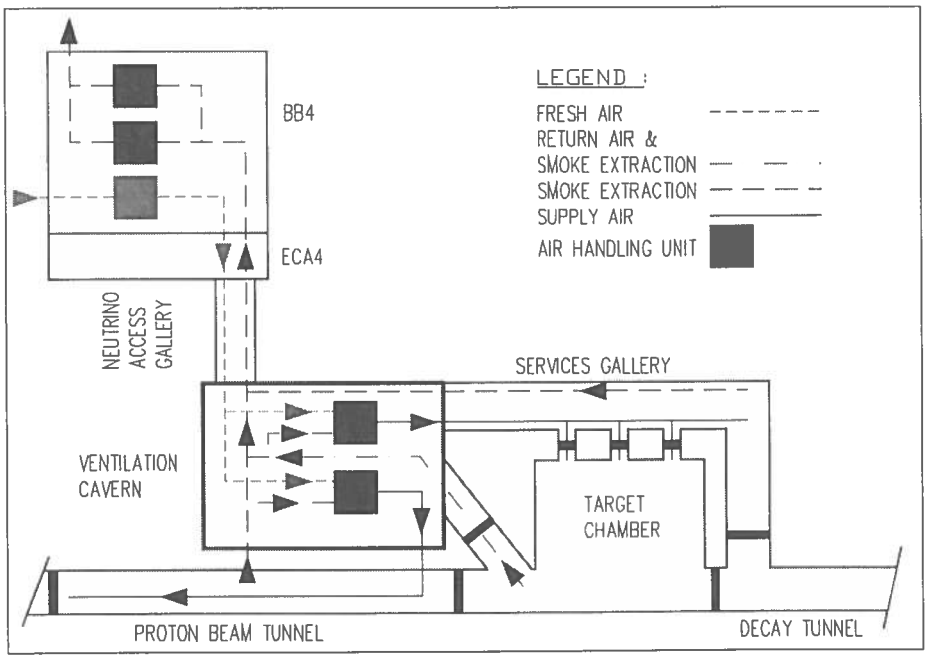

Fig. 45: Overview of the infrastructure for ventilation

Access gallery

Air handling: The air in the access gallery is treated by a unit at the surface in building BB4 or its annex and is operated only during access periods. The unit, operating entirely with fresh air, is used to heat and cool the area. It provides a flow rate of 16 000 m^3/h and its components are designed to provide the following ambient conditions:

i) dry temperature 19°C,

ii) dewpoint 10°C.

Fresh, clean air is supplied to the access gallery, via an air-handling link with the access gallery and the proton beam tunnel. The electrical power required for this unit amounts to 200 kW and chilled water at 6/12°C has to provide 120 kW of cooling power.

It is possible to start this unit from the surface or from the access point in ECA4. The criteria for this, which have to be drawn up to prevent any contamination hazards owing to the overpressure generated by the injection of fresh air, are to be defined in a detailed procedure.

Smoke removal (cold smoke $\leq$ 100°C): A system of smoke removal ducts is located in the access gallery and connected to two units at the surface (one on stand-by). It is possible to start this unit from the surface or from the access point in ECA4. A safety procedure for starting the unit has to be defined to prevent any contamination hazard due to the quality of the discharged air. In view of the physical link with the surface building via shaft PAM4, two smoke extraction fans are fitted on the roof of BHA4 (BB4). This equipment is powered from the no-break circuit at the required power of 10 kW.

Target chamber and service gallery

Air handling: The air in these two areas is treated in a shared unit placed underground in the second level of the tunnel junction labelled 'ventilation cavern' in Fig. 45. The unit cools and dehumidifies the air to prevent any risk of corrosion of the equipment. This unit operates entirely on recirculated air except during access periods, with a total treated air flow rate of 16 000 m^3/h. The components are designed to ensure the following ambient conditions:

i) dry temperature 19°C,
ii) dewpoint −15°C.

The power required is: (a) electric 320 kW, (b) cold (chilled water at 6/12°C) 120 kW. This air handling unit is equipped both with local and remote controls.

Smoke removal (cold smoke $\leq$ 100°C): A system of smoke removal ducts is located in the target chamber and its service gallery, connected to the one for the access gallery and controlled in the same way.

Proton beam tunnel

Air handling: The air in the proton beam tunnel is treated by a unit, placed underground in the ventilation cavern, which cools the air and thus the equipment in the proton beam tunnel. This unit operates entirely on recirculated air except during access periods, with a total treated air flow rate of 12 000 m^3/h. The components are designed to ensure the following ambient conditions:

i) dry temperature 19°C,
ii) dewpoint 10°C.

This unit requires 50 kW of electric power and 90 kW of cold (chilled) water at 6/12°C. It is equipped with both local and remote controls.

Smoke removal (cold smoke $\leq$ 100°C): A dual-purpose extractor and removal grid for smoke below 100°C is placed on the partition between the ventilation cavern and the proton beam tunnel, connected to the access gallery system and controlled in the same way.

Cooling and fire extinction The SPS primary circuit provides the primary cooling of the demineralized water circuit for the proton beam magnets (2000 kW, 115 m^3/h). It also serves as a fire extinction circuit ($\approx$ 5 bar static pressure available).

The equipment in the target chamber is cooled with a demineralized water circuit ($\approx$ 50 kW, 3 m^3/h) having either chilled water or the SPS water as primary circuit. The air handling units in the ventilation cavern are supplied with chilled water at 6°C (600 kW, 86 m^3/h). The primary water of these units is also cooled from the SPS primary circuit. As is usual, a fire extinction circuit is installed.

Finally, all seepage or leakage water is collected in a sump in the service gallery and pumped to BB4 where it is checked for contamination before discharge or treatment.

Hadron stop and muon chambers

Ventilation: The treated air from sector 8-1 of the LEP/LHC tunnel is supplied from a fresh-air handling installation on the surface at point 8. The hadron stop area is ventilated by air taken from this sector 8-1. The air is provided by two fans (one on stand-by) connected to a ducting system making it possible to take the air as far as the two muon chambers. The air is returned to the tunnel by overpressure. This device is controlled from RE88, the access point to the tunnel. The access procedure ensures that the equipment is started up before an access is given. The air quality is monitored. The unit is put into operation every time access to this area is required.

Smoke removal (cold smoke $\leq$ 100°C): The fans are reversible in order to remove smoke.

Cooling and fire extinction: The water required for fire extinction is supplied from the main LEP tunnel raw water circuit (available pressure around 10 bar). The cooling of the hadron stop uses the octant demineralized water as primary circuit (50 kW, 3 m^3/h, 27°C) to avoid any risk of contamination of the raw water circuits or the octant circuit. Any infiltration through the cavern walls or leakages from the cooling equipment is collected in a sump in the hadron stop area and then pumped to point 8 for checking before discharge or treatment.

4.8.2 Decay pipe accessories

The decay pipe consists of welded steel pipes of 2.45 m diameter, with a total length of 1000 m (see Section 4.1). The volume of the pipe is 4800 m^3, the inner surface amounts to 7700 m^2. The thickness of the steel pipes is 20 mm, solid enough to withstand the pressure under vacuum provided the surrounding spaces are filled with concrete.

Vacuum To provide the required vacuum of about 1 mbar in less than one week, two rotating pumps are foreseen. They are installed in the service gallery, near the end of the target cavern. Each pump has a capacity of 630 m^3/h and a final pressure near 0.1 mbar. The pumps are equipped with the necessary valves, filters, and pressure gauges, and they can be remotely controlled. The filtered exhaust gases are transported to the surface through a dedicated pipe equipped with a ventilator for extraction.

Using the two pumps, the required pressure of 1 mbar can be attained in three days. After that, one pump is switched to 'stand-by' and used as a spare.

Vacuum window and shutter The decay pipe is closed on the target chamber side by a 1 m diameter 2 mm thick titanium window. The other end (i.e. at the hadron stop) is closed by a massive steel plate, 5 cm thick.

For safety reasons, i.e. to protect against a possible implosion risk, it is necessary to install a motor-driven vacuum shutter (a thick circular steel plate) which is moveable along horizontal rails in front of the 2 mm titanium window. When run conditions are established, the plate is automatically driven out of the beam into a 'run position'. When access to the target area is requested, the shutter is automatically driven in front of the titanium window. This shutter must be interlocked with the access conditions for the NGS target area. Should the titanium sheet break, the shutter plate is pushed by the implosion effect against the titanium window flange thus reducing the leak to a tolerable level.

Decay pipe collimator In order to localize the induced radioactivity from defocused particles along the decay tunnel, a 10 m long iron collimator is foreseen in the very upstream part of the decay pipe (see Fig. 46). The detailed design of this collimator (COLL4) has to be optimized according to the final layout of the focusing elements and their strengths, i.e. once the final neutrino beam optics are available.

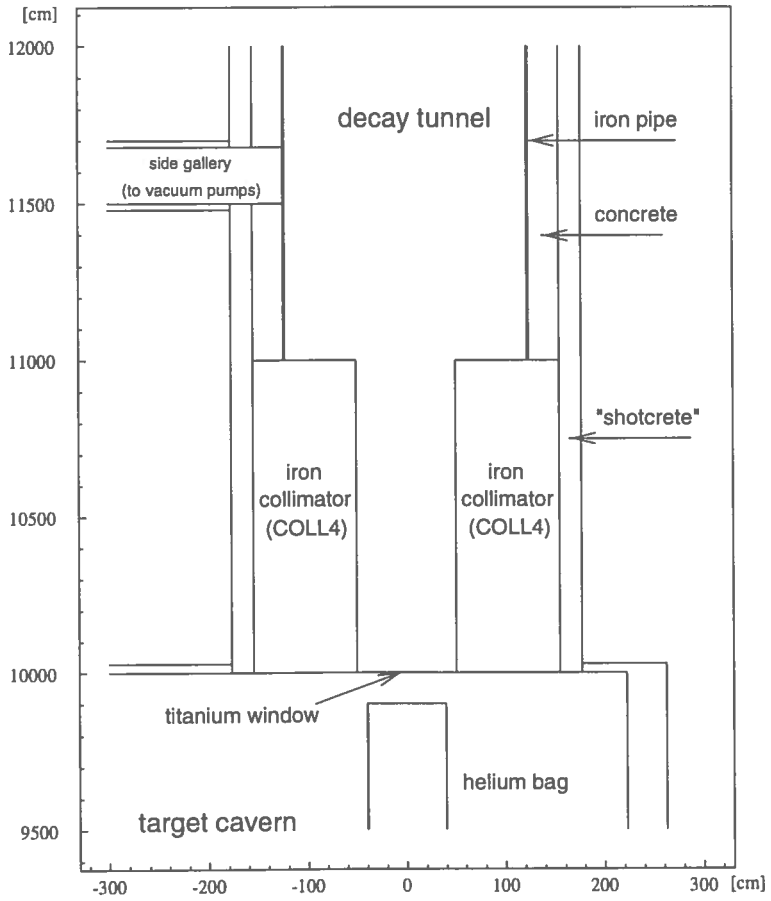

Fig. 46: Schematic view of the beginning of the decay tunnel

4.8.3 Power converters

For reasons of operational simplicity and maintenance, the whole system is designed to be an extension of the SPS. Apart from the corrector power converters, all the power converters are recovered from the SPS and LEP. All the power converters are pulsed and controlled by the MUGEF (microprocessor controlled function generator) system.

For the main bending magnets (MBs), it is planned to use the same power converter as for the TI8 MBs. This converter is made from two units connected in series, working in a 'master/slave' configuration and is located in building BA4. This power converter can be switched from the TI8 MB circuit to the TN4 (NGS) MB circuit and vice versa with the help of two remotely controlled power switches. In the TN4 MB circuit the number of magnets is lower and therefore needs a remotely controlled switchable current loop and may need only one power converter. The other dipoles are fed by the SPS and LEP power converters. The QD/QF chains and all the other quadrupoles are fed by the LEP power converters. Concerning the correctors, neither the quantity nor the electrical parameters are defined today, but it would be judicious to design the new coils to use new SPS COD (closed-orbit deflector) power converters.

The power converters coming from the SPS will be renovated. At the moment, a renovation project for the SPS auxiliary converters is planned. All needed power converters will be added to this programme. This programme includes a complete reconstruction/modernization of all components, with an upgrading of the regulation, control and interlock subsystems. The power converters coming from LEP will also be modified. The power part is retained, but the complete electronics has to be replaced by new SPS electronics, which can be controlled by the MUGEF system.

4.8.4 Power distribution and DC cabling

Power distribution Most of the electrical installations for the new neutrino facility are fed from BA4 of the SPS. The service installations in the new underground structures are cabled from this point.

Although the individual loads are fairly small, the total load combined with the distance to BA4, may mean that the optimal solution is an 18 kV cable from BA4 to an 18 kV/ 400 V transformer close to the target area. The distribution in the area is entirely low voltage, i.e. 230 V/ 400 V.

The major part of the load elements are in the short tunnels and small caverns around the target area. Here low-voltage switchboards are foreseen for the local distribution.

The part of the load to be installed in the muon pits and the tunnel leading to them is supplied from the LEP stub-tunnel RE88. Small sub-distribution panels are required for the distribution to the racks in the pits. Here the load is small, a few tens of kilowatts, so a 230 V/ 400 V link from RE88 is sufficient.

The lighting of the tunnels is similar to that of the LEP tunnel. Specific areas, where detailed work requires a higher luminosity, can be equipped with more powerful lighting.

The safety systems (emergency stops, 48 V supplies, anti-panic lighting and safe power) are prepared to the standards developed during the LEP and LEP 200 projects. All the equipment of such installations are part of long-term solutions, proven at CERN over years of operation.

The distribution of services requires cable routing in the structures, either in false floors or on cable ladders fixed to the walls. In the very narrow tunnels care is taken to reduce the space requirements for routing electrical cables.

DC cabling The DC cabling for the magnets in the primary beam tunnel also originate in point 4 of the SPS. These cables run through the primary beam tunnel on cable ladders in the upper part of the tunnel cross-section.

Water-cooled cables are used for the dipole circuit. Existing water-cooled cables in the SPS will be recovered to a maximum possible extent, i.e. from BA4 to ECA4, to reduce costs. From ECA4 and onwards, the major part of the water-cooled cables will be new.

Conventional cables are used for the other magnet circuits. The cross-section of the conventional cables has been selected to keep the heat dissipation in the tunnel low.

4.8.5 Access control and machine interlock systems

The realization of the NGS project implies the implementation of safety systems ensuring protection of personnel as well as of equipment.

Safety considerations The NGS tunnels are considered as a 'CERN Primary Beam Area'. At CERN the access to such areas follows safety rules:

- The access to a primary beam area must be forbidden and nobody should be present in the area during beam exploitation.
- The beam should be turned off and interlocked, and the level of remanent radiation must be acceptable in order to allow access to this primary beam area.

The general rules for the access control and machine interlock systems are equivalent to the ones found today at the SPS, and more specifically at the WANF.

Two access points are foreseen at the NGS:

1. Access to the target chamber is provided from point 4 of the SPS (see Fig. 6). The access point (door for material transport and turnstile for personnel traffic) is in the ECA4 cavern. Here, the neutrino access tunnel can be entered and the ventilation cavern, storage tunnel, as well as the service gallery and target chamber can be accessed.
2. Access to the muon pits, downstream of the hadron stop, is provided through the LEP/LHC tunnel, starting in point 8, and passing through the alcove RE88 (see Fig. 31). Access to this area, although rarely needed, requires that both the neutrino beam and the LHC be switched off.

Further details of the Access Control and the Machine Interlock System for the NGS are described elsewhere [70].

4.8.6 Alarms and fire detection

The installation of safety systems is planned in all the areas where equipment is located, i.e. in the proton beam tunnel, the target chamber and its service gallery, as well as the muon detector areas.

Evacuation Based on the principles used at LEP, the evacuation alarm systems consist of two control panels connected to sirens installed at least every few hundred metres. The control panels are installed in BA4 and at point 8 of LEP. The precise location of the sirens and of a few dozen glass plates with emergency stop buttons depends on the local equipment layout.

Red telephones Some 20 of these emergency telephones are foreseen. When activated, these telephones automatically generate an alarm of Level 3, thus informing the Fire Brigade Control Room of the precise location of the person calling. The detailed layout for the installation of these telephones will be given by the CERN Technical Inspection and Safety Commission (TIS), once the layout of the equipment is defined.

Fire detection Fire detection in an environment with long tunnels, coupled with high radiation, is a difficult problem. Since most areas of the NGS are not accessible when the accelerators are running, smoke detectors would have to be located in BA4 and at point 8 of LEP (see Fig. 6). Sampling tubes would have to be installed close to the ceiling of the areas with equipment — they would have to carry the smoke to the detectors. Considering a typical velocity of 3 m/s in such tubes, this implies that it takes about 6 minutes for the smoke generated, e.g. in the service gallery near the target, to be detected in BA4. In addition, the time for the smoke to reach the closest sampling tube might be about 2–5 minutes. For the time being, no manufacturer of smoke detection systems can guarantee that such a diluted smoke can be reliably detected.

It should be noted at this point that there is no fire detection installed over much of the length of LEP, with the exception of about 150 m to either side of the access points. Pending a detailed safety discussion, it is assumed that no fire detection is needed in the NGS caverns and galleries.

5 RADIOLOGICAL ASPECTS

5.1 Introduction

The most important items in the present proposals for a neutrino beam to Gran Sasso from a radiological viewpoint are the target chamber, the decay tunnel, and the hadron stop. Estimates must be made of possible dose rates to which maintenance personnel could be exposed, the total induced radioactivity in the structure and its surroundings, and the magnitude of any release to the environment via air or water pathways. Some of these quantities of interest have been estimated from simulations of the cascades induced by the interactions of the primary protons from the SPS in the neutrino production target and the hadron stop [71].

Simulations of these cascades were carried out using the 1997 version of the Monte Carlo cascade program FLUKA, see Refs. [47, 72] and the references therein. The study was based on the Reference Design detailed in this Report (see Section 3 and the Reference Parameter List in Appendix Appendix A). No attempt has yet been made to optimize the design with respect to minimizing the radiological quantities of interest. Thus the studies completed so far represent upper bounds of these quantities serving to show that the project is feasible without undue adverse effects on the environment.

5.2 Remanent dose rates due to induced radioactivity

The latest version of the present WANF has proved successful in keeping the doses to maintenance personnel to acceptable levels. It has been possible to make repairs to components in the vicinity of the target, horn and reflector. The design of the new facility allows for the increase in proton intensity by increasing the shielding around the target and collimators. Thus dose rates due to induced radioactivity should not increase over present levels in the WANF.

The situation in the new facility has been significantly improved by the provision of a service side-gallery which gives access to the target chamber without exposing people to the most radioactive items in the chamber. This allows necessary equipment to be installed close to the beam-line components and for this equipment to be maintained without radiation exposure.

In addition, people making repairs to the beam-line components themselves can make their preparations in the service gallery and spend the minimum amount of time in the highest radiation environment. Such a side-gallery is a feature of both SPS target stations in the North Area. They were included in these projects as a result of adverse criticism of the WANF Target Area design, where the civil engineering plans were completed at a very early stage in preparation for the SPS construction.

Another improvement has been the provision of a simple stub-tunnel as a storage area for radioactive items close to the target chamber. This means that a horn or reflector which has been in service and become faulty can be stored easily, reducing the dose to transport personnel.

These provisions ensure that the new facility does not increase the global exposure to personnel, despite the increased intensity of protons being targeted in the area. In fact the area has been designed rather to reduce the current level of exposure.

5.3 Radioactivity in the structure and components of the facility

On the assumption that the facility will run for ten years at the reference intensities, the radioactivity induced in the molasse around the underground structures and in the concrete of the structures themselves will decay to insignificant levels within 50–70 years after the end of target operation.

The iron shielding around the target and collimators, the TDX collimator and the collimator at the front of the decay tunnel, with a mass of the order of 700 t, will have average specific activities at the end of target operation between 10^4 and a few times 10^6 Bq/g. The decay of the isotopes in this iron will be relatively slow, reaching insignificant levels only after several hundred years. Disposal of these items as radioactive waste must therefore be foreseen.

The iron of the hadron stopper will have an average specific activity of a few times 10^3 Bq/g. Parts of this, about 200 t, will also need special disposal facilities.

The iron of the decay tunnel and the iron reinforcements in the concrete of the target chamber will probably stay in place at the end of the target operation. The reinforcements will reach insignificant levels of radioactivity within 50 years, but the time for the decay tunnel to reach similar levels will be of the order of 500 years.

The aluminium of the collimator COLL2, the horn, the reflector, and the two helium-pipes in the target cave, total mass about 3–4 t, will have specific activities, after 10 years of operation and a further ten years of decay, which are of the order of 10^6 Bq/g. Disposal of these items as radioactive waste must also be foreseen.

However, the activity in the graphite core of the hadron stop will probably reach levels where normal disposal will be possible after ten years of decay.

Demineralized water in the cooling circuits of the horn, reflector, collimators, and hadron stop will be kept in closed circuits. Emptying of these circuits will take place only after measurements have been made of the radioactivity contained. It is to be expected that the tritium concentrations will allow immediate emptying to the drains, but before that the water must pass through a demineralizing resin where any ^{7}Be and other radioisotopes will be removed.

5.4 Release of radioactivity via the air of the ventilation system and the drains

The air of the target chamber will be contained within a closed circuit during operation. After targeting stops, a cooling-down period of several hours will be imposed before flushing of the target chamber with fresh air is started. It will take at least several hours to flush all the original air from the target chamber. Control of the radioactivity by careful determination of the delay time, the flushing time, and the transit time for the air to reach the exhaust stack from the

target chamber will ensure that any radioactivity vented will be less than the relevant CERN Reference Release Constraints. Continuous monitoring of the radioactivity in the released air will be provided.

The radioactivity contained in the residual air of the decay tunnel and in the front part of the hadron stop area is significantly lower than the radioactivity in the target chamber.

Estimates have been made of the quantity of tritium that will be created in the closed helium-gas cooling circuit for the target and the helium containers in between the horn and reflector and the reflector and the end of the target chamber. It has been shown that the production is similar to that of tritium in the air of the target chamber. Since the release of tritium from this latter source is not of radiological importance, the regular flushing of one of the helium circuits will not create a significant release of tritium.

The drains in the target chamber and the LHC tunnel will collect any groundwater that might seep into the excavation as well as any spillage water. The radioactivity in the groundwater, even though at a low level, is such that it is prudent to impose controls on the release of the drain water. In addition to routine controls on drain water leaving the facility, water will not be released unless point controls have shown that the radioactivity in the water meets CERN Release Standards. Only then will the drain water be released. If the radioactivity exceeds such levels, then the drain water must be evaporated, as is done in some present CERN facilities, and the residue disposed of as solid radioactive waste.

5.5 Dose rates from neutrinos

As a postscript, it has been thought necessary to reply to questions concerning the dose rates due to neutrinos at the Gran Sasso (LBL) or the short-baseline facility (SBL). The neutrino fluence at the SBL and LBL facilities is $1.09 \times 10^{-3}\,\mathrm{m}^{-2}$ and $4.39 \times 10^{-9}\,\mathrm{m}^{-2}$, respectively, per proton on target (see Table 6 in Section 3). For an average of 5×10^{12} protons per second on target, this leads to a fluence rate of $1.9 \times 10^{9}\,\mathrm{cm}^{-2}\,\mathrm{h}^{-1}$ and $7.8 \times 10^{3}\,\mathrm{cm}^{-2}\,\mathrm{h}^{-1}$, respectively, at the SBL and LBL facilities. The factor to convert neutrino fluence to dose equivalent is close to $10^{-18}\,\mathrm{Sv\,cm}^2$. Thus the dose equivalent rates are $1.9 \times 10^{-9}\,\mathrm{Sv/h}$ at the SBL facility and $7.8 \times 10^{-15}\,\mathrm{Sv/h}$ at Gran Sasso. For comparison, natural background radiation levels at the ground surface are typically $100 \times 10^{-9}\,\mathrm{Sv/h}$ and are a factor of about three to four times lower than this in a limestone underground environment. The levels from neutrinos are thus insignificant.

6 PLANNING AND COST ESTIMATE

6.1 Installation procedure and planning

The schedule described here is based on the working hypothesis for the NGS study used in 1997. It assumes that funding would be available such that civil engineering could start in October 1998. This is now known not to be the case.

The effective planning must be based on the funding scenario and could be influenced by the duration of the authorization procedure for NGS in the CERN Host States. The latter can not be started before the authorization for the civil engineering of the LHC by the French authorities is obtained. Presently, a draft schedule for NGS is being prepared which assumes the start of civil engineering in spring 1999 and would allow a first NGS neutrino beam to be delivered early in 2003. The basic sequence of works follows the pattern described in this section.

Since the construction and installation of this new NGS facility interfere considerably with the LEP and SPS machine operation, as well as with the LHC project, the feasibility of this schedule is strongly linked to the following external time windows and milestones (see Fig. 29 to locate PGC8, TJ8 and TT40):

LHC project:

excavation of PGC8 and TJ8 in order to excavate the TT40 beam tunnel.	before end 1998

LEP and SPS operation:

winter shutdown: used to excavate the TT40 on the SPS side	Dec. 1998 to Mar. 1999
winter shutdown: to connect the hadron stop area to RE88 on the LEP side	Dec. 1999 to Mar. 2000
definitive LEP stop and start of LEP dismantling	Oct. 2000
long winter shutdown of the SPS: equipment installation in the SPS LSS4.	Nov. 2000 to May 2001 (7 months)

The planning for the construction and installation procedure is presented in Fig. 47. It is planned to launch the call for tender for civil engineering works by the end of April 1998 in order to reach the September 1998 Finance Committee for contract adjudication. The civil engineering construction can then start immediately. In this way, one can expect the first neutrino beam to Gran Sasso soon after May 2002. Should any delay in the start and/or execution of construction occur, the above time windows would be missed, and the operation of the NGS would be delayed until spring 2003 at the earliest.

Work starts by digging the NGS temporary access pit, followed by the excavation of the access gallery, the target chamber, the decay tunnel, and the hadron stop cave. It has been assumed that a tunnel boring machine (TBM) is used instead of a road header machine and/or explosives because of its higher progress rate (15 m/day). When the end of the hadron stop cave area is reached, the TBM is removed and may be reused to excavate the proton beam tunnel. The aim is to excavate the connecting tunnel between the hadron stop cave and the RE88 alcove during the LEP winter shutdown 1999–2000, and to finish the connection to the LSS4/ECA4 during the same LEP–SPS shutdown. The enlargement on the target chamber, the excavation of the adjacent caves and galleries, the enlargement of the hadron stop cave, and the final connection to the RE88 alcove are done simultaneously with the digging of the proton beam tunnel.

When the excavation is completed, i.e. 18 months after the site opening, the concrete lining or shotcreting of underground caverns is undertaken. The completion of civil engineering work is expected by the end of year 2000, leaving 16 months for: lowering and building the hadron stop and lowering the decay tunnel pipes (5 months); setting up services into the proton beam tunnel, the target chamber and adjacent galleries (2 months); installing the proton beam line and target chamber equipment (6 months); and commissioning the complete facility (3 months). In order to minimize interference with the dismantling of LEP in sector 8-1, a three-month time window is reserved to lower and install muon detectors and services in the hadron stop area.

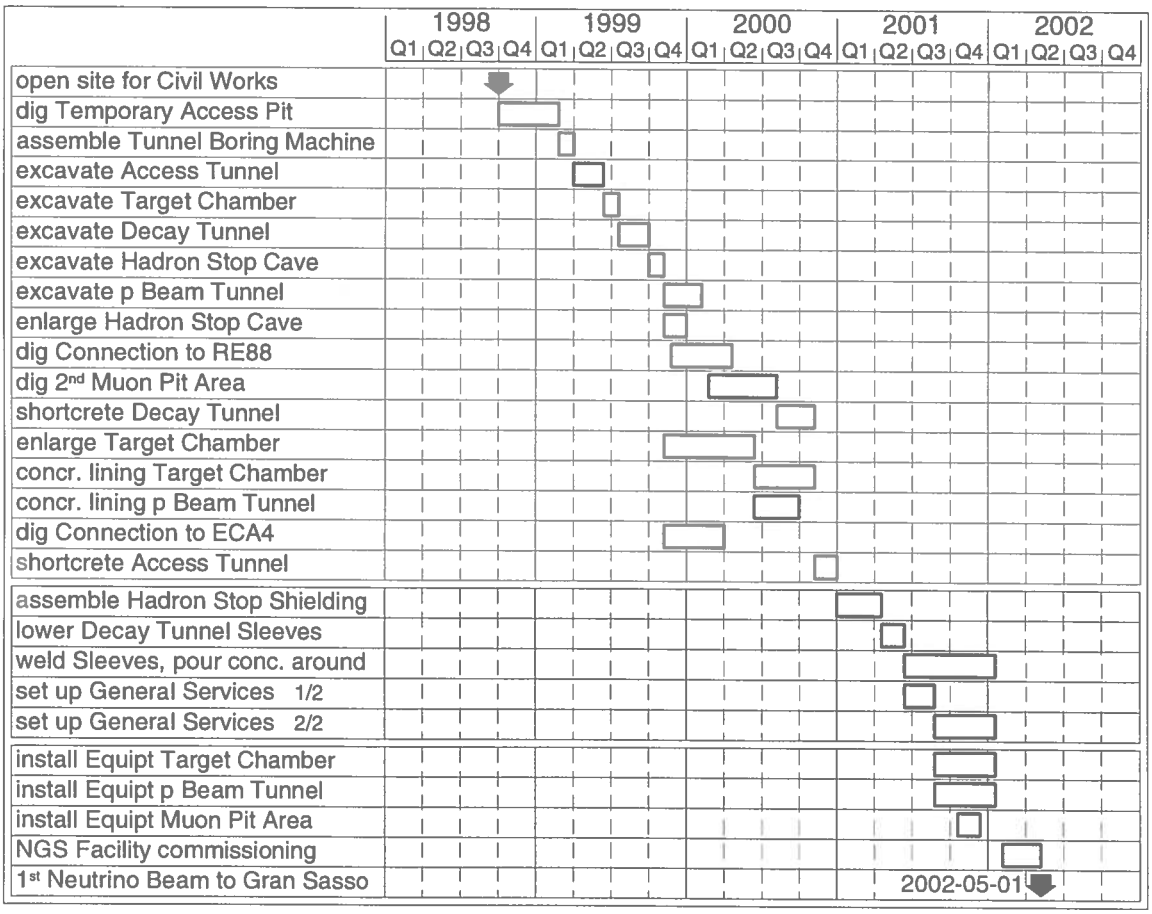

Fig. 47: Planning of the NGS beam project

6.2 Cost estimate

In Table 13 a summary is given of a detailed cost estimate (see CERN internal note [73]). Individual items do not contain any contingency, but a modest overall contingency of less than 5% has been added. Note that the cost for the short-baseline experimental area is not included here.

Manpower through industrial support contracts is included in these cost estimates. On the other hand, the CERN and INFN manpower needed for this project is not included. These manpower needs are currently being evaluated.

As is to be expected, the most expensive item in Table 13 is the civil engineering. The estimates given here are considered to be quite precise since they are extrapolated from the recently adjudicated tenders for the LHC civil engineering. The least expensive of the LHC tenders was chosen as the guideline for the NGS project. From experience, 10% for civil engineering design work, soil investigations, consultancies, etc., are then added. Note that the cost for the 1 km long decay tunnel, including its 2.45 m diameter steel tube, are included in the total for civil engineering.

Table 13: Cost estimate, in MCHF, of the NGS beam

Civil engineering		**41.6**
Proton tunnel, neutrino access gallery and civil engineering shaft (PGCN)	13.90	
Caverns (target area, hadron stop and access to muon chambers)	11.10	
Decay tunnel (including steel tube and concreting)	12.90	
Design work, soil investigations, consultancies	3.70	
Equipment		**19.2**
Proton beam	10.70	
Target	1.60	
Secondary beam	6.35	
Hadron stop	0.57	
Infrastructure		**7.0**
Cooling and ventilation	3.69	
Electrical infrastructure	1.26	
Handling equipment, crane, survey, safety, access system	2.03	
Contingency		**3.2**
Total (incl. industrial support)		**71.0**

A significant effort has been made to keep the cost of equipment low by re-using existing components from various facilities at CERN, such as from some West Area beam-lines (operation stopped at the end of 1996), from the present WANF facility as well as from LEP (not expected to run beyond 2000). In particular, all the iron needed for the hadron stop can be recovered from the WANF. All power supplies for the proton beam-line elements as well as for the focusing system (horn and reflector) can be recovered, together with a good fraction of the water-cooled cables needed for the high-power magnetic elements.

The cost for infrastructure is dominated by the need for cooling and ventilation equipment. Several ventilation circuits with filters are needed for the various beam and access tunnels. Smoke extraction systems are needed in all areas where equipment is to be installed.

The annual cost for the operation of the facility is currently under evaluation.

Acknowledgements

The contributions of a large number of people have made this report possible within a very short period of time.

Most importantly, the enthusiasm and skills of N. Pocock (SL-DI) were of invaluable help in editing and correcting the report.

Y. Bonnet (SL-EA), J.-P. Bouchet (EST-SU), A. Bronzini (ST-CV), J.-L. Caron (AC), M. Goujon (EST), C. Martel (ST-CV) and A. Vital (ST-CE) made important contributions to a number of the figures in the report. The assistance of J. Blondel (ST-TFM) and M. Vannier (ST-CE) in preparing and typing the civil engineering section is acknowledged.

M. Clément (SL-EA), P. Collier (SL-OP), M. Jones (EST-SU), M. Jonker (SL-OP), B. Pirollet (ST-CV) and M. Ross (SL-BT) have contributed at various stages of the preparation and during the evolution of this report.

We thank P. Bonnal (AC) and J.-L. Caron (AC) for the cover page of this report.

The fruitful discussions with members of NuMI at Fermilab, and in particular with J. Hylen, are gratefully acknowledged. We also thank N. Mokhov for an early calculation of the muon absorption.

Appendix A
REFERENCE PARAMETER LIST

Proton beam

Maximum proton beam momentum (design)	450 GeV/c
Proton beam momentum (assumed for operation)	400 GeV/c
Proton beam normalized emittance (1σ)	12π mm mrad
β^* at the focus (H and V)	2.5 m
$\rightarrow$ minimum beam size/maximum divergence (1σ)	0.27 mm, 0.1 mrad
Minimum repetition time (dedicated operation at 400 GeV/c)	7.2 s
Time between bursts	50 ms
Proton intensity (for hadron stop considerations)	5×10^{12} protons/second, 200 days/year
Proton intensity (for environmental considerations)	5×10^{19} protons/year

Expected integrated number of protons per 200 days ($\varepsilon = 50\%$), running with 2 subcycles for neutrinos and 16% duty cycle for slow extraction (cycle D, CERN-AC note 97–15)

at 350 GeV/c (SPS accel. limited)	3.4×10^{19} protons
at 400 GeV/c (SPS accel. + target limited)	3.0×10^{19} protons
at 450 GeV/c (graphite target limited)	2.0×10^{19} protons

Expected period of operation	10 years

Target chamber

Length of target chamber	115 m
Diameter of target chamber	6.5 m (int.)
Floor width of target chamber	5.6 m
[Enlargement at target (optional)]	7.4 m
Crane capacity	10 t
Free height under crane hook	3.7 m
Beam height in target chamber	1.6 m
Diameter of neutrino service gallery	3.4 m (int.)
Distance of service gallery from cavern	6.0 m
Length of junction tunnel to target chamber	8 m
Distance of proton focus to entrance of decay tunnel	100 m

Target

Start coordinate (w.r.t. proton focus)	−0.5 m
End coordinate (w.r.t. proton focus)	+1.5 m
Target material	carbon
Target rod length	10 cm
Diameter of rods	3 mm
Number of rods	11
Distance between rods	9 cm

Note: it is possible that a more compact target (i.e. more rods) will finally be used inside the defined space.

Collimators

COLL1 (at target exit)

Material	copper
Start coordinate (w.r.t. proton focus)	+1.70 m
End coordinate (w.r.t. proton focus)	+2.90 m
Cross-section: square	$1 \times 1\,m^2$
Opening: cylindrical, radius such that limitation at exit is (seen from the proton focus)	±20 mrad

COLL2 (before the horn)

Material	aluminum
Start coordinate (w.r.t. proton focus)	+4.30 m
End coordinate (w.r.t. proton focus)	+7.00 m
Cross-section: cylindrical	diameter 0.5 m
Opening: conical, opening angle seen from focus	±15 mrad

COLL3 (between horn and reflector)

Distance from proton beam focus to COLL3 entrance	25 m
Length of collimator	1.6 m
Opening of collimator	$0.8 \times 0.8\,m^2$

Outer dimensions of collimator: like WANF, see Fig. 36 of this report.

Horn and reflector (dimensions referring to **magnetic length**):

Distance from proton beam focus to horn entrance	7.85 m
Length of horn	6.65 m
Current in horn	120 kA
Distance from proton beam focus to reflector entrance	80.35 m
Length of reflector	6.65 m
Current in reflector	120 kA
Present design of conductors	see Section 3

Note: for the calculations, it is assumed that all spaces outside the horn and reflector are filled with helium at 1 atm.

Decay tunnel

Upstream end of decay tunnel (w.r.t. focus)	100 m
Length of decay tunnel	992 m
Diameter of decay tunnel (TBM)	3.50 m (ext.)
Length of decay pipe	994.5 m
Diameter of decay pipe (inner diam. steel pipe)	2.45 m (96 inch)
Wall thickness decay pipe	20 mm
Concrete filling around pipe	ca. 53 cm
Entrance window decay pipe	diameter 1 m, 2 mm titanium
Exit window decay pipe	5 cm steel
Pressure in decay pipe (min.)	1–2 Torr
Pumping down time (max.)	2 weeks

Decay pipe collimator (iron)

Start of collimator (w.r.t. proton beam focus)	100 m
Length of collimator	10 m
Inner diameter of collimator	1 m
Outer diameter of collimator (= inner diameter of shotcrete)	3.1 m

Hadron stop and muon chambers

Upstream end of hadron stop cavern (w.r.t. proton focus)	100 + 992 m
Length of hadron stop cavern	26 m
Diameter of hadron stop cavern	6 m (int.)
Length of hadron stop	18.2 m
Cross-section of hadron stop	$4 \times 4\,\mathrm{m}^2$
Length of graphite insert	3 m
Cross-section of graphite insert	$2.6 \times 2.6\,\mathrm{m}^2$
Wall thickness of aluminium box around graphite	0.1 m
Length of airgap upstream of hadron stop	0.25 m
Length of airgap downstream of hadron stop (= length of first muon chamber)	5 m
Length of 'muon filter': molasse	67 m
Length of 2nd muon chamber	3.5 m
Muon pit 'service alcove' surface	$10 \times 4\,\mathrm{m}^2$
Access gallery to hadron stop: diameter	3.1 m (int.)
Access gallery to 2nd muon pit: diameter	2.5 m (int.)

Short-baseline experiment

Distance proton focus to SBL cavern	approx. 1850 m

Appendix B
TECHNICAL DRAWINGS: CIVIL ENGINEERING AND TARGET STATION

In this Appendix, detailed drawings showing the civil engineering layout of the CERN-NGS facility are presented (Figs. B.1–B.3). They provide the necessary details for a more technically interested reader.

Similarly, the detailed drawings of the target station layout inside the target chamber are shown in the three views (Figs. B.4–B.6), together with an illustration of the complex target station shielding (Fig. B.7).

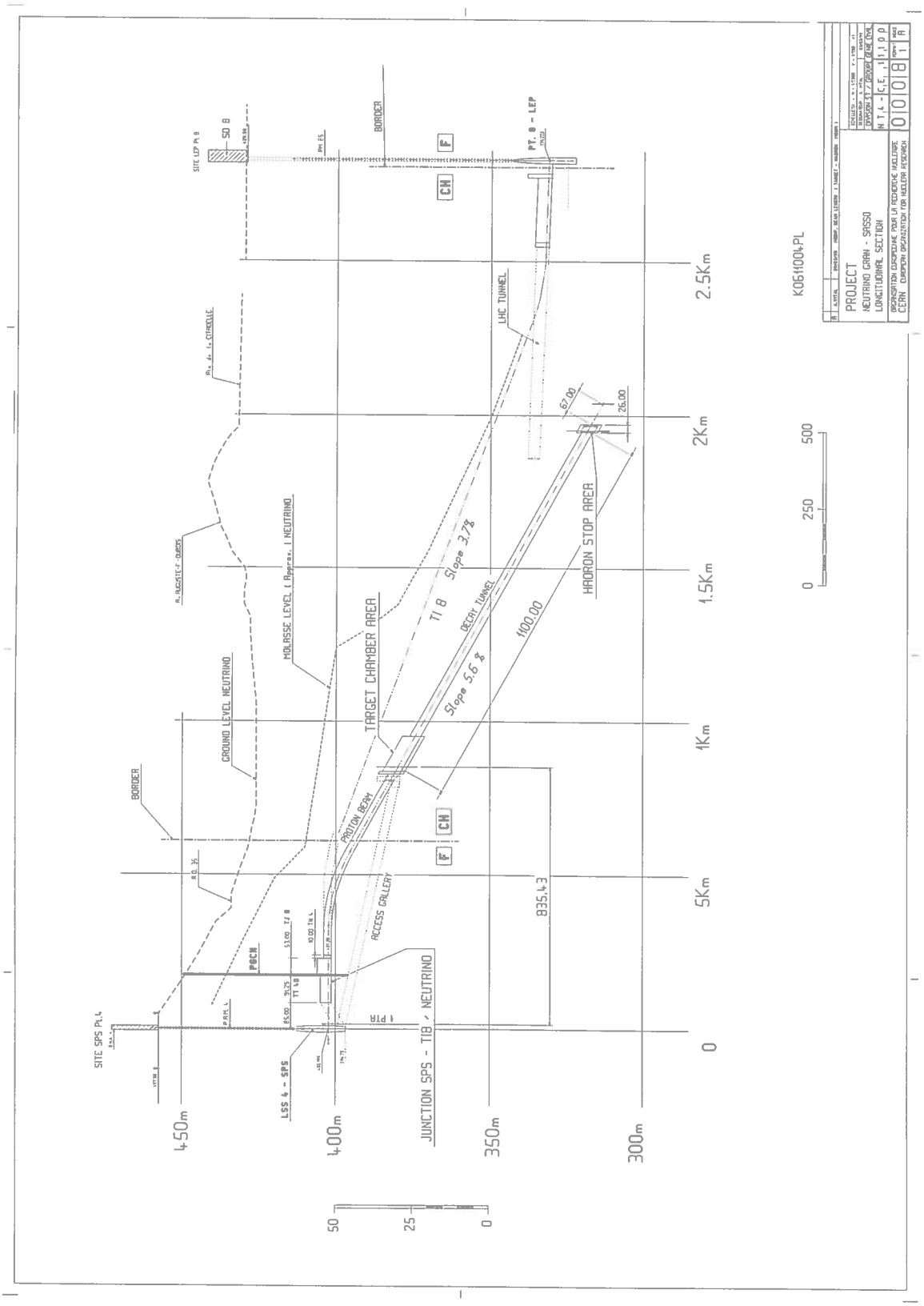

Fig. B.1: Components of the NGS (vertical cut)

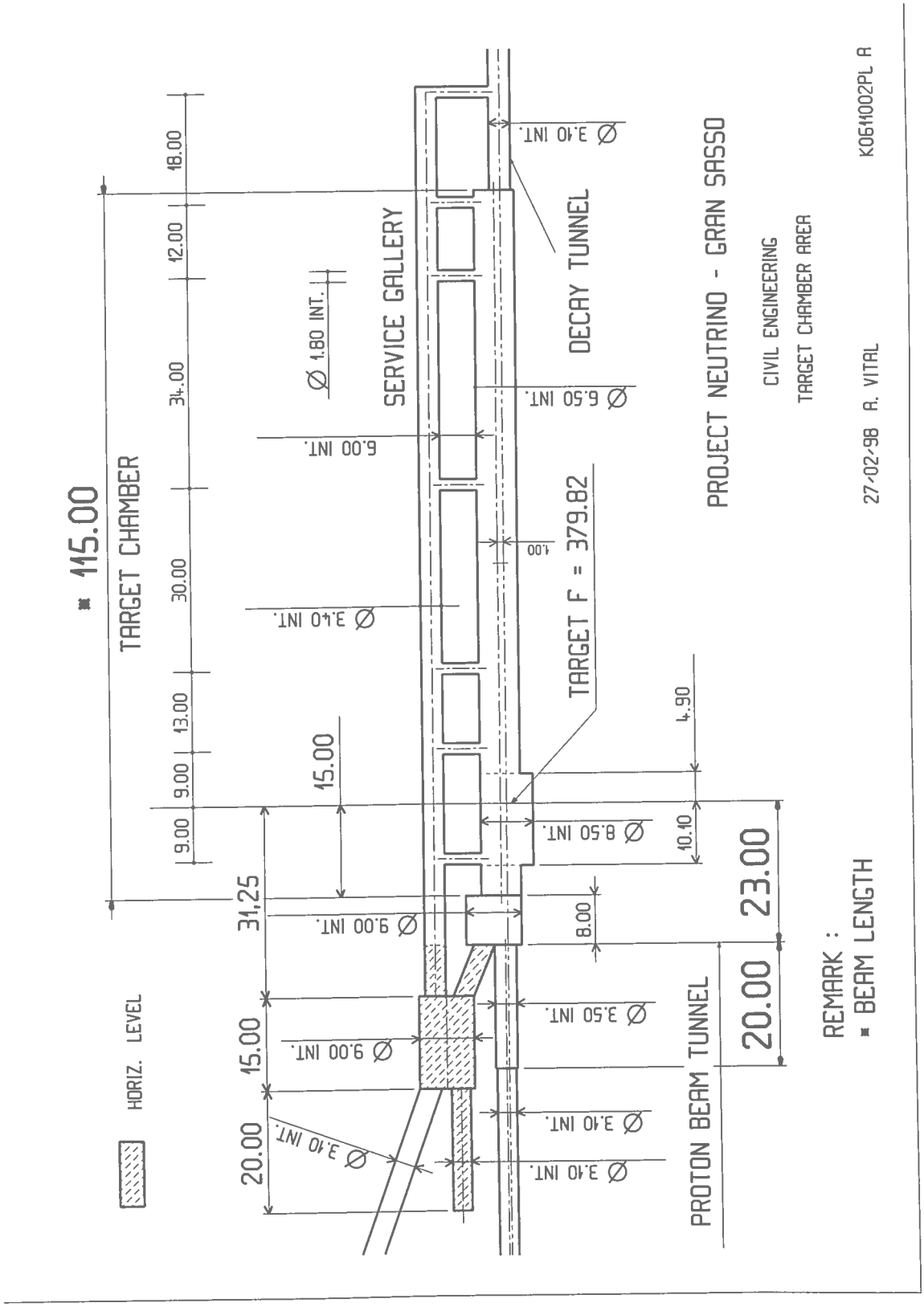

Fig. B.2: Civil engineering layout of the target chamber and the adjacent areas (dimensions in metres)

Fig. B.3: Civil engineering layout of the hadron stop chamber, the muon pits and their access tunnels (dimensions in metres)

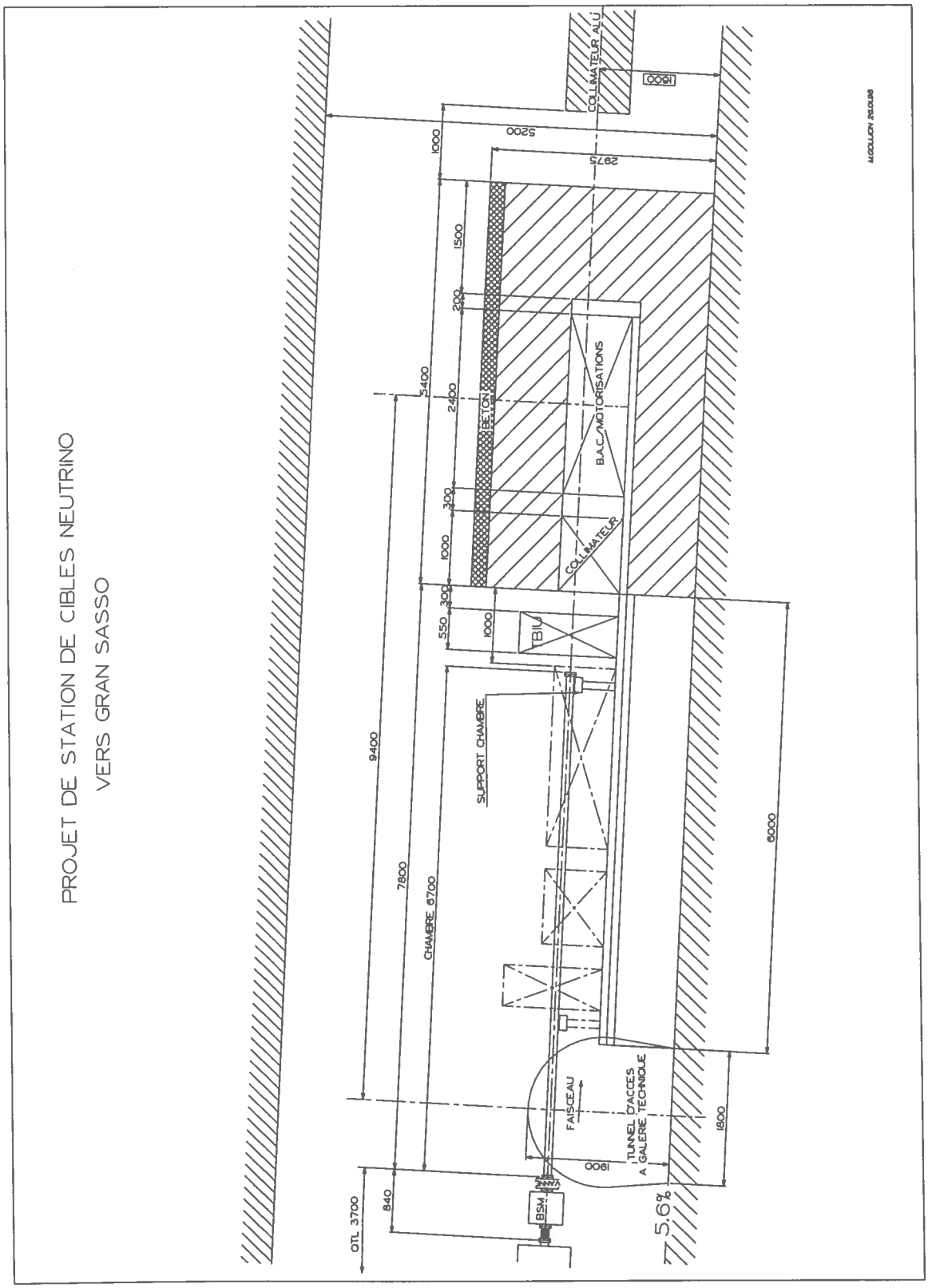

Fig. B.4: Side view of the NGS target region (dimensions in millimetres)

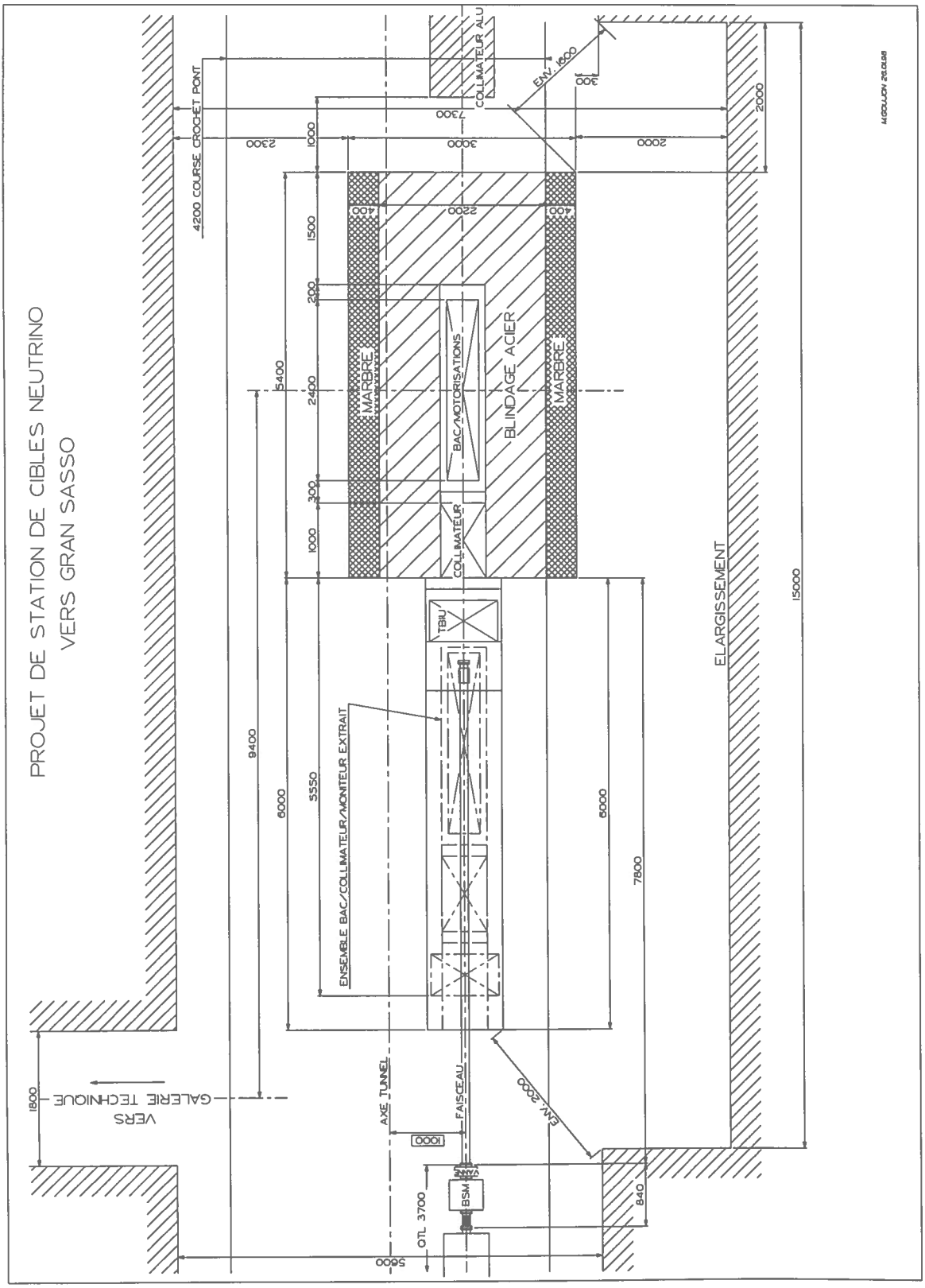

Fig. B.5: Top view of the NGS target station (dimensions in millimetres)

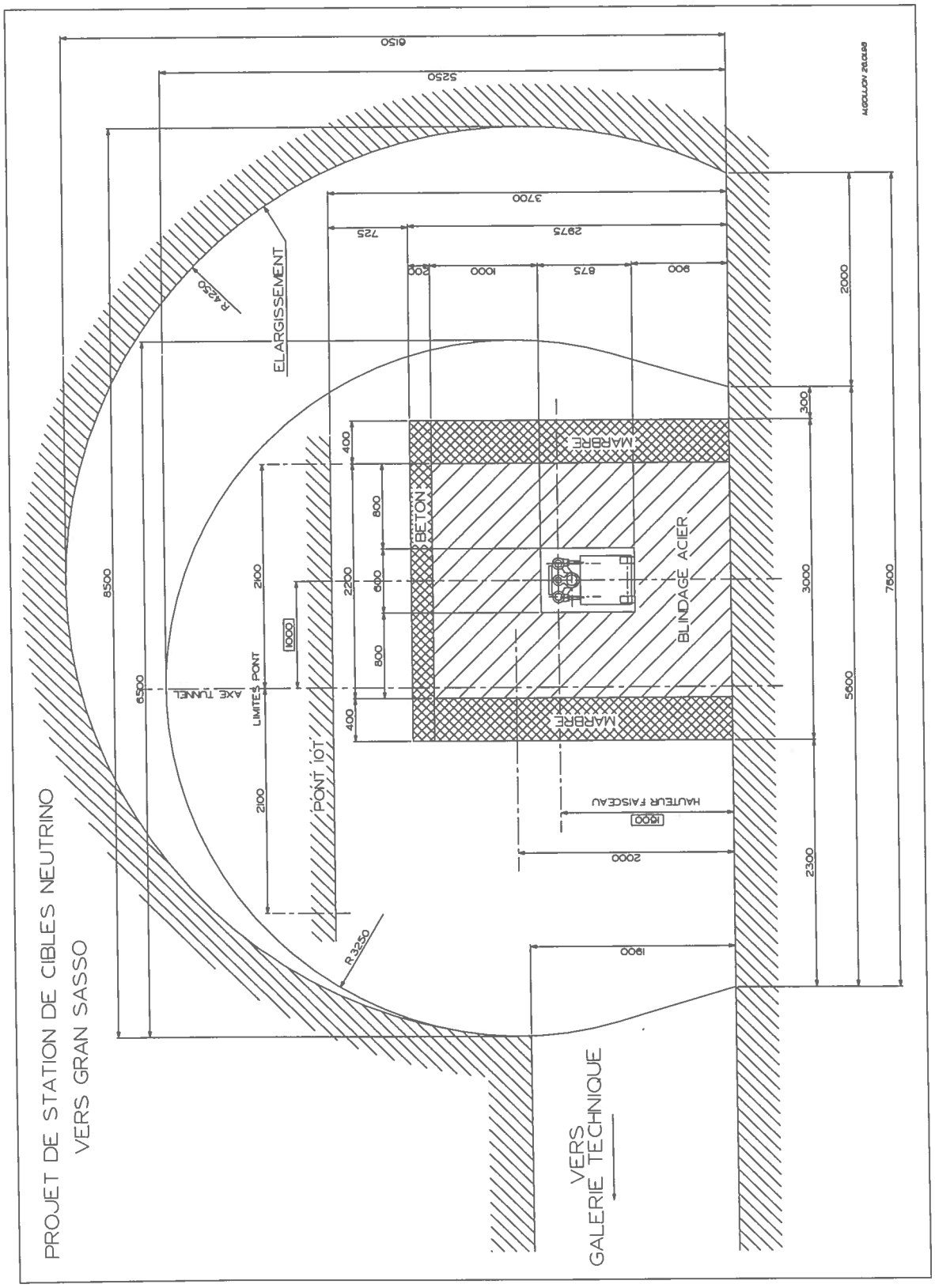

Fig. B.6: Front view of the NGS target station (dimensions in millimetres)

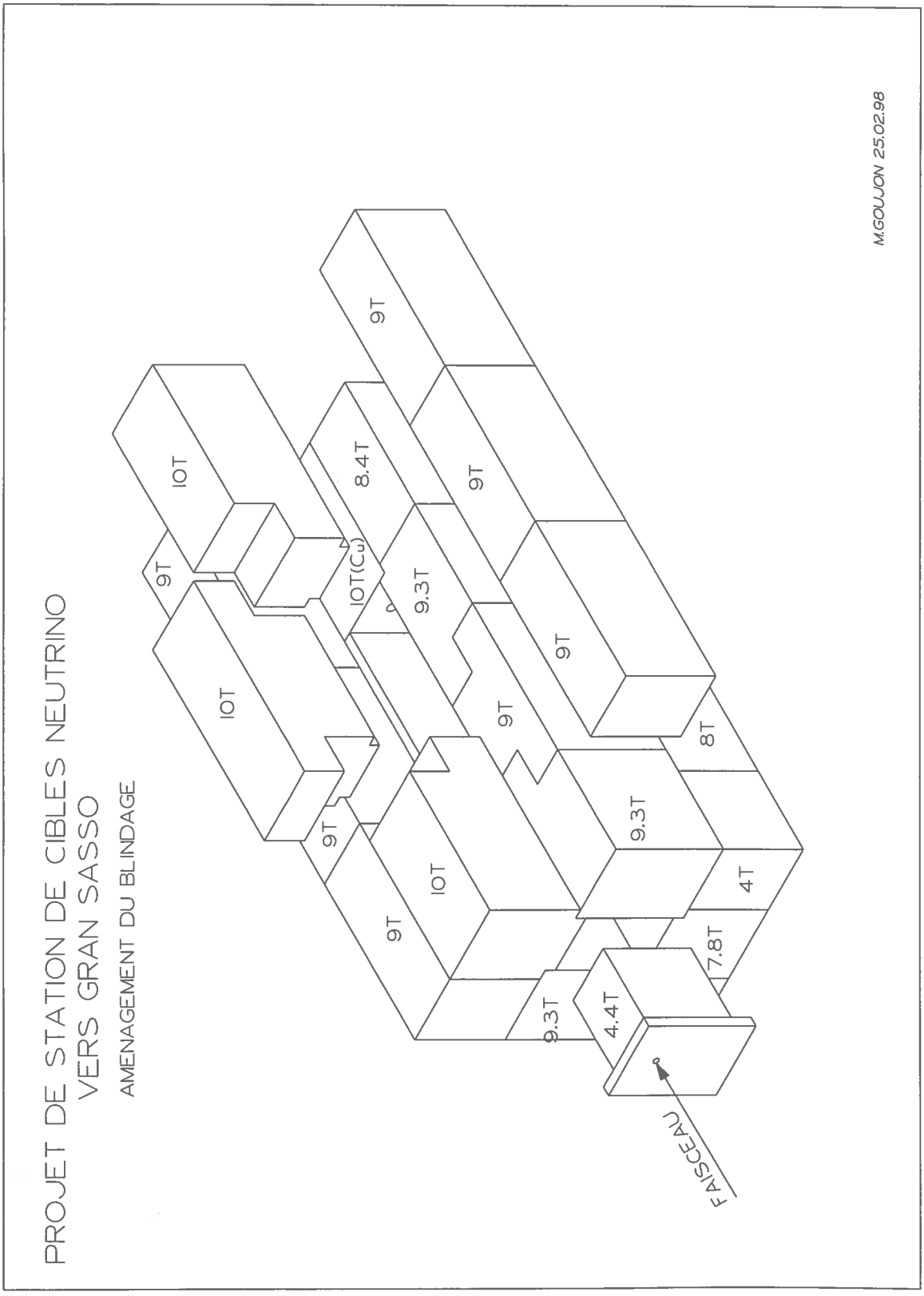

Fig. B.7: Shielding of the NGS target station

Appendix C
THERMOMECHANICAL ANALYSIS OF THE TARGETS

C.1 Energy deposition

The energy density per incident proton deposited on beryllium or graphite rods of 3 mm diameter and 10 cm long, is estimated from simulations with the Monte Carlo shower code FLUKA [46], using the beam parameters listed in Table 11, Section 4.4. This simulates the random injection of thousands of protons into the relevant transverse phase space. The interactions, transport, and energy deposition processes are followed down to 0.1 MeV for all charged particles, down to 10 keV for photons, and down to 0.4 eV for neutrons. The energy density on each rod is scored using a regular cylindrical binning mesh of 0.1 mm thick by 10 mm long. Other target box details are neglected for this analysis. Figure C.1 shows the total energy absorbed by successive beryllium rods, while Fig. C.2 displays, for several of them, the radial distribution of energy density averaged over the rod length.

The most critical rod is the first one, as the deposited energy density reaches its maximum value of 0.44 GeV/cm^3 per primary proton (at about 8.5 cm depth) and its steepest axial and radial gradients. Maximum thermal and mechanical constraints have thus to be expected in this rod, even though the second one absorbs slightly more integrated energy. Hence, only the behaviour of the first rod is considered in the subsequent analysis. The continuous curves of Fig. C.2 are fits to a Gaussian distribution; they suggest that the mean radial distribution of energy density in a rod can be modelled as:

$$d_0 \times \exp(-b \times r^2)$$

which is important for the 1-D analytical calculation. For the first rod, one finds the quantities given in Table C.1.

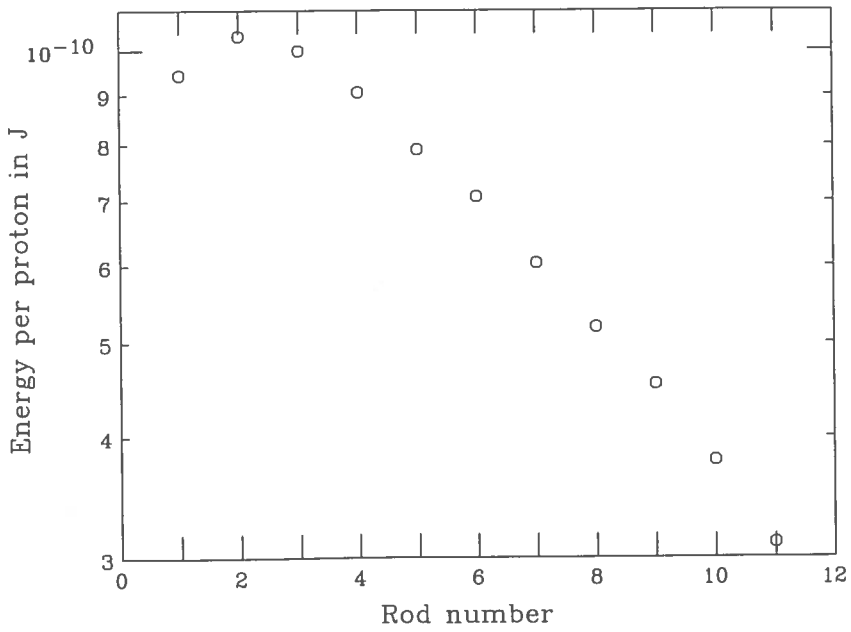

Fig. C.1: Energy deposited per proton in each beryllium rod

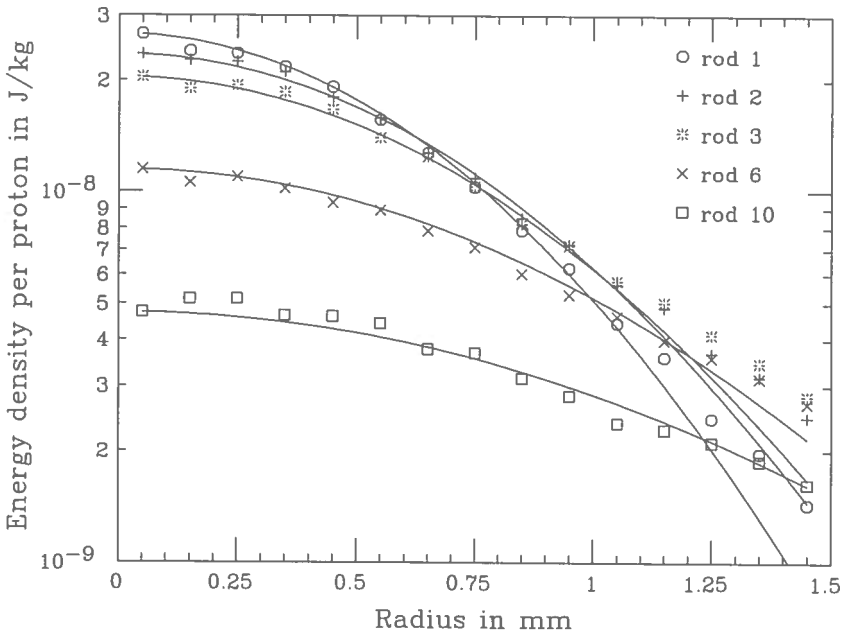

Fig. C.2: Energy density in various beryllium rods

Table C.1: Parameters of energy density deposition in beryllium and graphite

	Beryllium	Graphite
ρ (g/cm^3)	1.85	1.75
d_0 (J/cm^3 $\times$ 10^{13} protons)	495	535
b (mm^{-2})	1.60	1.77

C.2 Temperature

Any local energy deposition d is assumed to immediately result in a local temperature rise ΔT:

$$d = \rho \int_{T_\mathrm{i}}^{T_\mathrm{i}+\Delta T} C_\mathrm{p}(T) \times \mathrm{d}T \,,$$

T_i being the initial temperature, ρ the material density and C_p its specific heat. This equation links the FLUKA output (d) and the input (ΔT) of any thermal analysis. Most of the thermal and mechanical material properties are temperature-dependent (e.g. C_p), and thus lead to non-linear behaviour. Nevertheless, the mean radial distribution of an initial temperature rise can also be approximated by a Gaussian distribution. The time-dependence of the temperature distribution can either be estimated by 1-D analytical or 2-D finite-element method. Each model assumes an axially symmetric thermal load, unconstrained axial and radial expansion, and thermal convection as heat transfer boundary conditions. The 1-D method considers an instantaneous and Gaussian initial temperature distribution, identical over the whole rod length. The 2-D method, performed with the ANSYS [74] analysis system, uses an internal thermal load derived from FLUKA output and accounts for the burst duration.

Figure C.3 shows the temperature evolution of a beryllium rod submitted to a single 10 μs FE: the temperature rise reaches its maximum value at the end of the burst. Both transient

analyses highlight two main phases: a conduction process which leads to a quasi-uniform rod temperature after 30–40 ms, followed by an exponential-like homogeneous cooling. The latter, roughly defined by a time constant (τ), provides an easy estimation of the steady state stemming from periodic thermal cycling (τ is assumed to be 4.9 s for beryllium and 1.7 s for graphite). Figure C.4 displays the temperature evolution of two 10 μs FEs of 2×10^{13} protons each, 50 ms spaced, impinging on a graphite rod every 7.2 s: the axial temperature varies from 25°C to 640°C going through 160°C. This is the temperature at the start of the second burst, which is taken as the initial temperature (T_i) in the subsequent mechanical analysis.

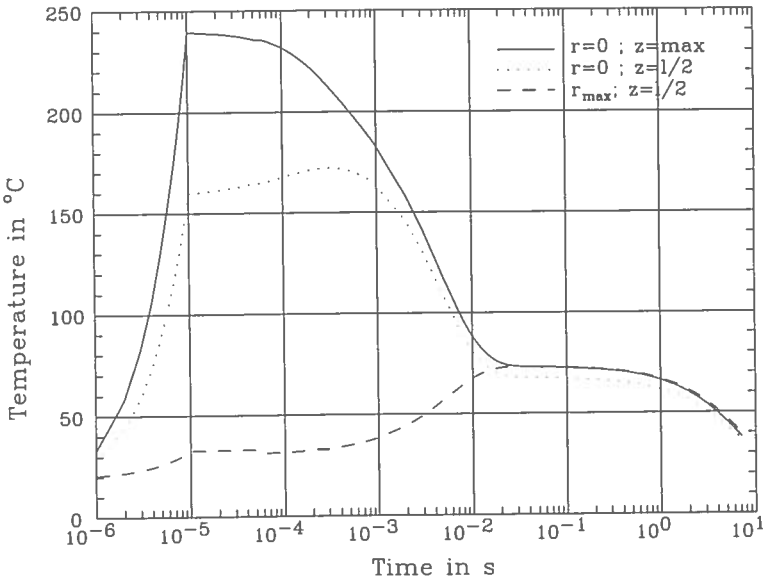

Fig. C.3: Temperature evolution of the first beryllium rod submitted to a single 10 μs FE

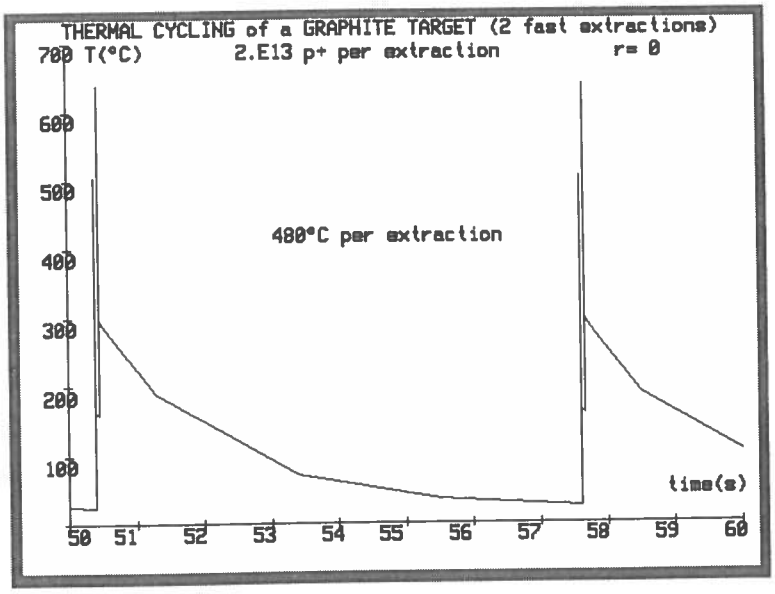

Fig. C.4: Temperature evolution of the first graphite rod submitted to two FE bursts of 10 μs each

C.3 Stresses

It is usual to distinguish between quasistatic and dynamic thermal stress components; this is rather artificial but a very useful method for an analytical approach. A quasistatic process can be taken as a sequence of stationary states, without any time limitation to meet the required thermal expansion constraints. Having estimated the radial distribution $\Delta T(r)$, the quasi-static thermal stress calculations can easily be performed (see Appendix A in Ref. [75]). A dynamic process should only be considered if the burst duration is shorter than or of the same order of magnitude as the time spent by the sound to travel from the rod centre to the edges. This is summarized in Table C.2.

Table C.2: Sound propagation in beryllium and graphite

	Beryllium	Graphite
Sound velocity c_s (mm/μs)	12.7	2.32
Axial travel duration over 50 mm (μs)	3.9	21.6
Radial travel duration over 1.5 mm (μs)	0.1	0.6

In this study, elastic waves of significant amplitude have thus to be expected in the longitudinal direction only. The ANSYS program performs a global thermal stress calculation, including the dynamic components provided that material density and time-dependence of thermal loads are specified. Figure C.5 shows the time evolution of the three main stresses stemming from an FE: the transverse stresses, σ_r and σ_θ, identical on-axis, have practically no dynamic component, whereas the longitudinal one (σ_z) displays a well-shaped dynamic wave superimposed over the quasistatic component. The 1-D analytical method to estimate the dynamic thermal stress component is described in Refs. [65, 75]. It assumes a hydrostatic pressure (p) stemming from the thermal inertia of the rod, instantaneously heated. It is worth noting that the dynamic wave amplitudes and periods are very similar, in both longitudinal and transverse directions, to those calculated by a 2-D analysis [66].

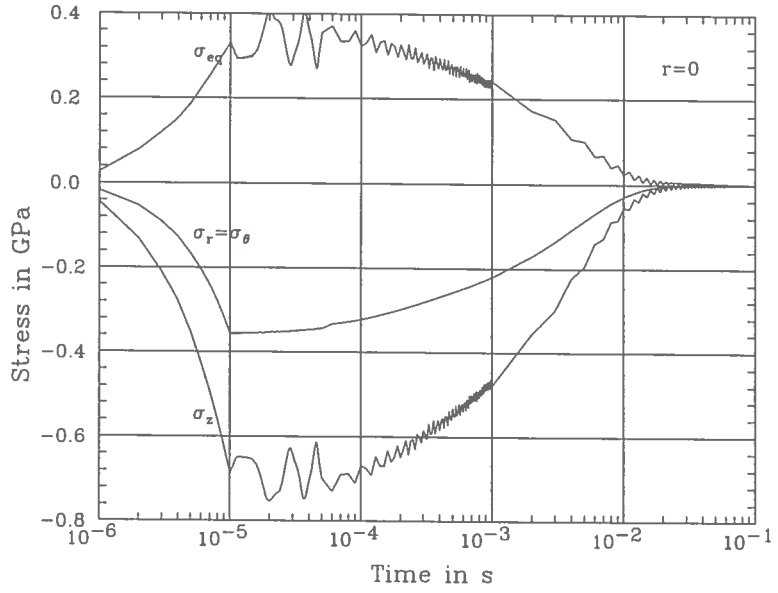

Fig. C.5: Time evolution of the three main stresses in the first beryllium rod submitted to a 10 μs FE

It is of little interest to perform a stress analysis if one has no clear and reliable equivalent strength criterion. These days, the one most commonly used for materials like beryllium with the same tensile (σ_0) and compressive (σ'_0) strength limits ($\sigma_{0,2}$), is the Von Mises equivalent stress (σ_{eq}) based on maximum shear energy. However, for materials like graphite the correct one, accounting for differing strength limit, is the Stassi criterion (σ_{teq}) [76]:

$$k \times \sigma_{teq}^2 - (k-1) \times (\sigma_r + \sigma_\theta + \sigma_z) \times \sigma_{teq} - \sigma_{eq}^2 = 0, \text{with } k = \sigma'_0/\sigma_0 \geq 1 \ .$$

Note that $\sigma_{eq} \leq \sigma_{0,2}$ (Von Mises) and $\sigma_{teq} \leq \sigma_0$ (Stassi), become identical if $k = 1$; the Stassi criterion is a generalization of the one introduced by Von Mises.

C.4 Beam intensity limitation

For the calculations, a material of maximum admissible strength σ_0 is assumed to be submitted to an FE of t_0 duration. The equivalent strength (σ_{teq}) is a function of two components: quasistatic and longitudinal dynamic. The quasistatic component depends only on the beam intensity I, while the longitudinal dynamic component is a function of the hydrostatic pressure p, the burst length t_0 and the rod half-length L; but since p is also dependent on I, this component is finally a function of I, t_0 and L, which can have a maximum value (σ_{z0}) reaching p [75]; in such a case it is no longer (t_0, L) dependent. The three parameters I, t_0 and L are optimized when the maximum of σ_{teq} equals σ_0: L and t_0 lead to the longitudinal stress σ_{z0} which, together with the quasielastic stresses stemming from I, adds up to σ_0. Figures C.6 and C.7 summarize the beam intensity limitation on rods of variable length submitted to FEs of various durations (6, 10 and 20 μs), for beryllium ($\sigma_0 = 29\,\text{daN/mm}^2$, $k = 1$) and graphite ($\sigma_0 = 1.6\,\text{daN/mm}^2$, $k = 4$). A maximum allowed intensity per burst of a given duration exists at any rod length. However, for some intensities many rod length values are possible, and L is no longer correlated to I if $2L \geq c_s \times t_0$. As one can see, very short rod lengths lead to extremely high intensities, but in particularly unstable (L, I) regions; such instabilities are explained by Fig. 5 of Ref. [75]. More probable length ranges, presently foreseen, lead to the maximum intensities per burst (10^{13}p^+ at 450 GeV) given in Table 12, Section 4.4

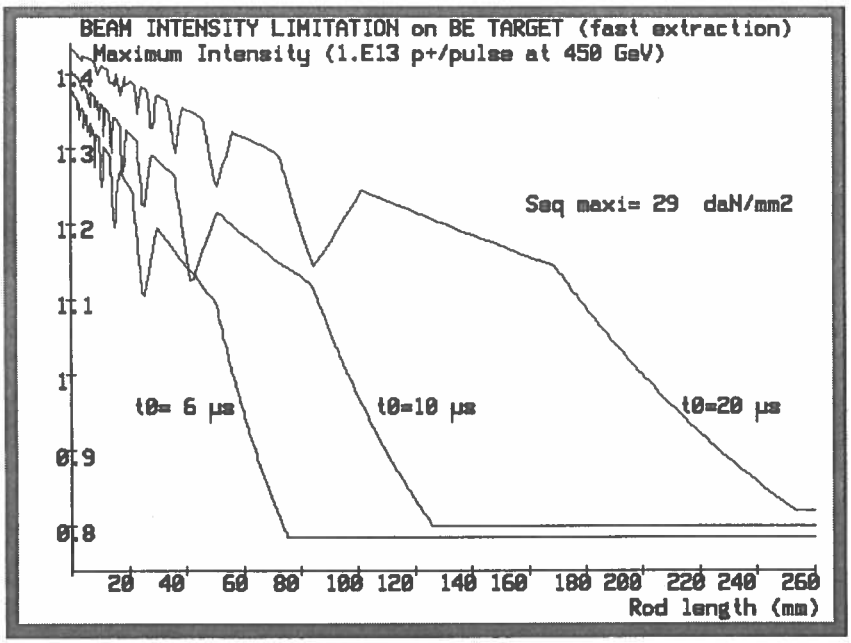

Fig. C.6: Beam intensity limitation for the beryllium target

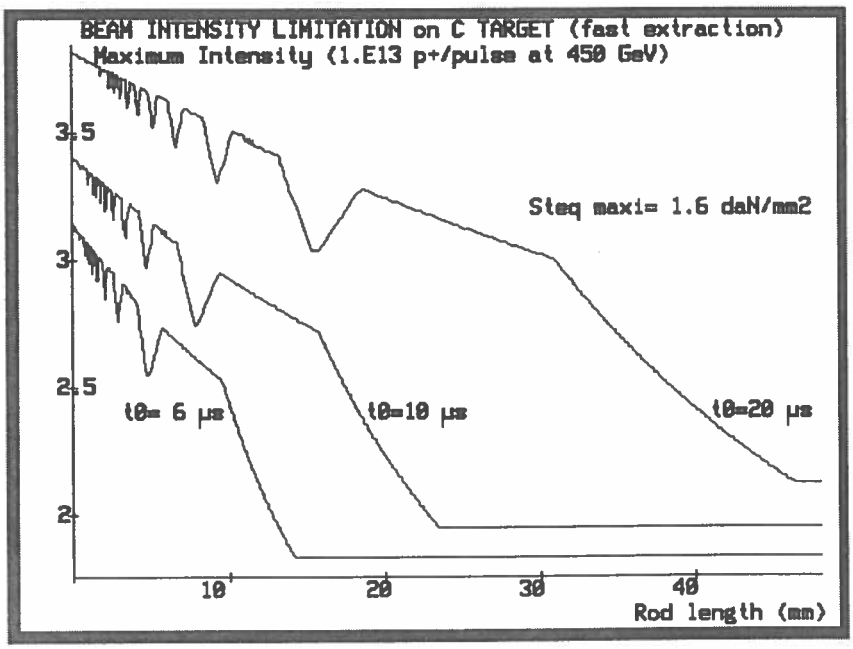

Fig. C.7: Beam intensity limitation for the graphite target

Appendix D
GEODETIC METROLOGY OF THE UNDERGROUND BEAM LINE

D.1 Metrological network

The alignment of the beam line components is done from a metrological network. This network, consisting of tripods, is determined from the position of the SPS quadrupoles around the departure of the beam line. The main problem for the determination of this network is that there is no access to any well-known points at the extremity of the decay tunnel, and the polygonal traverse therefore remains as an 'antenna'. As a matter of fact, the geometrical configuration for a link to LEP points is not good enough for this metrology.

In the vertical plane, the network is measured using optical levels and the accuracy can be expressed as follows:

$$\delta_\nu = \sigma_{\text{niv}} \times \sqrt{D}$$

Here σ_{niv} is the standard deviation over 1 km and D the distance in kilometres. At the end of the decay tunnel, $D = 1.8$ km and $\sigma_{\text{niv}} = 0.4$ mm, so the error can reach 0.5 mm. As already mentioned, these vertical measurements apply only to altitudes H (above the geoid) but not to ellipsoidal heights, which cannot be directly assessed.

In the XY plane, for the above-mentioned reasons and in order to ensure a good absolute determination of the network all along the tunnel, gyrotheodolite measurements are indispensable. The radial accuracy at the end of the network (in the area of the muon detectors) can be expressed as follows :

$$\delta_{\text{r}} = \sigma_{\text{gyro}} \times d \times \sqrt{n}$$

where σ_{gyro} denotes the standard deviation of the gyrotheodolite, d the span between two gyromeasurements and n the total number of sides of the traverse.

An optimization of the span d and therefore of the number of sides n has to be done, according to practical conditions. As an example, for $\sigma_{\text{gyro}} = 3$ arcsec, a distance $D = 1800$ m, a span $d = 50$ m, n is 36, the resulting radial error is 4.7 mm.

In addition to the gyrotheodolite measurements, overlapping offset measurements contribute to a better relative determination, in order to ensure a 'smoothness' quality of 0.1 mm r.m.s. all along the network.

D.2 Alignment of the curved proton beam line up to the target

The main quadrupoles are initially aligned from the metrological network using optical levels, theodolites and CERN 'ecartometers', which can accurately measure offsets to a straight line materialized by a stretched wire [77]. Then the position of these components are 'smoothed' so that the accuracy in the relative positions between three consecutive components remains lower than 0.2 mm in the XY plane and 0.1 mm for the altitude.

Finally, the remaining components are aligned according to these quadrupoles and with the same relative positional accuracy.

D.3 Metrology of the straight section and the magnetic horn

Particular attention is given to the alignment of the proton beam straight section, containing the final focusing quadrupoles, and to the magnetic horn, as all the components in this section have to be aligned to within 0.1 mm and must lie precisely in the absolute direction towards the Gran Sasso Laboratory. Therefore, offset measurements ensure the required accuracy for the

relative position, and gyrotheodolite measurements guarantee the absolute orientation within 3 arcsec.

The maintenance of the alignment of this area together with the level of radiation would certainly require the setting up of fixed reference tripods. Special attention must also be paid to the positioning and to the stability control of the magnetic horn.

D.4 Metrology of the muon detectors and final adjustment of the line

In the vertical plane, the error on the slope between the horn and the muon detectors is slightly dependent upon the error in the difference of measured altitudes (only 0.4 mm at 1 km), but it can be more strongly affected by the uncertainties of the geoidal parameters — i.e. errors on its absolute slope in the EUREF system and on local undulations in the interval. The local undulations are known to within a few millimetres (from the mass model) but there is no clear idea yet on the possible discrepancies in position and slope between the Swiss geoid, the French one, the EUREF one, and the CERN one. A good indication results from step 4 of the geodetic process mentioned in Section 4.2.3.

As for the azimuth, the situation can be more easily sketched and analysed as shown in Fig. D.1.

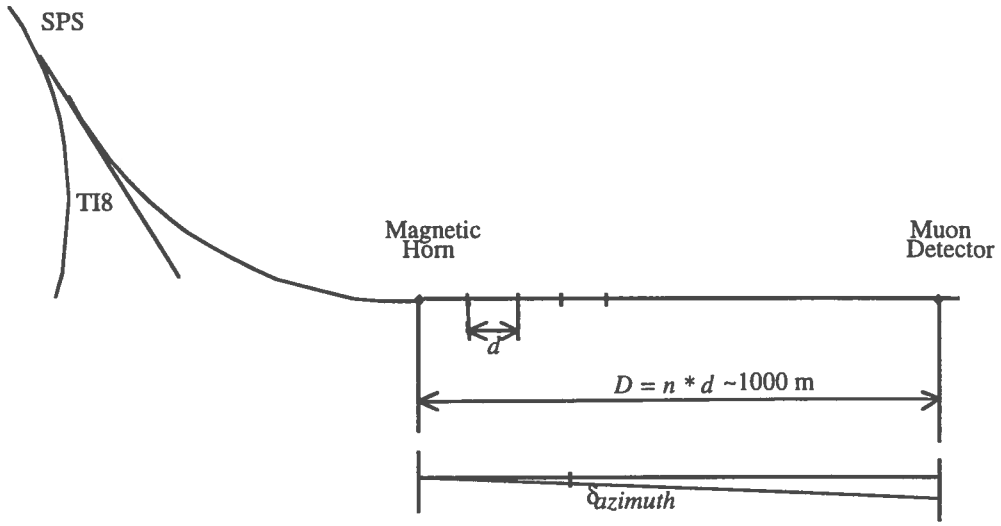

Fig. D.1: Schematic view of the (azimuthal) alignment of the NGS beam

The error on the azimuth between the magnetic horn and the muon detectors becomes:

$$\delta_{\text{azimuth}} = \frac{\delta_{\text{r}}}{D} = \frac{\sigma_{\text{gyro}} \cdot d \cdot \sqrt{n}}{d \cdot n} = \frac{\sigma_{\text{gyro}}}{\sqrt{n}} .$$

For a $\sigma_{\text{gyro}} = 3$ arcsec and $n = 20$, the r.m.s. error on the resulting azimuth could be limited to 3×10^{-6} rad.

As a by-product of the accurate GPS measurement required for the geoidal parameters, the orientation parameters in the EUREF system are accurately deduced. Considering an additional 2×10^{-6} rad random error in this determination, the final error in absolute orientation would be maintained to less than 4×10^{-6} rad r.m.s. — which makes a radial error of 3 m r.m.s. around the target point, at 732 km from the origin.

Appendix E
DETAILS OF THE ELECTRICAL SYSTEMS FOR HORN AND REFLECTOR

E.1 General layout

Horn and reflector electrical circuits are identical according to the scheme shown in Fig. E.1.

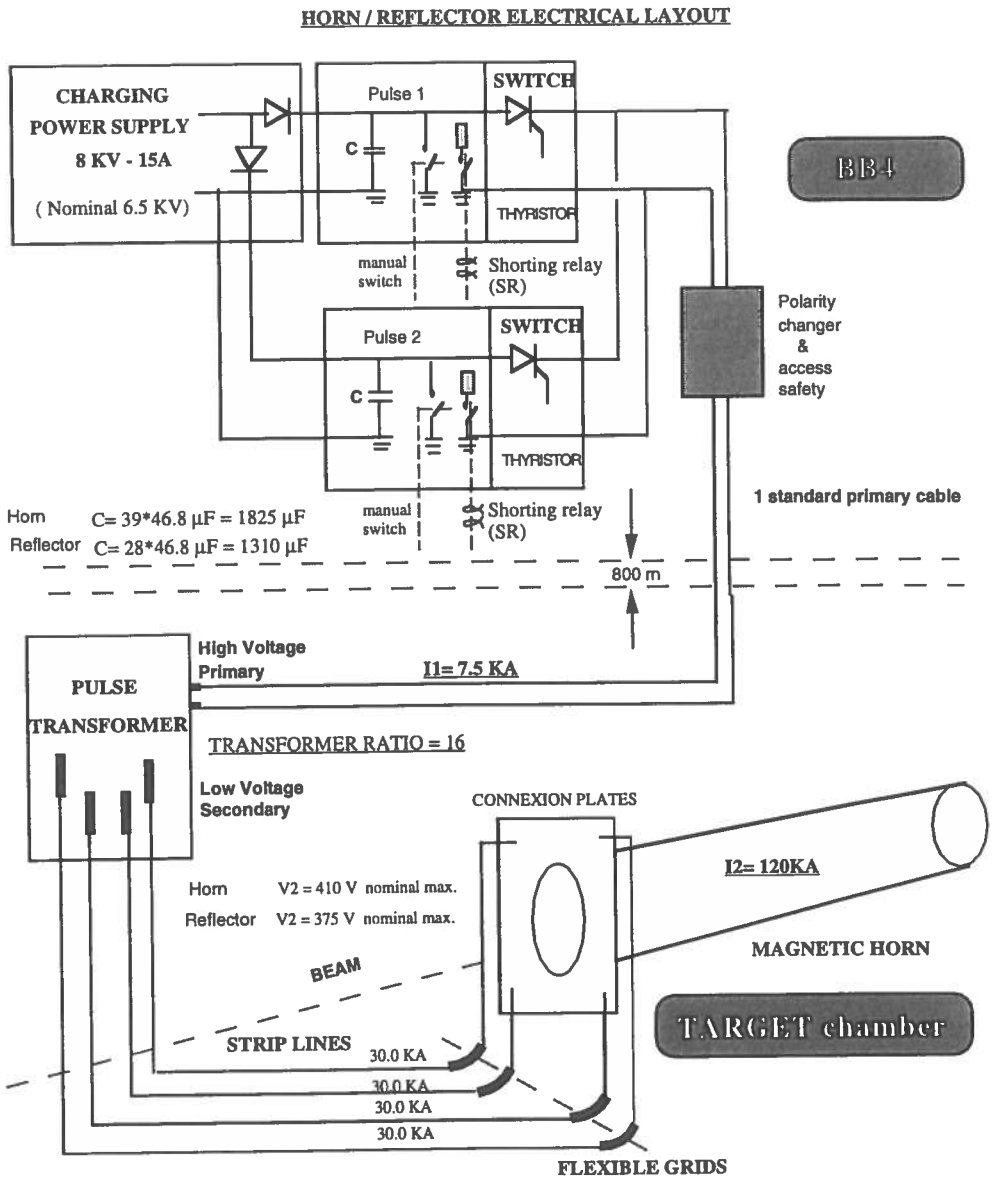

Fig. E.1: Horn/reflector electrical layout

The requirement is to produce a stable reproducible field (0.1% precision) in the element during the two 10 μs fast spill extractions. For each circuit, the currents (pulse 1 and pulse 2) are produced by the discharge of two capacitor banks into the element which acts as an inductive load with small resistance. This circuit L, C, R is undercritically damped and the top of the first half sine wave is used to produce the magnetic field needed during the extraction time.

The two capacitor banks are charged by one special 8 kV charging power supply. Between the load and pulse generator a pulse transformer of ratio 16 is inserted which results in the following advantages:

1. The primary current is the load current divided by 16. This allows the insertion of one remotely controlled and motorized polarity changer on the power line just after the thyristor switches. It is located in a separate cabinet and remote control is possible from within the supervisor panel provided by the beam control system. Only one primary high-voltage cable is necessary between the polarity changer and transformer, and this is useful since this distance is around 1000 m from the surface to the service tunnel where the transformer is located.
2. The voltage on the load is low since it is the pulse generator voltage divided by 16. This allows the use of radiation-resistant Arclex spacers for insulation of the connections and of the strip-lines.
3. The pulse transformer includes in fact four primary coils and four secondary coils interlaced. The leads of the four primaries are mounted in parallel externally to the coil mould; the four secondaries are attached to four strip-lines connected to the horn connection plates. This gives the possibility to tune their impedance by adjustment of the inductance of each line through remachining of the width. Hence it is possible to equalize the four secondary currents. This is used as an indirect measure of the correct field distribution in the horn.

E.2 Main electrical components

A schematic diagram of the horn or reflector charging circuit is shown in Fig. E.2. For each circuit, the main components are:

1. One 8 kV, 15 A charging supply:

By reception of the start pulse derived from the SPS timing system, the power supply starts charging the two capacitor banks with a constant charging current until the voltage reaches the requested preset value V_c *Set*. The reception of the stop pulse blocks the charging unit during the blocking time of 300 ms. The trigger pulse for pulse 1 is expected to arrive in this time interval to fire the first energy storage switching section producing the first discharge into the load, followed 50 ms later by the trigger pulse for pulse 2 firing the second energy storage switching section producing the second discharge into the load. The preset voltage V_c *Set* is calculated to precisely reach the required horn current of 120 kA. The stability of the power supply enables a precision of 5×10^{-4}.

The voltage and current settings and the control electronics consist of two parallel senseloops working respectively in sequence:

- first during the capacitor charging phase,
- and second during the voltage stabilization phase.

They act on the phase angle of the TH1–TH6 thyristor switch. A rectifier bridge D1–D6 is located on the secondary side of the power transformer TR1.

The charging current needed is:

$$I_{ch} = \frac{2 \times V_c \times C}{t},$$

where

$V_c =$ Voltage on capacitor,
$C =$ Capacitor of one energy storage switching section,
$t =$ Charging time = [Cycle time - (Blocking Time + stabilization time)],
$I_{ch} =$ 0 to 15 A $\pm$ 2%,
$V_c =$ 0 to 8 kV $\pm$ 0.05%.

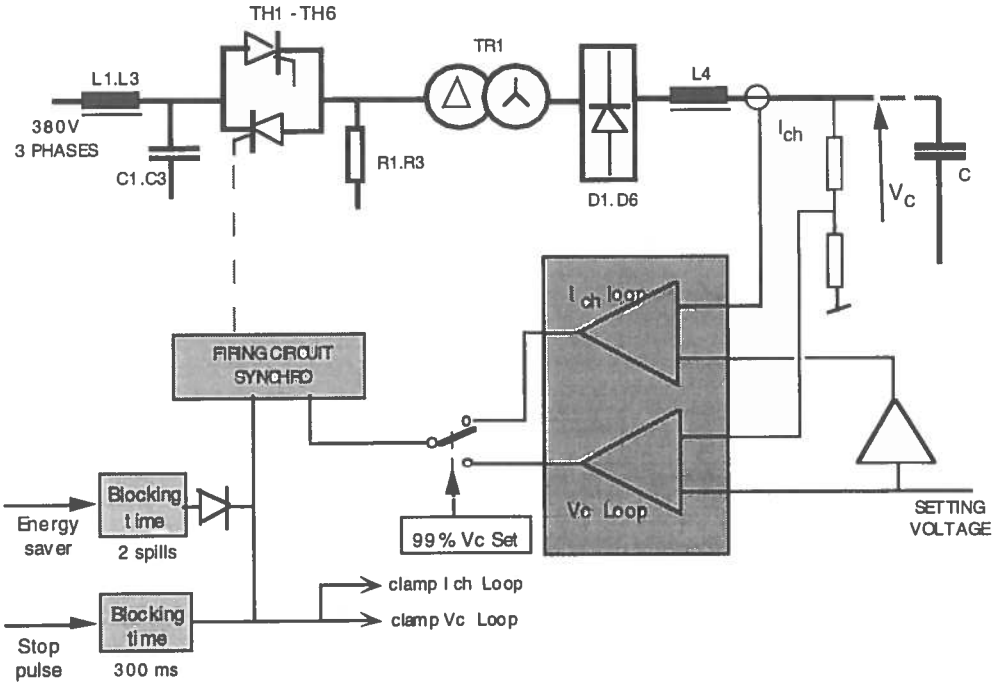

Fig. E.2: Diagram of the horn charging circuit

2. **Two capacitor banks:**
   Parallel mounting of 46.8 μF (10 kV) capacitors to build up two 1825 μF banks for the horn and two 1310 μF banks for the reflector.

3. **Two switching sections:**
   Each one has two series thyristors (10 kV peak, 7500 A peak) protected against excessive di/dt by one saturating choke.

4. **One interlock system:**
   Protecting against all faults related to the electrical circuit, water circuit, personnel access, etc.

5. **One polarity changer:**
   Already mentioned.

6. **One primary high-voltage cable:**
   Of approximately 1000 m in length has to be installed per system (EDF type: ROQUE V_N = 18 kV). Total section of the copper conductor is 240 mm^2. The 6.4 s cyclic double pulse of 7500 A amplitude corresponds to 180 A r.m.s.

7. **One pulse transformer:**
   A detailed description can be found in Ref. [43] and references therein.

8. **Four secondary low-voltage strip-lines:**
   Four sets of massive aluminium alloy parallel plates connect the pulse transformer to the horn passing. They need to pass through a trench to avoid blocking the runway along the beam.

E.3 Main electrical data

Only nominal operational data are given in Table E.1.

Table E.1: Electrical characteristics of the horn and reflector

	HORN SYSTEM		REFLECTOR SYSTEM	
Peak current in element	120 kA		120 kA	
Transformer ratio	16		16	
Primary current peak	7500 A		7500 A	
Inductance element	1.2 μH x 16^2	0.30 mH	0.4 μH x 16^2	0.12 mH
connections	0.12 μH x 16^2	0.03 mH	0.12 μH x 16^2	0.03 mH
striplines (30 m length)	20 nH x 30 x 16^2	0.15 mH	20 nH x 30 x 16^2	0.15 mH
transformer	0.10 mH		0.10 mH	
cable (800m) 240 mm^2	0.01 mH		0.01 mH	
TOTAL	0.50 mH		0.41 mH	
Resistance element	0.6 m Ω x 16^2	0.153 Ω	0.33 m Ω x 16^2	0.087 Ω
striplines (30 m length)	2.5 μ Ω x 30 x16^2	0.019 Ω		0.019 Ω
transformer	0.019 Ω		0.019 Ω	
cable (800m) 240 mm^2	0.125 Ω		0.125 Ω	
TOTAL	0.316 Ω		0.250 Ω	
Total capacitance for one switching section	46.8 μF x 39	1825 μF	46.8 μF x 28	1310 μF
Pulse duration	3.3 ms		2.5 ms	
Charging voltage	6500 V		6000 V	
Voltage on element	340 V		210 V	
Duty cycle	2 pulses 50 ms apart all 6 s		2 pulses 50 ms apart all 6 s	
r.m.s. current in element	2800 A		2400 A	
Power dissipation in element	4800 W		2400 W	
r.m.s. current in cable	175 A		150 A	
Current density in cable	0.73 A / mm^2		0.61 A / mm^2	
Voltage drop cable	937 V		937 V	
Power dissipation in cable	3830 W (5 W/m)		2700 W (3.5 W/m)	

E.4 Horn and reflector magnetic induction

The magnetic volume is confined between the inner and outer conductor of the element with the azimuthal magnetic induction B (Tesla) varying as $B = \mu_0 I/2\pi r$ in MKSA units. The maximum value is found on the surface of the neck at the smallest radius on the inner conductor. For $I = 120\,\text{kA}$:

HORN: at radius $r = 10.8\,\text{mm}$, the corresponding value is $B = 2.22\,\text{Tesla}$.
REFLECTOR: at radius $r = 100.0\,\text{mm}$, the corresponding value is $B = 0.24\,\text{Tesla}$.

It appears that the mechanical constraints on the inner conductor of the reflector compared with the horn are in the ratio $(0.24/2.22)^2$ and are hence much less of a problem.

References

[1] J. Primack et al., *Cold and hot dark matter cosmology with* $m_{\nu_\mu} \approx m_{\nu_\tau} \approx 2.4$ eV, Phys. Rev. Lett. **74** (1995) 2160;
S. Ghigna et al., *Statistical tests for CHDM and* λCDM *cosmologies*, preprint astro-ph/9611103 (1996).

[2] B. Pontecorvo, Zh. Ehksp. Teor. Fiz. **7** (1958) 172 [Sov. Phys. JETP **34** (1958) 247].

[3] N. Hata and P. Langacker, *Solutions to solar neutrino anomaly*, preprint hep-ph/9705339 (1997).

[4] S.P. Mikheyev and A.Yu. Smirnov, Yad. Fiz. **42** (1985) 1441;
L. Wolfenstein, Phys. Rev. **D17** (1985) 2369.

[5] Y. Fukuda et al., *Two-nucleon pion absorption in* ^{4}He *at* 1 GeV/c, Phys. Lett. **B335** (1994) 237.

[6] Y. Totsuka (for the Superkamiokande Collaboration), talk given at the *18th International Symposium on Lepton and Photon Interactions*, Hamburg, 28 July–1 August 1997.

[7] M. Apollonio et al., *Initial results from the CHOOZ long baseline reactor neutrino oscillation experiment*, Phys. Lett. **B420** (1998) 397.

[8] C. Athanassopoulos et al., *Evidence for* $\nu_\mu - \nu_e$ *neutrino oscillations from LSND*, Phys. Rev. **C54** (1996) 2658; Phys. Rev. Lett. **77** (1996) 3082.

[9] J.J. Gomez-Cadenas and M.C. Gonzales-Garcia, Z. Phys. **C71** (1996) 443.

[10] G.L. Fogli, E. Lisi and D. Montanino, *A consistent three-flavour approach to possible evidence of neutrino oscillations*, Phys. Rev. **D49** (1994) 3626.

[11] G.L. Fogli, E. Lisi and D. Montanino, *Matter-enhanced three-flavor oscillations and the solar neutrino problem*, Phys. Rev. **D54** (1996) 2048.

[12] P.F. Harrison, D.H. Perkins and W.G. Scott, Phys. Lett. **B349** (1995) 137.

[13] A. Acker and S. Pakvasa, *Three neutrino flavors are enough*, preprint hep-ph/9611423, vol. 2, 27 November 1996.

[14] C.Y. Cardall and G.M. Fuller, *Can a "natural" three-generation neutrino mixing scheme satisfy everything?*, Phys. Rev. **D53** (1996) 4421.

[15] C.Y. Cardall, G.M. Fuller and D.B. Cline, *Intermediate baseline appearance experiments and three-neutrino mixing schemes*, preprint hep-ph/9706426, 19 June 1997.

[16] G. Ewan et al., *Sudbury Neutrino Observatory Proposal*, SNO-87-12 (1987).

[17] The ICARUS Collaboration, *ICARUS II - A Second Generation Proton Decay Experiment and Neutrino Observatory at the Gran Sasso Laboratory*, Proposal, LNGS-94/99 Vols. I and II, May 1994;
The ICARUS Collaboration, *A First 600-ton ICARUS Detector Installed at the Gran Sasso Laboratory*, Addendum to Proposal LNGS-94/99, 19 May 1995.

[18] C. Arpesella et al., *Borexino Proposal*, 2 vols., eds. G. Bellini and R.S. Raghavan, University of Milan (1991).

[19] J. Kleinfeller (for the KARMEN Collaboration), talk given at the *17th International Conference on Neutrino Physics and Astrophysics*, Helsinki, 13–19 June 1996.

[20] N. Armeninse et al., *Letter of Intent: Search for $\nu_\mu - \nu_\tau$ Oscillation at the CERN PS*, CERN-SPSC/97–21, SPSC/I216.

[21] M. de Jong et al., CHORUS Collaboration, *A new search for $\nu_\mu - \nu_\tau$ oscillation*, CERN-PPE/93–131 (1993).

[22] P. Astier et al., NOMAD Collaboration, *Proposal: Search for the Oscillation $\nu_\mu - \nu_\tau$*, CERN-SPSLC/91–21 (1991), CERN SPSLC/91–48, SPSLC/P261 Add.1.

[23] E. Eskut et al., CHORUS Collaboration, *A search for $\nu_\mu - \nu_\tau$ oscillation*, submitted to Phys. Lett. **B** (1997).

[24] J. Altegoer et al., NOMAD Collaboration, *The NOMAD experiment at the CERN SPS*, Nucl. Instrum. Methods Phys. Res. **A404** (1998) 96, and references therein;
J. Altegoer et al., NOMAD Collaboration, *A search for $\nu_\mu - \nu_\tau$ oscillations using the NOMAD detector*, submitted to Phys. Lett. **B** (1998).

[25] N. Ushida et al., Phys. Rev. Lett. **57** (1986) 2897.

[26] H. Harari, *Light neutrinos as cosmological dark matter: a crucial experimental test*, Phys. Lett. **B 216** (1989) 413.

[27] J. Ellis, J.L. Lopez and D.V. Nanopoulos, *The prospects for CHORUS and NOMAD in the light of COBE and GALLEX*, Phys. Lett. **B292** (1992) 189.

[28] J. Ellis, *Outlook on neutrino physics*, pre-print CERN-TH/96–325, hep-ph/9612209 and in *Proceedings of the Conference on Pure Mathematics with Computers*, Helsinki, 3–4 June 1996.

[29] A.S. Ayan et al., *Letter of Intent: A High Sensitivity Short Baseline Experiment to Search for $\nu_\mu - \nu_\tau$ Oscillation*, CERN-SPSC/97–5, SPSC/I 213, 14 March 1997.

[30] G.L. Fogli, E. Lisi and D. Montanino, *Fourier analysis of real-time, high-statistics solar neutrino observations*, BARI-TH-276–97, preprint hep-ph/9706228 (1997).

[31] E. Ables et al., MINOS Collaboration, Fermilab Proposal P-875 (1995).

[32] M. Ambrosio et al., NOE Collaboration, *A new design scintillating fiber calorimeter to search for neutrino oscillations in massive underground detectors*, Nucl. Instrum. Methods Phys. Res. **A363** (1995) 604.

[33] T. Ypsilantis et al., *A long base line RICH with a 27kton water target and radiator for detection of neutrino oscillations*, Nucl. Instrum. Methods Phys. Res. **A371** (1996) 330.

[34] H. Shibuya et al., OPERA Collaboration, *Letter of Intent: The OPERA Emulsion Detector for a Long-Baseline Neutrino-Oscillation Experiment*, CERN-SPSC 97–24, LNGS-LOI-8-97 (1997).

[35] G. Baldini et al., *NICE Proposal*, LNGS-LOI 98/13 (1998).

[36] B. Van de Vyver et al., *Prompt ν_τ background in wide-band ν_μ beams*, CERN-PPE/96–113 (1996).

[37] M.C. Gonzales Garcia et al., NOMAD Collaboration, *Prompt ν_τ fluxes in present and future tau neutrino experiments*, CERN-TH 96–220, CERN-PPE 96–114, (1996).

[38] More information on the Gran Sasso Laboratory can be found on the World-Wide Web, http://www.lngs.infn.it/.

[39] P. Collier et al., *The SPS as Injector for LHC: Conceptual Design*, report CERN-SL/97–007 (DI), (1997).

[40] A.E. Ball, B. Bianchi, J.-P. Revol, G.R. Stevenson and E. Weisse, *CERN beams for long base line neutrino oscillation experiments*, CERN SL Note 92–75 (BT), (1992).

[41] L.K. Resvanis et al., NESTOR Collaboration, *NESTOR: a neutrino particle astrophysics underwater laboratory in the Mediterranean*, in *Proceedings of the Workshop on High-Energy Neutrino Astrophysics*, Honolulu, 23–26 March 1992.

[42] S. Péraire et al., *The SPS target station for CHORUS and NOMAD neutrino experiments*, CERN-SL/96–044 (BT), in *Proceedings of the 5th European Particle Accelerator Conference EPAC'96*, Sitges, 1996.

[43] G. Acquistapace, V. Falaleev, J.M. Maugain, G. Olesen, S. Rangod and J. Zaslavsky, *The West Area neutrino facility for CHORUS and NOMAD experiments (94–97 operation)*, CERN-ECP/95–014 (1995).

[44] A.E. Ball, S. Katsanevas and N. Vassilopoulos, *Design studies for a long-baseline neutrino beam*, Nucl. Instrum. Methods Phys. Res. **A383** (1996) 277.

[45] P. Lefèvre and T. Pettersson eds., LHC Study Group, *The Large Hadron Collider: Conceptual Design*, report CERN-AC/95–05 (LHC), (1995).

[46] A. Fassò et al., *Simulating accelerator radiation environment*, in *Proceedings of SARE*, Santa Fe, 11–15 January 1993, ed. A. Palounek, (Los Alamos Report LA-12835-C, Los Alamos, 1994) p. 134;
P. A. Aarnio et al., *Proc. MC93 International Conference*, Tallahassee, 1993, (World Scientific, Singapore, 1994), p. 88.

[47] A. Ferrari and P. R. Sala, *The Physics of High Energy Reactions*, lecture given at the *Workshop on Nuclear Reaction Data and Nuclear Reactors Physics, Design and Safety*, International Centre for Theoretical Physics, Miramare-Trieste, 15 April–17 May 1996, Proceedings in press (World Scientific);
A. Fassò et al., *Proceedings of the Third Workshop on Simulating Accelerator Radiation Environments (SARE-3)*, KEK-Tsukuba, 1997, H. Hirayama ed., (KEK report Proceedings 97–5, 1997) p. 32.

[48] A. Ferrari and P.R. Sala, GEANT *hadronic packages: a comparison at the single interaction level*, ATLAS Internal Note PHYS-NO-086, (1996).

[49] M. Bonesini (on behalf of the NA56/SPY Collaboration), *The NA56/SPY experiment at CERN*, presented at the *International Europhysics Conference on High Energy Physics*, Jerusalem, August 1997, proceedings in press;
A. Guglielmi (on behalf of the NA56/SPY Collaboration), *Report on SPY results*, presented at the *16th International Workshop on Weak Interactions and Neutrinos*, Capri, 22–28 June 1997.

[50] G. Ambrosini et al., *Measurement of pion and kaon fluxes below* 60 GeV/c *produced by* 450 GeV/c *protons on a beryllium target*, proposal CERN-SPSLC/96–01;
G. Ambrosini et al., Phys. Lett. **B**, in press.

[51] A. Guglielmi, private communication.

[52] I.M. Papadopoulos and the TOSCA Neutrino Beam Study Group, private communication.

[53] F. Pietropaolo, private communication.

[54] C. Richard-Serre, *Evaluation de la Perte d'Énergie Unitaire et du Parcours pour des Muons de* 2 *à* 600 GeV *dans un Absorbant Quelconque*, Report CERN 71–18 (1971).

[55] W. Lohmann, R. Kopp and R. Voss, *Energy Loss of Muons in the Energy Range* 1–10 000 GeV, Report CERN 85–03 (1985).

[56] J. Hylen et al., *Conceptual Design for the Technical Components of the Neutrino Beam for the Main Injector (NuMI)*, FERMILAB-TM-2018 (1997).

[57] *Proposal for a Long-Baseline Neutrino Oscillation Experiment Using KEK-PS and Superkamiokande* - E362 (1995).

[58] M. Mayoud, *Géométrie théorique du LEP*, CERN/LEP-SU/MM/sb (1983).

[59] B. Bell, *A simulation of the gravity field around LEP*, CERN/LEP-SU internal report (1985).

[60] M. Crespi (DITS/Università di Roma), private communication.

[61] C. Boucher (LAREG, France), private communication.

[62] E. Gübler (L+T, Switzerland), private communication.

[63] A. Hilaire, V. Mertens and E. Weisse, *Trajectory correction of the LHC injection transfer lines TI2 and TI8*, preprint LHC Project Report 122 (1997).

[64] G. Catanesi et al., *CERN West Area Neutrino Facility beam alignment*, preprint CERN-SL/96–24 (OP), in *Proceedings of the 5th European Particle Accelerator Conference EPAC'96*, Sitges, 1996.

[65] S. Péraire, *Comportement thermique et mécanique d'une cible en béryllium soumise à un cycle d'extractions rapides*, CERN SL/Note 95–54 (BT/TA) (1995).

[66] J.M. Zazula et al., *Thermomechanical effects induced by SPS beam in a beryllium rod of the T9 neutrino target*, CERN SL/Note 95–90 (BT/TA) (1995).

[67] R. Valbuena, CERN EST Division, private communications.

[68] E. Heijne, *Muon Flux Measurement with Silicon Detectors in the CERN Neutrino Beams*, Report CERN 83–06 (1983).

[69] L. Casagrande et al., *The Alignment of the CERN West Area Neutrino Facility*, Report CERN 96–06 (1996).

[70] E. Cennini, CERN-ST note, in preparation.

[71] G.R. Stevenson and H.H. Vincke, CERN/TIS-RP/98-draft.

[72] A. Ferrari, T. Rancati and P.R. Sala, FLUKA *applications in high-energy problems: from LHC to ICARUS and atmospheric showers*, in *Proceedings of the Third Workshop on Simulating Accelerator Radiation Environments (SARE-3)*, KEK, Tsukuba, 1997, H. Hirayama ed., (KEK report Proceedings 97–5, 1997) p. 165.

[73] *The NGS cost estimate*, CERN/AC Note (in preparation).

[74] Swanson Analysis Systems Inc., *ANSYS Release 5.3*, Houston, USA (1996).

[75] S. Péraire, *Vibration d'un cylindre soumis à un champ thermique radial*, CERN SL/Note 97–39 (BT/TA) (1997).

[76] J. Avril, *Encyclopédie Vishay d'Analyse des Contraintes* (Vishay-Micromesures, Malakoff, France, 1974).

[77] J. Gervaise, *Applied geodesy for CERN accelerators*, CERN/LEP-SU/84.3 (1984).

LIST OF CERN REPORTS PUBLISHED IN 1998

CERN 98-01
CERN. Geneva
Tavlet, M; Fontaine, A; Schönbacher, H
Compilation of radiation damage test data, Part II, 2nd edition: Thermoset and thermoplastic resins, composite materials; Index des résultats d'essais de radiorésistance, IIe Partie, 2e édition: Résines thermodurcies et thermoplastiques, matériaux composites
CERN, 18 May 1998. - 180 p

CERN 98-02
CERN. Geneva
Acquistapace, G; Baldy, J L; Ball, A E: et al.
The CERN neutrino beam to Gran Sasso (NGS); Conceptual technical design
CERN, 19 May 1998. - 126 p

CERN 98-02
ISSN 0007-8328